UNIVERSITY OF OKLAHOMA

GRADUATE COLLEGE

DECISION-MAKING FOR WELL PLACEMENT OPTIMIZATION IN OIL

FIELD DEVELOPMENT

A DISSERTATION

SUBMITTED TO THE GRADUATE FACULTY

in partial fulfillment of the requirements for the

Degree of

DOCTOR OF PHILOSOPHY

By

YUQING CHANG
Norman, Oklahoma
2015

DECISION-MAKING FOR WELL PLACEMENT OPTIMIZATION IN OIL
FIELD DEVELOPMENT

A DISSERTATION APPROVED FOR THE
MEWBOURNE SCHOOL OF PETROLEUM AND GEOLOGICAL
ENGINEERING

BY

_____
Dr. Deepak Devegowda, Chair

_____
Dr. Chandra S. Rai

_____
Dr. Carl Sondergeld

_____
Dr. Xingru Wu

_____
Dr. S. Lakshmivarahan

_____
Dr. Theodore B. Trafalis

To my family.

ACKNOWLEDGEMENTS

I also thank all my friends in Norman for the accompany and for the best memories in Oklahoma. The hiking and camping trips we had together are what I miss the most.

Most of the studies in this dissertation cannot be done without the support of the team members led by Dr. Henry Neeman in OU Supercomputer Center (OSCER). They always provide the most efficient helps in time in person, which made all the research possible.

The finalization of this dissertation is done while I work in the reservoir group of IRIS in Bergen, Norway. I appreciate my research group director Randi Valestrand for her kindness, her understanding and support during this time.

A special thanks goes to my boyfriend Kurt Rachares Petvipusit, who has walked with me through all the ups and downs in the past few years, who shares the joy and relieves the pain. I appreciate what he did for everything!

No word can express my deep appreciation to my parents, who are always there whenever wherever, who always give me full support and encouragement for all the critical points I have gone through. This dissertation is especially dedicated to my father, the greatest man in my life. His diligence, optimism and courage have shaped me and will continuously motivate me. A sudden brain stroke on my father in November 2012 gave me the darkest winter ever. I am grateful that the effort of the doctors and the whole family brought his life back, but he lost the capability of long-distance travels. Although he missed the chance to see where I studied in Oklahoma, I hope he recovers enough one day, to see where I live now in Bergen - a beautiful city of Norway.

TABLE OF CONTENTS

LIST OF TABLES

LIST OF FIGURES

ABSTRACT

Well placement is a method to improve oil recovery by drilling new infill wells in a reservoir. Drilling new wells is a critical yet very challenging task in field development, because the optimal well locations are rarely known and difficult to decide in practice due to complex reservoir and depletion situations. This dissertation focuses on the development of mathematical optimization techniques to assist decision-making for well planning and placement. The following topics are included in this dissertation.

- To study and develop two stochastic approximated gradient-based approaches: the ensemble based optimization method (EnOpt) and the fixed-gain simultaneous perturbation stochastic approximation (FSP) for well placement; Evaluate the performance and effectiveness of these two methods on case studies.

- To develop an efficient method to decide optimal number of wells and the corresponding locations, evaluate the performance on study cases.

- To handle geological uncertainty and decision-making risk, propose a new workflow for multi-objective well placement optimization.

- To ensure an efficient decision-making and a fast turnaround time, the use of engineering prior knowledge and a few acceleration routines are discussed in the context of optimization.

All approaches are evaluated on synthetic reservoir models, some are performed on real field-like cases. This dissertation provides various optimization methods with an enhanced capability of addressing geological uncertainty for well placement in oilfield

development. However, it should also be noted that while the techniques proposed in this dissertation are applicable to a diverse set of reservoirs with no known limitations, the additional value of this dissertation lies in its ability to address well placement needs for highly complex reservoirs. For reservoirs that lack the complexity seen, for example, in deepwater basins, conventional well placement methods may be sufficient.

CHAPTER I

INTRODUCTION

1.1 Introduction

The World Energy Outlook (WEO) 2015 report from the U.S. Energy Information Administration (EIA) states that the generation capacity of electricity, has been and will be mainly supported by natural gas and oil in the near and long-term future (Figure 1.1). Consequently, ensuring energy security through judicious management of oil and gas resources becomes vital.
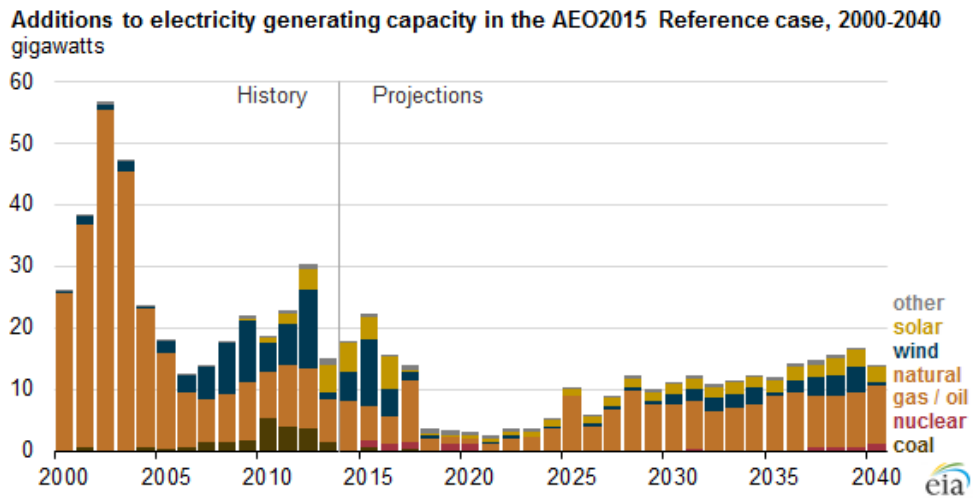
Figure 1.1: Electricity generating capacity mainly comes from natural gas and oil (Source: Annual Energy Outlook 2015, EIA).

Figure 1.2 shows the decline of oil production from the currently producing fields worldwide along with projections for future production from new and existing oil fields. Well placement has a direct impact on the development of new and existing plays and therefore is critical to the oil field development.

Currently, energy produced from the existing fields account for 30% to 70% of the
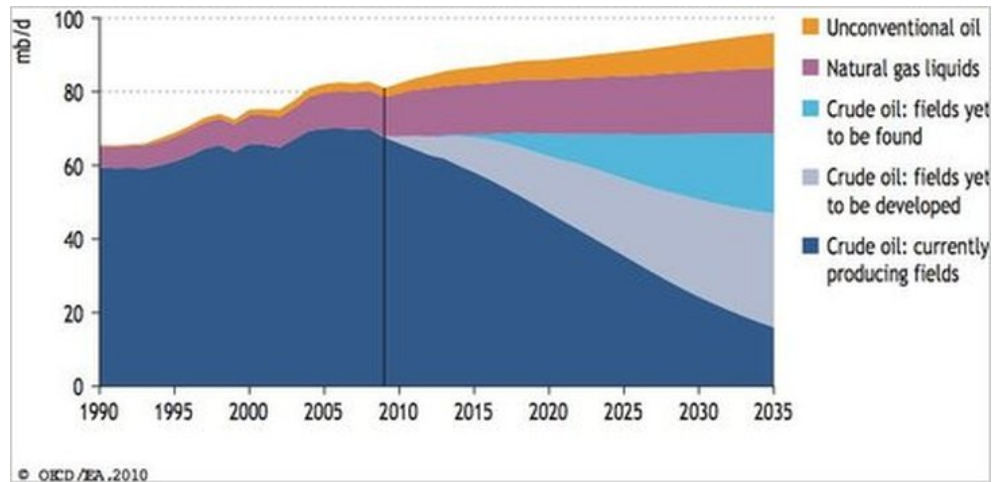
Figure 1.2: Projections of the world's liquid energy source to 2035 (Source: Annual World Energy Outlook 2010, EIA).

hydrocarbons in place (Mullins, 2014) and the number of production wells and their locations can have a considerable impact on the energy recovery factor. Although drilling as many wells as possible can improve recovery of hydrocarbon resources, this is not an optimal strategy. Firstly, drilling and completing wells can be very expensive with costs varying between 5 million and 150 million US dollars. Secondly, typical drilling success rates are not high. For example, deep water drilling success rates have only averaged around 30% since 1985 (before which they averaged around 10%) Pettingill (2006). Finally, the number of planned wells is a function of current and expected future oil prices.

Mullins (2014) demonstrates the objective of well placement as shown in Figure 1.3. The goal of drilling the production wells is to target the hydrocarbon-rich zones. A few injection wells may also be required for pressure support during the reservoir production. The orientation of the wells also becomes important and depends on the subsurface geology interpreted from seismic data, gravity data, magnetic data, well log analysis, well testing data, production data or core data from rock/fluid samples obtained during the drilling process and geological interpretation. This data is

then utilized to construct geological models that are representations of the subsurface reservoirs. However, these models are still associated with considerable heterogeneity because of the sparsity of data and/or the resolution of the measurements. Consequently, optimal well placement is still a challenging task and continues to be a topic of active research.
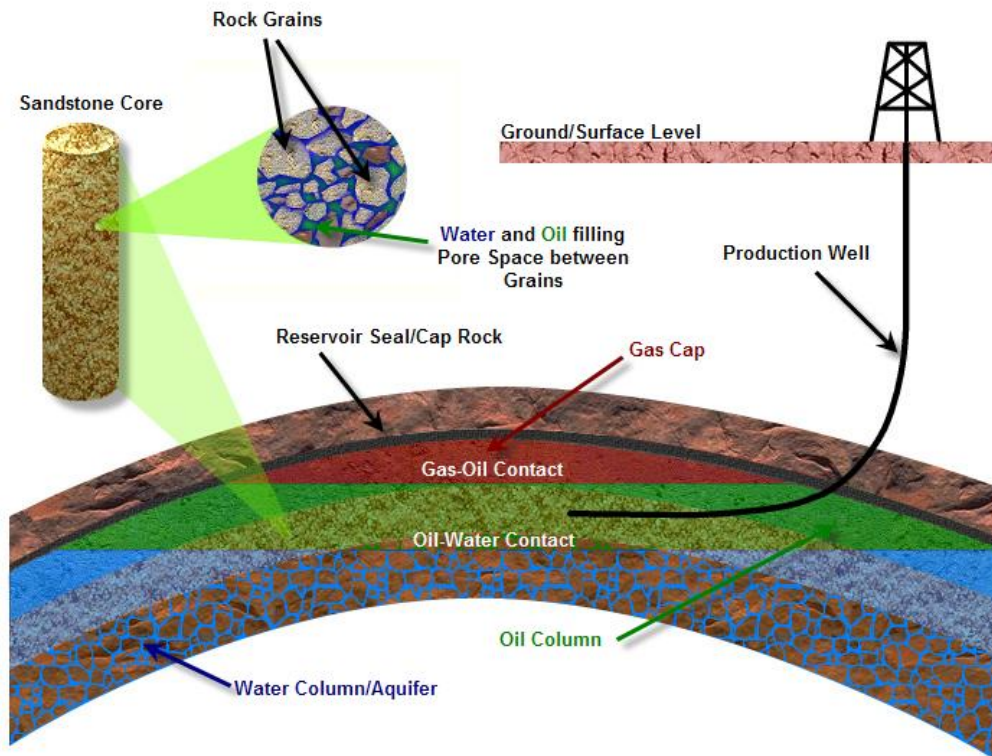
Figure 1.3: Schematic of subsurface oil and gas reservoir (Mullins, 2014).

In this chapter, I review the existing optimization approaches for well placement and introduce the motivating factors for the work done in this dissertation.

1.2 Optimization Algorithms

Locating new wells is a complex and challenging problem because of complex reservoir structure, the presence of existing well patterns, surface equipment specifications,

infrastructure, environmental conditions, geological uncertainty and economic considerations. Most traditional optimization methods for well placement focus on placing a new well or a group of new wells in order to maximize contact with the most productive regions of the reservoir, to target bypassed hydrocarbon or to maximize some predefined reservoir performance metric, such as the Net Present Value (NPV) or the cumulative oil production (Yeten et al., 2003; Bouzarkouna, 2012). NPV is the most widely used objective function in reservoir optimization, which is the difference between the present value of cash inflow and the present value of cash outflow. In recent years, several authors have developed optimization approaches to deal with well placement problems (Beckner and Song, 1995; Bittencourt and Horne, 1997; Pan and Horne, 1998; Guyaguler and Horne, 2000; Yeten et al., 2003; Bangerth et al., 2006; Ozdogan and Horne, 2006; Handels et al., 2007; Wang et al., 2007; Sarma and Chen, 2008; Onwunalu and Durlofsky, 2009; Forouzanfar et al., 2010; Wang et al., 2011; Bouzarkouna, 2012; Ding et al., 2014). Generally, these studies use algorithms which can be categorized into three different groups:

1. Gradient-based methods: For example, the steepest ascent/descent method, conjugated-gradient method and the adjoint method (Handels et al., 2007; Wang et al., 2007; Sarma and Chen, 2008; Forouzanfar et al., 2010).

2. Gradient-free methods: For example, genetic algorithms (GA) (Bittencourt and Horne, 1997; Guyaguler and Horne, 2000; Yeten et al., 2003; Artus et al., 2006), covariance matrix adaptation evolutionary strategy (CMA-ES) (Bouzarkouna, 2012), particle swarm optimization (Onwunalu and Durlofsky, 2010) and simulated annealing (Beckner and Song, 1995).

3. Stochastic approximate gradient methods: For example, ensemble-based methods (EnOpt) (Leeuwenburgh et al., 2010) and simultaneous perturbation stochastic approximation (SPSA) (Bangerth et al., 2006), etc.

In the following sections, I review these methods for well placement optimization. Some of these techniques are originally introduced to address production optimization and the application to well placement optimization is very limited; therefore, a few algorithms of interest are also introduced whose applications have been restricted to production optimization only.

1.2.0.1 Gradient-Based Methods

In well placement optimization, the objective functions can be formulated as predefined functions, such as net present value (NPV), cumulative oil production, sweep efficiency, etc. Gradient-based methods are the algorithms that utilize the gradient of the objective function with respect to decision variables to guide the search for optimal solutions. The most popular gradient-based algorithm in petroleum engineering optimization problems is the adjoint method (Brouwer et al., 2004; Wang et al., 2007; Sarma and Chen, 2008; Forouzanfar et al., 2010). For example, Sarma and Chen (2008) apply gradient-based algorithms to determine well locations by replacing the discrete well location parameters with their continuous counterparts in the real domain and obtain a continuous function that provides the adjoint and gradient for optimization. In another application, Vlemmix et al. (2009) apply the adjoint method to determine optimal well trajectories. In their work, the well trajectory is surrounded with side-tracks to all adjacent grid blocks, and the approximate gradients of the side-track contribution is used to search for the solution with maximum NPV. The curvature (dog-leg severity) of the trajectory is constrained with a predefined drilling feasibility limit. The results show that the gradient-based algorithm can seek the path that leads to a better (improving) NPV. The gradient information for these algorithms may be obtained from evaluating an explicit form of the objective function, however may not be readily available in practical applications such as well placement problems that involve black-box reservoir simulations. If the objective function is

multi-modal with several local optima, gradient-based search path may only resolve suboptimal solutions as it may get stuck at the local optimum. For this reason, other types of algorithms can be used, such as the gradient-free (Guyaguler and Horne, 2000; Yeten et al., 2003; Bouzarkouna, 2012) and/or stochastic approximate gradient methods (Bangerth et al., 2006; Leeuwenburgh et al., 2010).

1.2.0.2 Gradient-Free Methods

Gradient-free algorithms may require considerable computational effort, however, they do have a greater potential likelihood to reach the global optimum (Spall, 1998b; Nwaozo, 2006; Bangerth et al., 2006; Chen, 2008; Leeuwenburgh et al., 2010; Bouzark-ouna et al., 2010). The most well-known gradient-free algorithm is the genetic algorithm (GA) and has been widely applied to many optimization problems in different engineering and geophysical disciplines. However, because GA necessitate a huge computation effort for real field applications, the efficiency of the algorithm becomes extremely important. There have been several developments to accelerate the performance of GA, and these include artificial neural network, hill climber, krigging and polytope (Guyaguler and Horne, 2000; Yeten et al., 2003), etc.

In the study of hybrid genetic algorithm towards well placement in Guyaguler and Horne (2000), the optimal well pattern is found by applying a hybrid genetic algorithm. At each generation of the GA, new members of the population are added using the polytope and krigging methods. The polytope algorithm is the direct search hill-climbing method. They compare the hybrid GA with the traditional GA by running exhaustive simulations to generate the function values as a base case. Their results show that the hybrid algorithm can reduce the necessary number of simulation runs by 4.4 and converges at 125 simulation runs while the classical GA provided a good solution only after 1000 simulation runs. Later, Yeten et al. (2003) use genetic

algorithm combined with several acceleration routines including artificial neural network, hill climber and a near-well upscaling technique to optimize well type, location and trajectory of non-conventional wells. However, as is mentioned in their work, the polytope and krigging methods require a huge number of simulation runs and are time consuming in terms of the convergence rate and function evaluations.

Well placement planning for reservoir management can include placing a single well, a group of wells or choosing well patterns. Instead of placing individual wells sequentially or simultaneously, Onwunalu and Durlofsky (2009) propose a particle swarm approach (PSO) for well pattern optimization in large-scale field development. They first choose some well pattern types, and then optimize the geometry for the promising pattern in the second step. The optimization includes variables that define well pattern types, well pattern operators and the sequence of these operator applications. The geometric transformation in the second step includes the size, shape and orientation of the well patterns that are optimized in the first step. They prove that PSO is robust and efficient for well placement optimization problems. In a further study, Onwunalu and Durlofsky (2010) also consider other optimization variables, involving deviated and dual-lateral wells and single or multiple reservoir models. They compare PSO with GA to demonstrate that PSO outperforms GA on all the reservoir realizations. However, they also indicate that the superior performance of PSO can be case dependent.

Despite the improvements in terms of acceleration routines to minimize function evaluations, gradient-free methods still have drawbacks when applied to well placement problem as the slow convergence rate necessitate expensive computational resources. In the next subsection, I describe the stochastic approximate gradient approaches that shares the advantages of both gradient-based and gradient-free methods.

The third class of optimization algorithms, stochastic approximate gradient optimization methods (Bangerth et al., 2006; Leeuwenburgh et al., 2010), are based on the estimation of the gradient of a suitably constructed objective function. The algorithms combine the advantages of both gradient-based and gradient-free stochastic algorithms in that they do not require an explicit form of the objective function evaluation as does the adjoint method. Additionally, the stochastic gradient methods tend to be more efficient because they require fewer function evaluations. For these reasons, I consider stochastic gradient method in this dissertation. Here, I focus on two approaches: ensemble based optimization method (EnOpt) (Chen, 2008) and Simultaneous Perturbation Stochastic Approximation (SPSA) (Spall, 1992).

Ensemble-based optimization (EnOpt) method is a relatively new method compared to other stochastic gradient methods. EnOpt is an gradient method with the gradient information acquired from an ensemble. An ensemble is a group of possible optimization solutions generated at each optimization searching step. The gradient is estimated based on the correlation between the ensemble and the corresponding objective function values. The first few applications of this algorithm are restricted to production optimization (Lorentzen et al., 2006; Nwaozo, 2006). Lorentzen et al. (2006) first introduce this algorithm to dynamic optimization of water flooding problems. In production optimization, Nwaozo (2006) presents an ensemble-based optimization (EnOpt) of a water flooding application by varying the bottom-hole pressure (BHP) of producing wells to maximize NPV for a constant injection rate. They demonstrate that EnOpt performs well and leads to an increase in cumulative oil production. Nwaozo (2006) also suggests that the advantage of this method over adjoint-based method is that it does not require explicit knowledge of simulator flow equations. Chen (2008) applies ensemble-based closed loop method to a production optimization problem. In a manner similar to the EnKF, multiple realizations of

control parameters (either control rate or BHP) are generated and sensitivity of the objective function is approximated from the ensemble. For a known geological reservoir model, the objective function depends only on control variables. In order to accelerate the convergence rate of this algorithm, several authors have applied this method in combination with different optimization algorithms (Nwaozo, 2006; Chen, 2008; Chaudhri et al., 2009; Leeuwenburgh et al., 2010; Su and Oliver, 2010; Dehdari and Oliver, 2011). Chen (2008) combines EnOpt method with steepest ascent algorithm, while Chaudhri et al. (2009) combine this algorithm with conjugated gradient method and Dehdari and Oliver (2011) combine sequential quadratic programming to improve the convergence of EnOpt for production optimization. The computation time of this algorithm does not strictly depend on the problem dimensions. Thus, for problems with a large number of variables, EnOpt is comparatively efficient but requires a certain number of realizations to approximate the gradient. Because the accuracy of the gradient approximation is sensitive to the size of the ensemble, a large number of realizations is necessary as the problem dimensions increase.

Even though there are various studies on the application of ensemble-based methods for production optimization problems, there is limited literature focusing on the application to well placement optimization. Leeuwenburgh et al. (2010) apply ensemble-based optimization (EnOpt) to optimize well locations in two different reservoir models. The example is tested with 9 wells (3 injectors and 6 producers) for fixed production settings. They show that by repositioning the producers and injectors, they are able to improve the sweep efficiency and increase the NPV. However, a comparison with other methods is lacking.

SPSA is another stochastic gradient method suitable for the problems with non-differentiable objective functions. This method is first proposed by Spall (1998b) where the underlying principle is based on a Kiefer-Wolfowitz type of stochastic algorithm (Kiefer and Wolfowitz, 1952), which is in fact motivated by the Robbins-Monro

algorithm. Robbins and Monro (1951) introduce the idea of stochastic approximation (SA). The Robbins-Monro algorithm is a methodology for solving the root finding problem where the function values cannot be observed directly and the measurements of a few random variables are obtained instead. This algorithm generates iterations that can make the variables converge to the unique root in finite number of iterations. Spall (2003) introduced simultaneous perturbation stochastic approximation (SPSA) by incorporating a random search technique into a finite difference gradient approximation which employs a unit vector searching a direction towards the highest value of objective function. SPSA is first explained in Spall (1987) and fully analyzed in Spall (1992). The theoretical convergence and a few adaptations of SPSA have been reported in the literature, such as discrete SPSA (Gerencsér and Hill, 1999; Gerencsér et al., 2001; Hill, 2005), adaptive SPSA (Spall, 2000) and global search SPSA (Maryak and Chin, 2008). Spall (2003) and Spall et al. (2006) compare SPSA with other optimization methods such as genetic algorithm and simulated annealing and they show that SPSA is quite competitive in terms of computation time to achieve comparable solution accuracies.

Chin (1997) compares random-direction SA, SPSA, and finite-difference SA (FDSA) algorithms numerically to solve a problem when only noisy measurements from the system are available but the gradient of the objective function is not. They utilize the root mean square errors computed from asymptotic distributions to evaluate these algorithms and indicate that SPSA is superior from both the theoretical and practical standpoints. SPSA requires fewer function evaluations than finite difference gradient approximation (FDG) per iteration. With a Bernoulli distribution to sample random search directions, SPSA requires only 2 function evaluations (forward and backward steps) per iteration regardless of the dimension of search space. On the other hand, FDG would require $2p$ function evaluations per iteration, where p represents the dimension of the problem.

SPSA has also been applied to problems in petroleum engineering. Gao et al. (2007) introduce SPSA into the history matching problem and Wang et al. (2009) apply SPSA in production optimization. Gao et al. (2007) give a detailed explanation for the formulation of basic SPSA, SPSA with line search and adaptive SPSA (Spall, 2001) and the application of SPSA in history matching. They also prove that for a quadratic objective function the expectation of the stochastic gradient is the true gradient. Wang et al. (2009) compare the performance of average SPSA gradient, single SPSA gradient, steepest ascent method and ensemble Kalman filter (EnKF) gradient. Single SPSA gradient is the gradient calculated at the current iteration, and average SPSA gradient is the average of all the gradients calculated at each step before and including the current iteration. EnKF gradient is another type of gradient averaging derived from the ensemble using statistics (Lorentzen et al., 2006; Nævdal et al., 2006). They conclude that excluding the steepest ascent method with adjoint gradient, average SPSA gradient works better than the other two methods. Maryak and Chin (2008) also prove that the basic SPSA algorithm can achieve global optimization convergence under certain conditions without the need for injected noise.

For application to well placement, Bangerth et al. (2005) use SPSA to search for optimal location. Later, Bangerth et al. (2006) review and compare the performance of different optimization algorithms. The authors investigate three methods in details, including simultaneous perturbation stochastic approximation (SPSA), FDG and very fast simulated annealing (VFSA). Two examples were tested to compare the performance of these algorithms. In the first example, a single well with known global optimum is placed, and in the second example, seven wells are placed simultaneously with the algorithms. The authors compare the algorithm performance in term of robustness, effectiveness, and efficiency. They indicate that SPSA has the potential to identify very good well locations for an arbitrary starting point. In high dimensional search space, FDG is not as efficient as the other two methods because

it requires $2p$ function evaluations. Moreover, FDG is reported to have a tendency to get stuck at the local minima.

Other optimization methods are also investigated by Bangerth et al. (2006), .i.e., Nelder-Mead algorithm (N-M) and Genetic Algorithm (GA). The N-M method turns out to be the approach with the least merits because it requires the maximum number of function evaluations without identifying a competitive solution while GA is reliable and more effective although it requires a higher number of function evaluations than VFSA and SPSA. The authors conclude that SPSA and VFSA are highly suited for this optimization problem. However, even though VFSA has low efficiency (higher number of function evaluations than SPSA), it is the most robust algorithm in terms of finding global optimum. For future studies, they suggest the use of VFSA during the initial optimization stage replaced by SPSA once it slows down.

Well placement is a discrete optimization problem. This type of optimization problem with discrete variables also plays an important role in the process of design and analysis for discrete event systems, such as resource allocation in manufacturing systems (Gerencsér and Hill, 1999), communication networks (Gokbayrak and Cassandras, 2001), admission control (Bhatnagar and Kowshik, 2005; Mishra et al., 2007) and routing in communication/wireless networks (Barnhart et al., 1995). For the application of SPSA on discrete optimization problems, Gerencsér and Hill (1999) first modify SPSA to a fixed gain version, which is called fixed gain SPSA method (referred as FSP in our study), to solve multiple discrete resource allocation problems by applying SPSA on discrete grids. Whitney et al. (2001) implement this method to the constrained optimization problem of resource allocation to distribute a finite number of discrete resources to finite users such that the specified objective function would be optimized. They compare results of rounding operations performed at different steps of the optimization calculations, such as the calculation for the gradient, the step size and the updated variables. They observe that better results are achieved

when the rounding operations is performed on the updated variables. Gerencsér et al. (2004) combine the truncated fixed gain SPSA method with Markov-Chain Monte-Carlo method to improve the convergence properties during the process of minimizing a convex function defined over the discrete grids. They conclude that the choice of the step size and the gain was critical to the performance of the algorithm.

A few studies have compared the performance of EnOpt and SPSA. Yan and Reynolds (2013) discuss the calculation of a few stochastic gradient methods, including a simplex gradient (Custódio and Vicente, 2007; Custódio et al., 2010; Conn et al., 2009), a modified simplex gradient (Do, 2012) and an EnOpt gradient (Chen and Oliver, 2009). They add smoothing by multiplying a covariance matrix to the approximated gradient and they conclude that by imposing temporal smoothness they are able to improve the convergence rate and the computational efficiency of the Monte Carlo gradient proposed by Pradlwarter (2007). Li and Reynolds (2011) modify SPSA in the context of reservoir history matching using the Stochastic Gaussian Search Direction which referred as G-SPSA in Do et al. (2012). They find that the expectation of the random search direction in G-SPSA is similar to that of the simple second order SPSA algorithm in Gao et al. (2007). Do and Reynolds (2013) compare EnOpt and G-SPSA with the application to the production optimization step of closed-loop reservoir management. They state that EnOpt algorithm can be derived from the modified SPSA-type algorithm.

In summary, the choice of optimization algorithms depends on the form of the objective function as well as the selection of the variables for optimization. All methods discussed above are capable of handling continuous functions; however, gradient-free methods tend to be more generalizable to discrete problems when generating new search points for each iteration in the optimization procedure. Although all methods can handle continuous optimization variables, the options for discrete variable problems are simple truncation or mapping techniques. Other forms of optimization

such as integer programming (Wolsey, 1998; Papadimitriou and Steiglitz, 1998) and branch and bound methods (Land and Doig, 1960; Little et al., 1963) are well suited for discrete variables. However the additional computation effort required by these methods may be prohibitive.

1.2.0.4 Relevance to This Dissertation

Although there are a variety of applications of EnOpt and SPSA on production optimization, few studies have focused on the performance of the well placement problem. In this work, I investigate the performance of EnOpt and SPSA on well placement further. First, I also investigate the sensitivity of the fixed-gain SPSA (FSP) solutions to the step size and gain size with the applications on a few synthetic case studies. Then, I apply a constant gain and the Bernoulli random search direction to the well placement optimization on the 2-D and 3-D heterogeneous cases. Last, I address the question of the computational efficiency for EnOpt and FSP by comparing the studies of the synthetic 2-D and 3-D reservoir cases for single well placement in terms of computation time, the number of function evaluations, and the effectiveness of algorithm based on the maximum NPV values achieved.

1.3   Well Placement with Quality Maps

Reservoir development by successively placing one or two wells can however be suboptimal and may lead to bypassed reservoir volumes and poor recovery. Consequently, it may be more appropriate, whether at the initial or later phases of reservoir development, to develop a strategy of optimally placing a specified number of wells to maximize the recovery, the economics of the project or any other desired criteria. However, this task can be challenging in reality. Firstly, for any given reservoir and a limited development budget, it becomes challenging to determine the optimal number of wells. This is likely to be a function of the underlying heterogeneity, fluid properties, existing well locations and their corresponding drainage patterns, and the

criteria for optimization. Secondly, sequential application of the single well placement routine can also be inefficient, time-consuming and may provide only limited guidance regarding the optimal number of wells.

In order to address the multiple well placement problem, reservoir engineers usually optimize the locations of a pre-specified number of wells (Bangerth et al., 2006). If the number of wells is not known a priori, a fixed number of wells will be placed and the proposed number of wells are increased progressively till they reach an optimum. Salmachi et al. (2013) study how to determine the number of wells in coal bed methane reservoirs. They first obtain the maximum NPV from different scenarios of the fixed number of wells and plot NPV versus the numbers of wells. Then they approximate the regression curve to find what is the optimal number of wells. This can be extremely time consuming and prohibitively expensive for large reservoirs requiring the placement of 10 or more wells. Other researchers attempt to optimize the number of wells with adjoint methods (Wang et al., 2009) or particle swarm optimization (Onwunalu and Durlofsky, 2009) by controlling the wells to be open or close (eliminated) in the optimization process. But these methods require either large computer storage or more function evaluations. Therefore, several authors (Cruz et al., 1999; Badru, 2003; Nakajima and Schiozer, 2003; Maschio and Schiozer, 2008) have also proposed the use of quality maps to restrict the search to feasible regions of the reservoir, thereby accelerating convergence.

A quality map is a 2-D representation of an appropriately chosen reservoir response, such as the net present value (NPV), cumulative oil production or some predefined production potential index. Cruz et al. (1999) introduce the concept of quality map where the quality unit is the cumulative oil production. The total quality is obtained by averaging the well quality at each grid blocks with an inverse distance weight. They observe that the mean quality map has good correlations with the production potential, and the average value of the uncertainty quality map is also

in line with the flow response uncertainty. Later, Badru (2003) applies the basic quality map to determine the optimal well locations, and the modified quality map approach, which is the basic quality map combined with genetic and polytope algorithms to determine the optimal well locations. Nakajima and Schiozer (2003) use analytical method, numerical simulation, and fuzzy system to improve the quality map for horizontal well placement.

Although quality maps have been applied for well placement in several studies, these work rely on exhaustive simulation runs with a single well placed in different regions of the reservoir to generate quality maps. This process tends to be inefficient, tedious and may not extend easily to multiple well placement. Some work may use interpolation or krigging to save some simulations runs, but because interpolation and response surfaces are essentially smooth functions derived from a limited sampling of the reservoir, they may not be entirely appropriate when the scale of heterogeneity is small. Additionally, such methods do not provide a reasonable framework to demarcate anticipated drainage volumes. In order to calculate the quality maps efficiently, one novel idea from Liu and Jalali (2006) propose to obtain the production potential through the use of parameter group to calculate the productivity potential by incorporating information from oil saturation, oil phase pressure, the natural log of permeability and the natural log of distance to the closest boundary. This is computationally more efficient compared to the traditional methods. Ding et al. (2014) modify this work and add the effect of bottom water and gas cap to the quality map calculation. Apart from the parameters considered in Liu and Jalali (2006), they add the distance from a certain grid to the water-oil contact and oil-gas contact, to calculate the productivity potential. Their work combine the modified quality map with a modified version of PSO and is applied to well placement optimization. However, this approach is more well suited to moderately homogeneous reservoirs and can fail if the reservoir is highly heterogeneous.

To mitigate the challenges and develop a method suitable for large field-scale problems, in this dissertation, I focus on developing quality maps that map regions of high connectivity and high oil (or gas) production potential. Connectivity in numerical reservoir simulation can easily be quantified through the use of inter-block transmissibility. The advantage of utilizing transmissibility to generate quality maps is the following: First, the transmissibility is easily obtained during simulator initialization and do not require any simulation runs. Consequently, even for large models, the computational effort required is on the order of a few seconds. Second, the transmissibility is directly linked to the underlying heterogeneity and do not require interpolation or generation of response surfaces. Moreover, I also introduce a quality map-assisted fixed-gain SPSA method (QM-FSP) to determine the optimal number of wells and their corresponding locations. Fixed-gain SPSA (FSP) (Gerencsér and Hill, 1999) is a modification of simultaneous perturbation stochastic approximation (SPSA) algorithm (Spall, 1992) designed to handle discrete variables associated with the well placement problem. I demonstrate the application of QM-FSP to several case studies to highlight the computational efficiency, accuracy and feasibility of the proposed approach.

1.4 Multi-Objective Optimization

The approaches described in the previous sections are restricted to seeking optimal solutions for one single objective for a specified reservoir model (Beckner and Song, 1995; Yeten et al., 2003; Bangerth et al., 2006; Maschio et al., 2008; Zandvliet et al., 2008; Onwunalu and Durlofsky, 2010; Emerick et al., 2009; Bouzarkouna et al., 2013). However, there are two main drawbacks with these traditional optimization approaches: Firstly, geological uncertainty is often ignored (Beckner and Song, 1995; Bangerth et al., 2006) and not properly treated. Optimization may rely on a single

reservoir model (Do et al., 2012) or may consider multiple geological realizations by using the expected value of the objective functions evaluated over all geological models as the overall objectives (Li et al., 2013) which may bias the optimization results (Wang et al., 2011). Secondly, traditional optimization techniques normally cannot meet the requirement of optimizing two or more conflicting objectives simultaneously (Ferraro and Verga, 2009). This means that optimal solutions achieved by optimizing one objective is often compromised by the degradation of another objective function. Previous work has relied on the use of weight coefficients for each objective to augment multiple objective functions into a single objective function (Yoon and Hwang, 1995). This method, though effective for some case studies, is subjective in defining weight factors for each objective. As a single objective optimization approach, it narrows the decision choice for decision-makers (Das and Dennis, 1997).

In fact, the trade-off relationship of multiple objective can be handled by using multi-objective optimization techniques. Therefore, in recent decades, multi-objective optimization has attracted much attention (Zitzler and Thiele, 1998; Deb et al., 2002; Zitzler et al., 2004; Emmerich et al., 2005; Ishibuchi et al., 2008).

There are many algorithms for solving multi-objective optimization problems (Marler and Arora, 2004). Based on fitness assignment and selection, multi-objective optimization approaches can be classified into criterion selection, aggregation selection and Pareto selection (Zitzler et al., 2000). Among these, aggregation selection is the most popular and widely used approach. In this method, optimization problems with multiple conflicting objective functions are solved by augmenting the objectives into a single function and solving the problem with single-objective optimization methods. But the selection of weight coefficients for each objective may be difficult; improper values of weight coefficients may eliminate the effect of some objectives that may in turn bias the optimal solutions. Moreover, aggregation selection does not work well

for non-convex objective functions because single objective function tend to emphasize optimizing one of the objective functions which has the highest weight factors. Ferreira et al. (2007) compare the solutions obtained for different weight factor settings and they show a clear bias of the solutions on the Pareto front. The Pareto front is a group of optimal solutions plotted in the objective function space and the shape appear as a pareto. Ferreira et al. (2007) show that the results tend to accumulate to different portions of the Pareto front with different weight factor settings. However, Pareto selection based algorithms can avoid the bias caused by improper weight coefficients and provide a group of solutions which take into account different combinations of multiple objective functions.

Among all the Pareto selection based algorithms, NSGA-II appears to be one of the most efficient algorithm in solving multi-objective optimization algorithms (Zitzler et al., 2003). NSGA-II (Deb et al., 2002) is a modification of Non-dominated Sorting Genetic Algorithm (NSGA). It introduces two new concepts: elitism and non-domination. The elitism is to describe how good is a solution in terms of objective functions. The non-dominated solutions are the ones that have equal elitism - no solution is absolutely better than the others in terms of all objective functions. NSGA-II aims at finding a good spread of non-dominated solutions and have better convergence to the true Pareto front. A few literatures report different Pareto-based evolutionary optimization algorithm, such as Niched Pareto Genetic Algorithm (Horn et al., 1994), NSGA-II (Deb et al., 2002) and Strength Pareto Evolutionary Algorithm (SPEA) (Zitzler and Thiele, 1999), etc. Among which, NSGA-II shows superior performance on different types of objective functions. Even though there is a huge body of work on multi-objective optimization (MOO) algorithms, most of them focus on solving explicit mathematical objective functions where computational problems are not in the major considerations. For simulation-based engineering optimization problems, particularly reservoir optimization problems, multiple objective optimization

19

attracts increasing interests yet facing computational challenges.

In engineering optimization problems, the goal of optimizing multiple objectives such as minimizing different types of data mismatches in history matching, maximizing NPV or minimizing the decision risk has become increasingly important in the recent past years (Schulze-Riegert et al., 2007; Ferraro and Verga, 2009; Hajizadeh et al., 2011; Mohamed et al., 2011; Schulze-Riegert et al., 2011; Fonseca et al., 2012; Park et al., 2015). There are several applications of MOO on reservoir history matching problems. Schulze-Riegert et al. (2007) apply an improved version of Strength Pareto Evolutionary Algorithm (SPEA2) to history match a synthetic reservoir model. This is the first application of multi-objective optimization to reservoir history matching problem. Ferraro and Verga (2009) compare SPEA as the multi-objective evolutionary algorithm (MOEA) and the multi-objective genetic algorithm (MOGA) on history matching of the PUNQ-S3 model (Imperial College, 2009). The difference between MOEA and MOGA is whether they have an external set to select individuals and generate the new population. MOEA has an archive set which keeps the good candidate solutions from each iteration, but MOGA does not have such a set. But they observe that the best performance was obtained from MOGA. They also compare the solutions of MOGA and single-objective GA and find that MOGA is able to find better solutions. The work from Ferraro and Verga (2009) is known as one of the early attempts to compare Pareto-based multi-objective solutions with the single objective experiments in history matching. Later, Hajizadeh et al. (2011) propose a new algorithm in history matching, which is called differential evolution for multi-objective optimization using Pareto ranking. They find their multi-objective optimization algorithm has a twice faster convergence and better history match compared to the conventional aggregation-based single objective approach. Mohamed et al. (2011) apply Multi-Objective Particle Swarm Optimization (MOPSO) to history matching and they also observe the fast convergence of MOO method. Park

et al. (2015) apply Multi-Objective Evolutionary Algorithm (MOEA) to reservoir history matching problem. They compare MOEA with the classical aggregation-based (single-objective) method (GA-SOP) and they observe that the GA-SOP solutions are clustered in one side of the Pareto depending on assigned weighting factors. Their studies show MOEA tend to find multiple plausible solutions compared to single-objective optimization methods. Other recent studies from Reynolds and Liu (2014) and Liu et al. (2015) apply gradient-based multi-objective methods to water flooding optimization. They apply gradient-based method to an augmented single objective function. The improvement from their work is that, instead of using constant values as the weights, they propose rescaled weights calculated from the optimal value of each objective function. All these work show the capability of MOO in assisting multi-criteria decision-making.

A critical concern about using multi-objective optimization technique is the prohibitively high computation cost. It should be noted that the *fast convergence* mentioned above in Hajizadeh et al. (2011) and Mohamed et al. (2011) refers to the number of iterations required to reach a convergence. It is a relative statement compared to single objective methods, but the number of function evaluations required is still high. For simulator-based optimization problems, the number of function evaluations for each iteration is proportional to the population size and the number of simulations required to evaluate the objectives, which can be a very computationally intensive process. In order to accelerate the convergence efficiency, some acceleration routines have also been presented in the literatures. Aanonsen et al. (1995) apply multiple regression and krigging to optimize well locations with the response surfaces and experimental design. Guyaguler and Horne (2004) consider the reservoir uncertainty in their well placement problem by carrying out the experiments on 23 history matched realizations for a simple but realistic model. A hybrid genetic algorithm is applied for the optimization, and a random realization is selected for objective

function evaluation using the well location proposed by GA. They observe that their approach can approximately incorporate the risks associated with the decision making process. Later, Bouzarkouna et al. (2012) and Bouzarkouna et al. (2013) apply meta-models and neighborhood approach to accelerate the well placement optimization process while considering geological uncertainty. Additionally, the quality map approach introduced previously has also been applied to accelerate the convergence efficiency.

Generally, we assume reservoir simulator can simulate subsurface flow accurately, however, the simulation forecasts are associated with uncertainty that come from the input data or reservoir model itself (Bléhaut, 1991; Liu et al., 2001; Devegowda and Gao, 2007; Schulze-Riegert et al., 2010). In reservoir characterization and modeling, a multiple-realization approach has been recognized as an important tool to address the uncertainty estimation (Cottini-Loureiro and Araujo, 2005; Ozdogan and Horne, 2006). Guyaguler and Horne (2004) consider the reservoir uncertainty in their well placement problem, by carrying out the experiments on 23 history matched realizations with the PUNQ-S3 model. Additionally, a few studies also combine quality map with uncertainty quantification. For example, Cruz et al. (2004) use the cumulative oil production after a specified production time as the quality unit and defined the total quality by weighting the quality units with the distance between each grid block and the closest well location. The quality map is obtained by repositioning one vertical producer in each grid block, and the producer is completed through all the reservoir layers. The quality map is then applied for 11 scenarios (number of wells) on 20 realizations of 50 reservoir models. A realization ranking methodology is proposed for visualization purpose, decision making, and uncertainty evaluation in the flow response. These realizations are ranked based on the total quality and the profit where the ranking of the total oil volume is obtained for a reference to compare the previous realization ranking results. They point out that by utilizing the quality

22

map, especially the L-optimal quality map, such as the lower-quartile quality map, it is possible to determine suitable vertical producer locations and to incorporate the geological uncertainty into the decision making during reservoir management process. However, their study requires a huge number of simulation runs and can potentially be very time consuming.

1.4.0.6   Relevance to This Dissertation

In this dissertation, I develop a new robust and efficient workflow of well placement optimization under geological uncertainty. I use multi-objective optimization techniques and consider both mean and variance of net present value for all geological realizations to obtain robust solutions. In order to accelerate the optimization process, a physical surrogate - upscaling of the reservoir models is utilized and a quality map is applied to constraint the search domain and limit the search area to the region around the optimal solutions. The quality map is defined as an oil in place (OIP) map, which is calculated by using the pore volume and the oil saturation. These are easily obtained from the initialization of the reservoir model without the need for any simulation runs. The OIP map can then provide a guide for the well placement. The case study results indicate that the proposed approach, quality map assisted multi-objective optimization method, significantly improves the computational efficiency for the well placement optimization problem.

1.5   Dissertation Structure

In this dissertation, Chapter 1 provides the introduction concerning the optimization problems exist in reservoir management and a review of the algorithms that have been applied in single objective and multi-objective optimization problems. Chapter 2 introduces the proposed stochastic approximate gradient algorithms, and the performance of the proposed methods are evaluated on three synthetic case studies. In Chapter 3, the engineering prior knowledge is taken into account and a novel

idea of using quality maps is proposed to place multiple wells optimally and efficiently. In Chapter 4, in consideration of the geological uncertainty in real problems, I propose the mean-variance approach to handle geological uncertainty, and use the multi-objective optimization method to optimize vertical or inclined well placement on a synthetic case and a field case. Chapter 5 summarizes the work in this dissertation and gives principle conclusions obtained from all the studies. The content and research focus of the main chapters are listed in Table 1.5.

Table 1.1: Key contents of each chapter

Chapters	Type of Objectives	Number of Wells	Geological Uncertainty	Methods
Chapter II	Single	Single	No	EnOpt, FSP
Chapter III	Single	Multiple	No	QM-FSP
Chapter IV	Multiple	Multiple	Yes	NSGA-II

CHAPTER II

STOCHASTIC APPROXIMATE GRADIENT METHODS

2.1 Introduction

The main concept of reservoir optimization is to combine the optimization algorithms, the optimizer (reservoir control parameters) and the reservoir simulator into a workflow and search for optimal solutions (Figure 2.1). *Optimal* refers to the solutions that give the best objective function values.
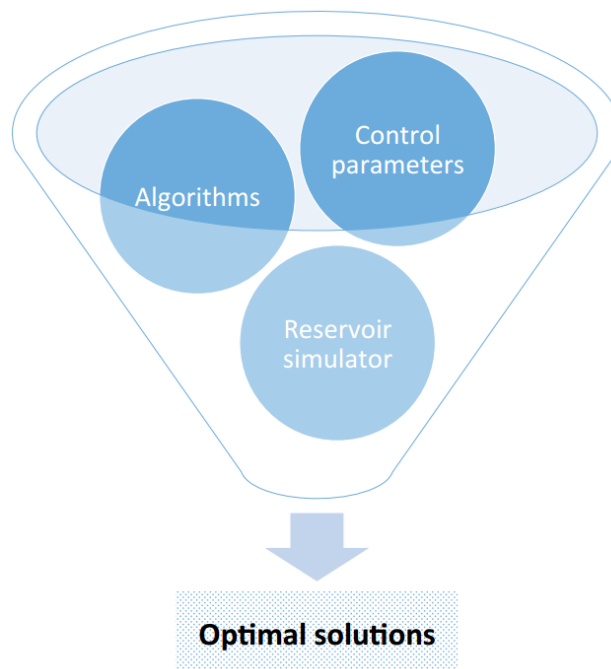
Figure 2.1: Illustration of the key contents in the reservoir optimization workflow

In oil field development, well planning and placement is a critical process for reservoir management. In general, reservoir engineers plan the wells based on their experience and make decisions by visualizing the reservoir model constructed from geological informations, such as the seismic data, well logging data, well testing data, core data, etc. Although this eye-aided approach is easy to implement, obtaining an optimal solution is nearly impossible. Well placement optimization, however, can solve this problem more efficiently and effectively. This chapter introduces the workflow of well placement optimization and the development of two stochastic approximate gradient methods that are suitable for well placement problems.

The workflow is illustrated in Figure 2.2. Generally, given a reservoir model, the optimization is started at some candidate locations; then the candidate locations are evaluated by running reservoir simulator followed by collecting production data and calculating the production profit. Then, the optimization algorithm is used to search for better solutions. This process is performed iteratively until the predefined stopping criteria are satisfied.
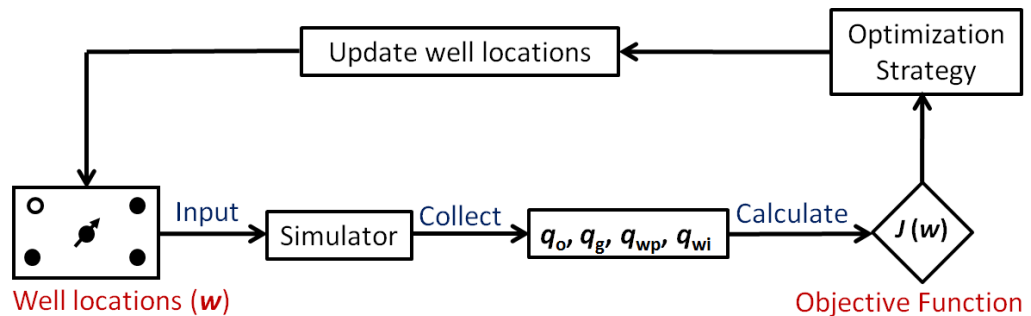
Figure 2.2: Well placement optimization workflow

The descriptions of the objective function and the optimization strategies developed in this work are introduced in the following sections.

2.2　Objective Function

In this work, I maximize Net Present Value (NPV) by optimizing well locations in the reservoir. The NPV function is in general the difference of cash inflow and outflow where the future value of money is discounted to its present value, as given in the following,

$$J(\mathbf{x}) = \sum_{k=1}^{N_t} \left(\frac{C_o \Delta q_{o,k}(\mathbf{x}) + C_g \Delta q_{g,k}(\mathbf{x}) - C_{wp} \Delta q_{wp,k}(\mathbf{x}) - C_{wi} \Delta q_{wi,k}(\mathbf{x})}{(1+d)^{k\Delta t}} \right) - C_d, \quad (2.1)$$

where $J(\mathbf{x})$ is the NPV to be maximized. C_o and C_g are the oil price and gas price in USD per barrel (USD/bbl), respectively. C_{wp} and C_{wi} are the cost to dispose and inject water (in USD/bbl), respectively. d is a daily discount rate. N_t is the simulation time step; Δt is the time period (in days) of each simulation step; C_d is the drilling cost for all the wells. If the wells are vertical wells, C_d is defined as

$$C_d = N_w C_{capex}, \quad (2.2)$$

where N_w is the number of wells and C_{capex} is the capital expenditure for drilling each well. For the applications in this chapter and Chapter 3, I place only vertical wells, and the drilling cost of each well is assumed to be constant.

2.3　Stochastic Approximate Gradient Algorithms

With the objective function defined above, this section focuses on introducing and adapting two algorithms to solve well placement problem: Ensemble-Based Optimization (EnOpt) and Fixed-Gain SPSA Algorithm (FSP).

2.3.1　Ensemble-Based Optimization Method (EnOpt)

Ensemble-Based Optimization (EnOpt) is applied in combination with the steepest ascent method to find the optimal location for a single well. In the following, I

describe an underlying principle of the ensemble method and show how the gradient can be approximated from the information of an ensemble.

2.3.1.1 Ensemble Generation

The idea of ensemble-based methods is to use the information from an ensemble to approximate the gradient. This gradient can then be used in any gradient-based algorithm for optimization. Each ensemble member is obtained from a normal distribution $X \sim N(\mu, \sigma^2)$, with μ and σ^2 representing the mean and the predefined variance of the variables. The variance of the ensemble represents the perturbation size which should be reduced iteratively as the variables get closer to the optimum. In this dissertation, the selection of the values for the ensemble variance is given as a predefined value in this dissertation. For different reservoir models, the variance is selected based on the heterogeneity of the reservoir. For example, in our illustrative homogeneous reservoir model, the variance of 2 is chosen for the first three successful search while the variance of 1 is used for the study in Section 2.4.1. The probability function for the normal distribution to generate ensemble realizations is given in the following,

$$f(\mathbf{x}) = \frac{1}{\sqrt{2\pi\sigma^2}} e^{\frac{-(\mathbf{x}-\mu)^2}{2\sigma^2}}. \tag{2.3}$$

2.3.1.2 Mathematical Formulation

Ensemble-based optimization is based on the steepest ascent method where the gradient is estimated from the ensemble of variables and the corresponding objective function values. Given N_w as the number of wells and let i and j be the Cartesian coordinates of well locations, the vector of well locations is given below,

$$\mathbf{x} = [x_{1i}, x_{1j}, \ldots, x_{N_w i}, x_{N_w j}]^T. \tag{2.4}$$

If considering single well placement for instance, the vector $\mathbf{x}$ is reduced to as

$$\mathbf{x} = [x_{1i}, x_{1j}]^T. \tag{2.5}$$

The flowchart in Figure 2.3 presents a simplified workflow for EnOpt. Initially, the ensemble of control variables is generated from Eq. 2.3. Then each ensemble member is used as inputs to the reservoir simulator where the objective function values (NPVs) are obtained such that the gradient can be approximated. This approximated gradient is then used in the steepest ascent method for optimization. The detailed description is provided in the following paragraph.
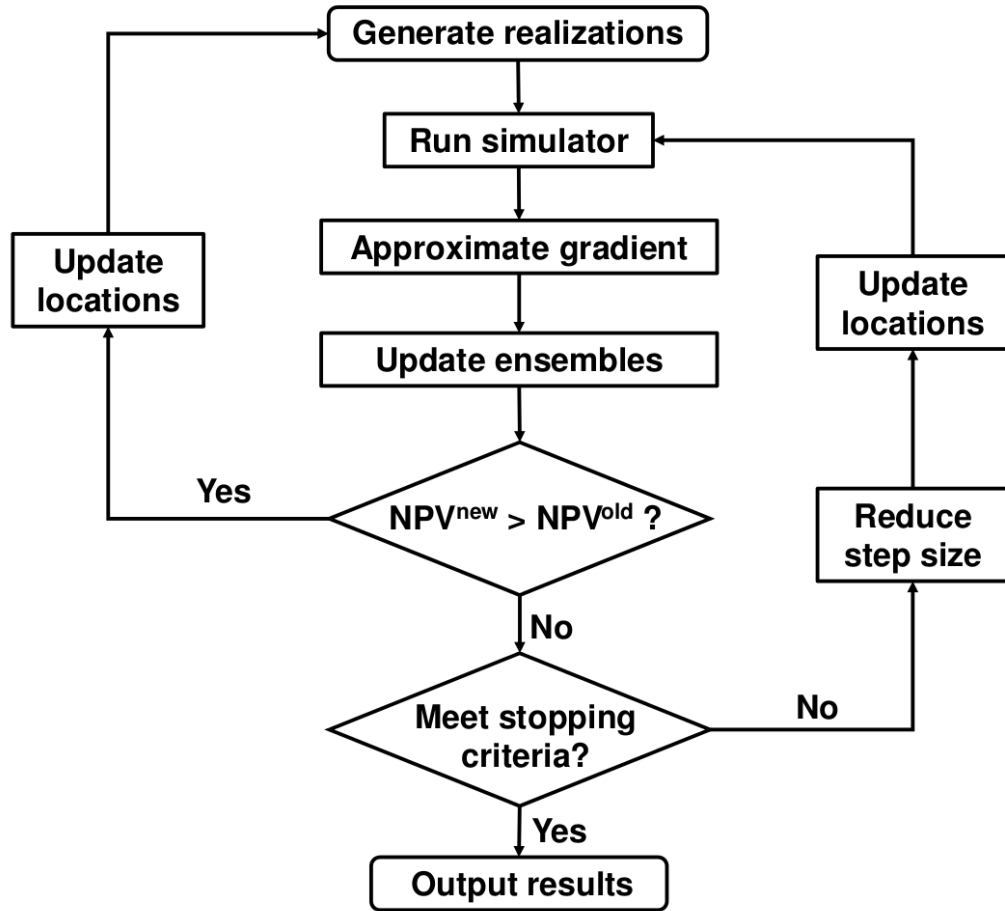
Figure 2.3: Flowchart of ensemble-based optimization method

For mathematical expression of the EnOpt method, I first define the following objective function where it is augmented by a penalty term (the right-hand side of

29

the equation) for the smoothness of variable changes.

$$f(\mathbf{x}) = J(\mathbf{x}) - \frac{\alpha}{2}(\mathbf{x} - \mathbf{x}_p)^T \mathbf{C_x}^{-1}(\mathbf{x} - \mathbf{x}_p), \tag{2.6}$$

where $J(\mathbf{x})$ denotes the NPV function given in Eq. 2.1; $\mathbf{x}$ is the vector of well locations; $\mathbf{x}_p$ is the well locations at the previous iteration and $\mathbf{C_x}$ is the covariance matrix of the well location variables. The α is the weighted factor of the NPV function $(J(\mathbf{x}))$ and the regularization term for variable smoothness. The α is simply a reciprocal of the step size in traditional steepest ascent optimization.

The Jacobian and Hessian matrix of the scalar valued function $f(\mathbf{x})$ with respect to the state vector $\mathbf{x}$ can be written as

$$\mathbf{D}(\mathbf{x}) = J'(\mathbf{x}) - \alpha \mathbf{C_x}^{-1}(\mathbf{x} - \mathbf{x}_p), \tag{2.7}$$

$$\mathbf{H}(\mathbf{x}) = J''(\mathbf{x}) - \alpha \mathbf{C_x}^{-1}. \tag{2.8}$$

Using the second-order Taylor's expansion, the objective function around $\mathbf{x}$ can be approximated as

$$f(\mathbf{x} + \Delta\mathbf{x}) = f(\mathbf{x}) + \mathbf{D}^T(\mathbf{x})\Delta\mathbf{x} + \frac{1}{2}\Delta\mathbf{x}^T\mathbf{H}(\mathbf{x})\Delta\mathbf{x}. \tag{2.9}$$

Based on the Newton-Raphson method, a suitable step size $\Delta\mathbf{x}$ is determined that maximizes the second order Taylor's expansion.

$$\frac{\partial f(\mathbf{x} + \Delta\mathbf{x})}{\partial \Delta\mathbf{x}} = \mathbf{D}(\mathbf{x}) + \mathbf{H}(\mathbf{x})\Delta\mathbf{x} = 0. \tag{2.10}$$

Substitute $D(\mathbf{x})$ from Eq. 2.7 and $H(\mathbf{x})$ from Eq. 2.8 into Eq. 2.10, yields

$$\Delta\mathbf{x} = \mathbf{x}_p - \mathbf{x} + \frac{J'(\mathbf{x})}{\alpha \mathbf{C_x}^{-1}}. \tag{2.11}$$

Because of the non-linearity of the equation, the iterative approach can be used to

solve Eq. 2.11 as given in the following.

$$
\begin{aligned}
\Delta \mathbf{x}^k &= \mathbf{x}_p - \mathbf{x}^k + \frac{J_k'(\mathbf{x})}{\alpha_k \mathbf{C_x}^{-1}} \\
&= \mathbf{x}^k - \mathbf{x}^k + \frac{J_k'(\mathbf{x})}{\alpha_k \mathbf{C_x}^{-1}} \\
&= \frac{J_k'(\mathbf{x})}{\alpha_k \mathbf{C_x}^{-1}} \\
&= \frac{1}{\alpha_k} \mathbf{C_x}^k J_k'(\mathbf{x}).
\end{aligned}
\tag{2.12}
$$

where k is the iteration index. Then the updated ensemble is given as

$$
\begin{aligned}
\mathbf{x}^{k+1} &= \mathbf{x}^k + \Delta \mathbf{x}^k \\
&= \mathbf{x}^k + \frac{1}{\alpha_k} \mathbf{C_x}^k J_k'(\mathbf{x}).
\end{aligned}
\tag{2.13}
$$

In the vicinity of x_k, given that the relationship between $\mathbf{x}$ and $J(\mathbf{x})$ is linear, the gradient can be approximated as

$$
J_k'(\mathbf{x}) = \frac{\mathbf{C}_{\mathbf{x}, J(\mathbf{x})}^k}{\mathbf{C_x}^k},
\tag{2.14}
$$

so the update scheme of the vector $\mathbf{x}$ becomes

$$
\mathbf{x}^{k+1} = \mathbf{x}^k + \frac{1}{\alpha_k} \mathbf{C}_{\mathbf{x}, J(\mathbf{x})}^k.
\tag{2.15}
$$

The cross covariance $C_{\mathbf{x}, J(\mathbf{x})}^k$ is the approximated gradient from the ensemble method, and the parameter α_k controls the step size. This equation is the same form as the update function for the traditional steepest ascent method. The value of α_k is generally subjective; I use the standard deviation of the objective function values obtained from the ensemble.

To improve the search direction, a pre-conditioning term $C_\mathbf{x}$ can be used to correct the abrupt changes for the state vector, and mitigate ill-posed conditions (Tarantola, 2005). The preconditioning is a procedure to condition the updated variables with prior knowledge or to exploit the physical knowledge of real engineering problem for

31

a better(faster) search direction. The precondition term $C_\mathbf{x}$ has been successfully applied in the EnOpt method (e.g. Chen and Oliver (2009), Nwaozo (2006), Petvipusit (2011)). In this work, I use the same pre-conditioning $C_\mathbf{x}$ for the EnOpt method as shown below

$$\mathbf{x}^{k+1} = \mathbf{x}^k + \frac{1}{\alpha_k}\mathbf{C}_\mathbf{x}^k\mathbf{C}_{\mathbf{x},J(\mathbf{x})}^k. \tag{2.16}$$

The EnOpt method is demonstrated in Figure 2.4 where the black dots denotes the well location from each ensemble member while the blue circle represents the mean of the ensemble. The algorithm is started from random starting points by generating the ensemble $\mathbf{x}^k$ (black dots), then the objective function is evaluated through the reservoir simulator. The gradient $\mathbf{g}^k$ is then approximated and used to update the variable for the next iteration. The variance of the ensemble decreases with the iterations in this figure. The algorithm stops when the stopping criteria are satisfied. The hollowed blue arrow represents multiple iterations before reaching the optimal point ($\mathbf{x}^*$).

2.3.2 Fixed-Gain SPSA Algorithm (FSP)

The Fixed-Gain SPSA Algorithm (FSP) is an adaptive SPSA algorithm. I will introduce SPSA, integer SPSA and FSP in the following.

Simultaneous Perturbation Stochastic Approximation (SPSA) is a stochastic type of algorithm (Kiefer and Wolfowitz, 1952) where it was originally proposed for optimization problems when the objective function is differentiable, and the variables of interest are real numbers. For well placement optimization problem, since the well location coordinates are integer numbers, I modify the algorithm for discrete variables from which the updated well locations are truncated to the center of the grid blocks. This section introduces the SPSA approach for solving problems with continuous variables and integer variables, and later I will also discuss the relationship between the estimated gradient and the true gradient method.
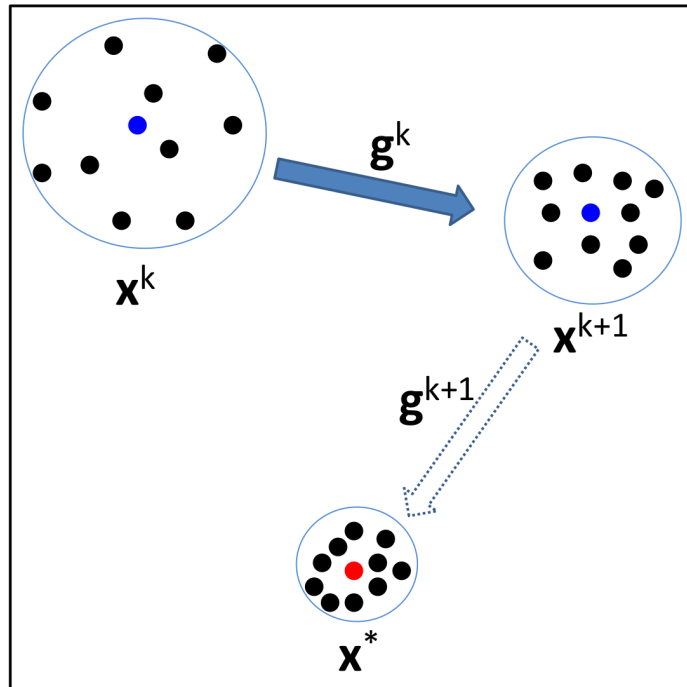
Figure 2.4: A demonstration of the searching routine in EnOpt algorithm. The blue dots represent the ensemble mean and the black dots represent the random points generated from the ensemble mean. The red dot represents the optimal solution.

I first describe the original algorithm of the SPSA approach, followed by its modified version used in this dissertation. Let $\mathbf{x} \in \mathbb{R}^p$ be the vector of well locations, where $p = 2N_w$. The algorithm of SPSA is given as follows:

1. Parameter initialization $(\alpha, \gamma, a, c, A, k_{max})$. The parameters α, γ and A are used to control the step size a_k and the perturbation size c_k for each iteration. While the term k_{max} is the user defined maximum number of iterations for the algorithm.

$$a_k = \frac{a}{(k + A)^\alpha}, \tag{2.17}$$

$$c_k = \frac{c}{k^\gamma}. \tag{2.18}$$

2. Generating perturbation vector $\mathbf{\Delta}_k$. The vector $\mathbf{\Delta}_k$ is a p-dimensional random vector generated by Monte Carlo methods from a zero-mean probability distribution. Sadegh and Spall (1998) showed that the optimal distribution for $\mathbf{\Delta}_k$ is the Bernoulli distribution. For the application of this work, this perturbation vector is used to compute the gradient of NPV from well locations.

3. Evaluating the NPV function from $\mathbf{x}_k \pm c_k\mathbf{\Delta}_k$ where $\mathbf{x}_k$ is the current well location. The objective function evaluations can be expressed as $J(\mathbf{x}_k^+)$ and $J(\mathbf{x}_k^-)$ for

$$\mathbf{x}_k^+ = \mathbf{x}_k + c_k\mathbf{\Delta}_k, \tag{2.19}$$

$$\mathbf{x}_k^- = \mathbf{x}_k - c_k\mathbf{\Delta}_k. \tag{2.20}$$

4. Gradient approximation. The approximated gradient at position $\mathbf{x}_k$ can be

expressed as

$$\mathbf{g}(\mathbf{x}_k) = \frac{J(\mathbf{x}_k + c_k\boldsymbol{\Delta}_k) - J(\mathbf{x}_k - c_k\boldsymbol{\Delta}_k)}{2c_k} \begin{bmatrix} \Delta_{k1}^{-1} \\ \Delta_{k2}^{-1} \\ \vdots \\ \Delta_{kp}^{-1} \end{bmatrix}. \tag{2.21}$$

5. Updating well locations.

$$\mathbf{x}_{k+1} = \mathbf{x}_k + a_k\mathbf{g}(\mathbf{x}_k). \tag{2.22}$$

6. Determine iteration or termination. The stopping criteria for the algorithm are: the maximum number of iterations, or the value of objective function with the predefined threshold $\varepsilon_J = 10^{-4}$.

$$0 \leq J(\mathbf{x}_k) - J(\mathbf{x}_{k-1}) < \varepsilon_J \tag{2.23}$$

It should be noted that when the stopping criteria in Eq. 2.23 is satisfied for the first time, I regenerate the searching direction instead of stopping the algorithm immediately. This is to avoid being trapped at a local optimum.

For the relation of the estimated gradient by the SPSA method and the true gradient, Spall (2003) showed that the estimated gradient on average approaches the true value of the gradient for repeated experiments. Later, Gao et al. (2007) provided a detailed proof of the equality relationship between true gradient and estimated gradient with application to production optimization. Here, I briefly review this method with the variables defined for the well placement problem.

Given that $\mathbf{x} \in \mathbb{R}^p, J : \mathbb{R}^p \to \mathbb{R}$, the Taylor's series expansion is

$$J(\mathbf{x}_k + c_k\boldsymbol{\Delta}_k) = J(\mathbf{x}_k) + c_k\boldsymbol{\Delta}_k^T\nabla J(\mathbf{x}_k) + \frac{1}{2}c_k^2\boldsymbol{\Delta}_k^T\nabla J(\mathbf{x}_k)\boldsymbol{\Delta}_k + O(c_k^3\|\boldsymbol{\Delta}_k\|^3), \tag{2.24}$$

$$J(\mathbf{x}_k - c_k\boldsymbol{\Delta}_k) = J(\mathbf{x}_k) - c_k\boldsymbol{\Delta}_k^T\nabla J(\mathbf{x}_k) + \frac{1}{2}c_k^2\boldsymbol{\Delta}_k^T\nabla J(\mathbf{x}_k)\boldsymbol{\Delta}_k - O(c_k^3\|\boldsymbol{\Delta}_k\|^3). \tag{2.25}$$

Therefore,

$$\frac{J(\mathbf{x}_k + c_k\boldsymbol{\Delta}_k) - J(\mathbf{x}_k - c_k\boldsymbol{\Delta}_k)}{2c_k} = \boldsymbol{\Delta}_k^T \nabla J(\mathbf{x}_k), \qquad (2.26)$$

and the estimated gradient of SPSA can be expressed as,

$$\begin{aligned}
\mathbf{g}_k(\mathbf{x}_k) &= \frac{J(\mathbf{x}_k + c_k\boldsymbol{\Delta}_k) - J(\mathbf{x}_k - c_k\boldsymbol{\Delta}_k)}{2c_k}
\begin{bmatrix}
\Delta_{k1}^{-1} \\
\Delta_{k2}^{-1} \\
\vdots \\
\Delta_{kp}^{-1}
\end{bmatrix} \\
&= \frac{J(\mathbf{x}_k + c_k\boldsymbol{\Delta}_k) - J(\mathbf{x}_k - c_k\boldsymbol{\Delta}_k)}{2c_k} \boldsymbol{\Delta}_k^{-1} \\
&= \boldsymbol{\Delta}_k^{-1} \boldsymbol{\Delta}_k^T \nabla J(\mathbf{x}_k).
\end{aligned}$$

Then,

$$E[\mathbf{g}_k(\mathbf{x}_k)] = E[\boldsymbol{\Delta}_k^{-1}\boldsymbol{\Delta}_k^T]\nabla J(\mathbf{x}_k), \qquad (2.27)$$

and the expectation of the estimated gradient is

$$E[\mathbf{g}_k(\mathbf{x}_k)] = E[\boldsymbol{\Delta}_k^{-1}\boldsymbol{\Delta}_k^T]\nabla J(\mathbf{x}_k). \qquad (2.28)$$

Since the expectation of $\boldsymbol{\Delta}_k^{-1}\boldsymbol{\Delta}_k^T$ can be written as

$$E[\boldsymbol{\Delta}_k^{-1}\boldsymbol{\Delta}_k^T] =
\begin{bmatrix}
1 & \frac{\Delta_{k2}}{\Delta_{k1}} & \cdots & \frac{\Delta_{kp}}{\Delta_{k1}} \\
\frac{\Delta_{k1}}{\Delta_{k2}} & 1 & \cdots & \frac{\Delta_{kp}}{\Delta_{k2}} \\
\vdots & \vdots & \ddots & \vdots \\
\frac{\Delta_{k1}}{\Delta_{kp}} & \frac{\Delta_{k2}}{\Delta_{kp}} & \cdots & 1
\end{bmatrix}, \qquad (2.29)$$

where,

$$\boldsymbol{\Delta}_k^{-1} = \left[\frac{1}{\Delta_{k1}}, \frac{1}{\Delta_{k2}}, \cdots, \frac{1}{\Delta_{kp}}\right]^T, \qquad (2.30)$$

$$\boldsymbol{\Delta}_k^T = [\Delta_{k1}, \Delta_{k2}, \cdots, \Delta_{kp}], \qquad (2.31)$$

and $\boldsymbol{\Delta}_k$ is symmetric distribution, so we have

$$E[\Delta_{ki}] = 0, i = 1, 2, \cdots, p. \tag{2.32}$$

$$E\left[\frac{1}{\Delta_{kj}}\right] = 0, j = 1, 2, \cdots, p. \tag{2.33}$$

From the Bernoulli distribution, it is known that $\mathbf{\Delta}_k^{-1}$ and $\mathbf{\Delta}_k^T$ are independent, so I can get

$$E\left[\frac{\Delta_{ki}}{\Delta_{kj}}\right] = E[\Delta_{ki}]E\left[\frac{1}{\Delta_{kj}}\right] = \begin{cases} 1, & i = j \\ 0, & i \neq j \end{cases} \tag{2.34}$$

$$\Rightarrow E[\mathbf{\Delta}_k^{-1}\mathbf{\Delta}_k^T] = I \tag{2.35}$$

$$\Rightarrow E[\mathbf{g}_k(\mathbf{x}_k)] = \nabla J(\mathbf{x}_k). \tag{2.36}$$

2.3.2.2 Integer SPSA Algorithm

Spall (1992, 2003) introduce the assumptions for the strong convergence of $\mathbf{x}_k$. The smoothness of objective function $J(\mathbf{x})$ should be three-times continuously differentiable and bounded on $\mathbb{R}^p$. Later, Bangerth et al. (2006) show that a variant of SPSA (integer SPSA) can be used to solve the well placement problem. The integer SPSA algorithm is as follows:

1. Parameter initialization $(\alpha, \gamma, a_0, c_0, A, k_{max})$. Set $k = 1$. $\alpha = 0.602, \gamma = 0.101$. The values for α and γ are taken from the guideline in Spall (1998a).

2. Generate perturbation vector $\mathbf{\Delta}_k$ from the Bernoulli distribution. $\mathbf{\Delta}_k$ is the random direction generated to perturb the current well locations for the gradient approximation using finite central difference method.

3. Compute the parameters c_k and a_k for the step size computation.

$$a_k = \frac{a}{(k+A)^\alpha}, \tag{2.37}$$

$$c_k = \left\lceil \frac{c}{k^\gamma} \right\rceil. \tag{2.38}$$

4. Objective function evaluations $J(\mathbf{x}_k^+)$ and $J(\mathbf{x}_k^-)$, where

$$J^+ = J(\Pi(\mathbf{x}_k + c_k\boldsymbol{\Delta}_k)), \qquad (2.39)$$

$$J^- = J(\Pi(\mathbf{x}_k - c_k\boldsymbol{\Delta}_k)). \qquad (2.40)$$

5. Gradient approximation.

$$\mathbf{g}(\mathbf{x}_k) = \frac{J^+ - J^-}{2c_k}\boldsymbol{\Delta}_k^{-1}. \qquad (2.41)$$

6. Updating the well locations.

$$\mathbf{x}_{k+1} = \Pi(\mathbf{x}_k + \lceil a_k\mathbf{g}(\mathbf{x}_k)\rceil). \qquad (2.42)$$

7. Set $k = k+1$, and check the stopping criteria. If the stopping criteria is satisfied, stop; Otherwise, go to step 2.

The operator $\lceil\cdot\rceil$ is to round a real number to the closest integer number, and the operator Π is used to map the updated variables that are outside the bounds back to the domain, while keeping the interior points unchanged. The stopping criteria for the algorithm are the maximum number of iterations and the change in the objective function values during the last 6 iterations.

2.3.2.3 Fixed-Gain SPSA Algorithm

The fixed gain SPSA (FSP) algorithm is a simpler form of the integer SPSA algorithm. The step size a_k and perturbation size c_k are set as a constant equal to 1, and the gain u is added as a new parameter and its value is set as a constant. The value of u depends on problems. In our heterogeneous reservoir case, I set $u = 1$. The algorithm can be stated as follows:

1. Set $k = 1$.

2. Generate perturbation vector $\boldsymbol{\Delta}_k$ from the Bernoulli distribution.

3. Evaluate objective functions $J(\mathbf{x}_k^+)$ and $J(\mathbf{x}_k^-)$, where

$$J^+ = J(\Pi(\mathbf{x}_k + \boldsymbol{\Delta}_k)), \qquad (2.43)$$

$$J^- = J(\Pi(\mathbf{x}_k - \boldsymbol{\Delta}_k)). \qquad (2.44)$$

4. Approximate gradient.

$$\mathbf{g}(\mathbf{x}_k) = \frac{J^+ - J^-}{2}\boldsymbol{\Delta}_k^{-1}. \qquad (2.45)$$

5. Update well locations.

$$\mathbf{x}_{k+1} = \Pi(\mathbf{x}_k + u\frac{\mathbf{g}(\mathbf{x}_k)}{\|\mathbf{g}(\mathbf{x}_k)\|}). \qquad (2.46)$$

where the operator $\|\cdot\|$ is the Euclidean norm of the gradient in order to get a unit gradient vector.

6. Set $k = k + 1$, and check the stopping criteria. If the stopping criteria are satisfied, stop; Otherwise, go to step 2.

The stopping criteria for the algorithm are the maximum number of iterations and the change in the objective function values during the last few iterations. In this problem, I use 30 as the maximum number of iterations, and the algorithm is terminated if the objective function values are not improved during the last 6 iterations.

The searching sequence of the FSP algorithm is demonstrated in Figure 2.5 where the blue dot represents the initial starting point and the blue dots with black edges represent the solutions used for the gradient approximation. The black dot is the updated solution based on the FSP algorithm. The dotted line represents multiple iterations of the algorithm before reaching the optimum at $\mathbf{x}^*$.

2.4 Application on Single Well Placement

The mathematical formulation of the stochastic search algorithms EnOpt and SPSA are described in the previous section. In this section, the application of these two
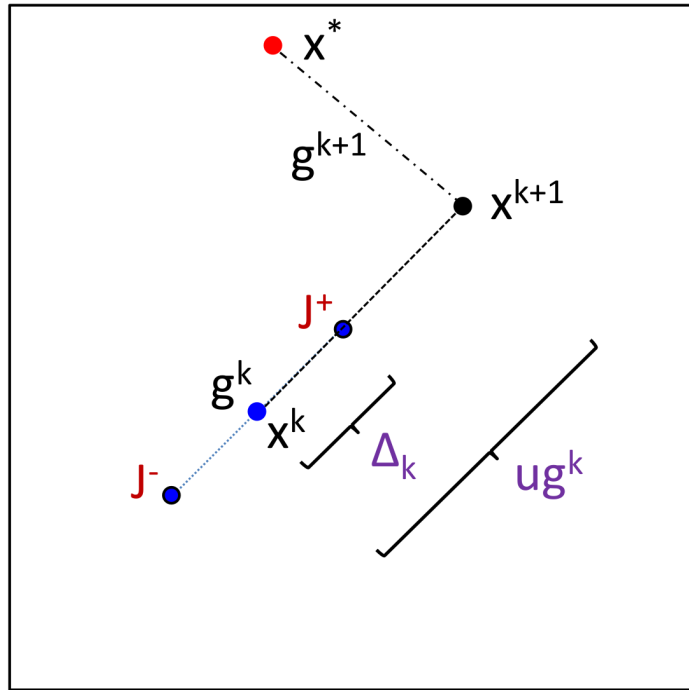
Figure 2.5: A demonstration of the searching routine in the FSP algorithm. The blue dot represents the initial starting point and the blue dots with black edges represent the solutions used for the gradient approximation. The black dot is the updated solution based on the FSP algorithm. The dotted line represents multiple iterations of the algorithm before reaching the optimum at $\mathbf{x}^*$.

algorithms are demonstrated on synthetic case studies. In Section 2.4.1, a 2-D homogeneous case is used to investigate the effect of various factors on the performance of the algorithms, and in Section 2.4.2, two heterogeneous reservoir models are used to compare the performance of these two methods. First, the following assumptions are made for the case studies.

1. The geology of the reservoir is presumably known. The geological uncertainty is therefore not considered.

2. Well controls are predefined at certain limits such as fluid target rate or bottom hole pressure (BHP). For the well placement problem, we constrain the wells to operate at a fixed BHP.

3. All wells are perforated through all layers of the reservoir.

4. Operation, maintenance, drilling costs, water injection and separation costs, and the prices for oil and gas are constant and are assumed to be independent of well locations and time.

Note that geological uncertainty and well perforation are taken into consideration in Chapter 4.

2.4.1 Illustrative Example for EnOpt and SPSA

In this section, both EnOpt and SPSA are applied to an illustrative example to test the factors that are significant to the performance of the algorithms. The illustrative example is a 2-D homogeneous reservoir model with an optimal solution known *a priori*. Therefore, I can test the distance between the solutions obtained from EnOpt, SPSA and the real optimal solution.

The illustrative example is a two-dimensional homogeneous reservoir model. The size of this reservoir is 2400 ft $\times$ 2400 ft $\times$ 30 ft where it was discretized to a 24 $\times$ 24

grid lattice, with each grid block dimension as 100 ft × 100 ft × 30 ft. The thickness of the reservoir is 30 ft. The reservoir properties are summarized in Table 2.1. The optimization algorithms are applied to seek for an optimal well location of a single vertical producer. The constant parameters used in this study are shown in Table 2.2. The 3-D surface and the contour plot of NPV are obtained from an exhaustive search, where I reposition 1 producer in each of the grid blocks of the reservoir model, run the simulator to get the liquid production and calculate the NPV thereafter. The exhaustive search shows the global optimal solution for the well location is at the center of the reservoir, as is shown in Figure 2.6.

Table 2.1: Homogeneous reservoir properties

Description	Properties
Number of grid blocks	24 × 24 × 1
Number of layers	1
Grid Block size	100 ft × 100 ft × 30 ft
Reservoir thickness	30 ft
Reservoir top depth	9000 ft
Water oil contact	9035 ft
Porosity	0.30
Permeability	30 mD
Initial reservoir pressure	3600 psia
Production time	5 years
BHP	500 psia

Table 2.2: Constant parameters for NPV calculation

Oil price, USD/bbl	80.0
Water disposal cost, USD/bbl	5.0
Water injection cost, USD/bbl	8.0
Drilling cost, USD/well	2,000,000
Discount rate	0.1

In this section, different parameters used in EnOpt algorithm are evaluated on the homogeneous reservoir model described previously. These parameters are starting points, ensemble size, ensemble generation, and the variance of ensemble. The reasons for the selection of these factors are provided in the following.
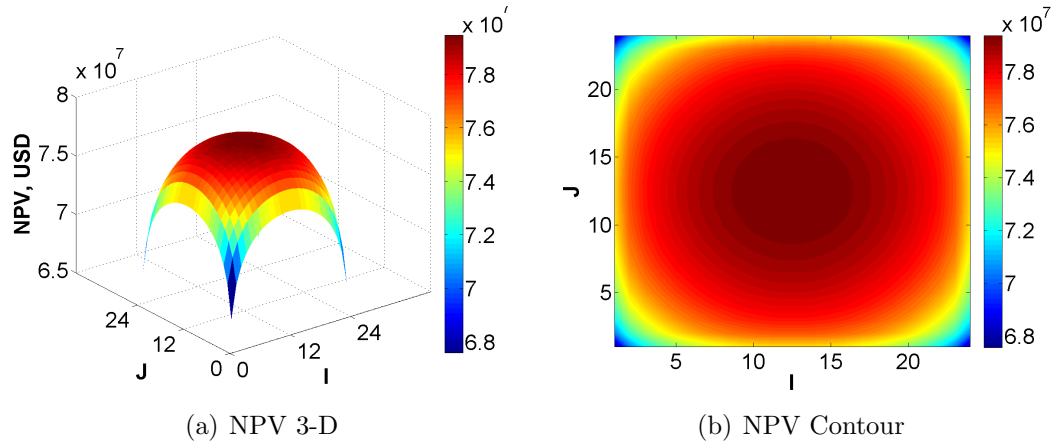
Figure 2.6: NPV 3-D and contour plot for homogeneous reservoir model (unit: USD). The maximum NPV appears to be at the center of the reservoir.

1. Starting Points: the effect of starting points is an important factor that can impact the performance of the gradient-based algorithms. Because EnOpt is also based on a approximate-gradient-based algorithm, it can sometimes obtain a local optimum. This work therefore focuses on the performance of this algorithm from different starting points. By using multiple starting points, we can increase the possibility of achieving the global optimum.

2. Ensemble size: an ensemble size can impact the accuracy of the sensitivity (gradient) estimation between the objective function and the variables. Large ensemble size tends to allow the algorithm to achieve a more accurate gradient estimation, but large ensemble size also requires many function evaluations (simulation runs) and consequently requires longer computation time. Therefore, the appropriate ensemble size is critical to the performance of the algorithm.

3. Randomness in the ensemble generation: new ensemble members generated from a normal distribution for each iteration can be different. Thus, different experiments will get different ensembles even though the same mean value is used. From our observation, this can affect the random search direction and

43

the performance of the algorithm.

4. The variance of the ensemble: the variance is an indicator to determine the variation of the ensemble measured from its mean value. Therefore, the greater value of the variance allows the algorithm to search in a larger area. However, the variance should be reduced when the solution gets closer to the optimum point. Because as the search gets closer to the optimum, the ensemble perturbed from a smaller variance can increase the accuracy of the gradient estimation. Otherwise, if the variance is too large, the approximate gradient tend to reduce to zero.

In each experiment, I test the algorithm using 5 different starting points. A group of experiments are conducted to test the algorithm performance when the values of the ensemble size are 2, 5, and 10 respectively, as shown in Figure 2.7. When the ensemble size is 2, it appears that the algorithm fails at some selected starting points, but the performance generally improves as the ensemble size increases. When the ensemble size is increased to 10, regardless the starting points, the optimal location can be reached as we see that the search path is comparatively shorter than the other experiments. The results imply that the performance of EnOpt is sensitive to the ensemble size as EnOpt approximates the gradient from the ensemble and this gradient tends to be more accurate as ensemble size increases.

For the impact from ensemble generation, each ensemble is generated independently from the normal distribution. Therefore, different tests can yield different results even though starting from the same starting point. These results are shown in Figure 2.8. For the test 1 of this experiment, there are two points which stop close to the boundary, while the second, test 2, generally shows satisfactory convergence. This result indicates that the performance of EnOpt depends on the choice of samples from which it may be necessary to conduct more experiments to obtain the true optimum.
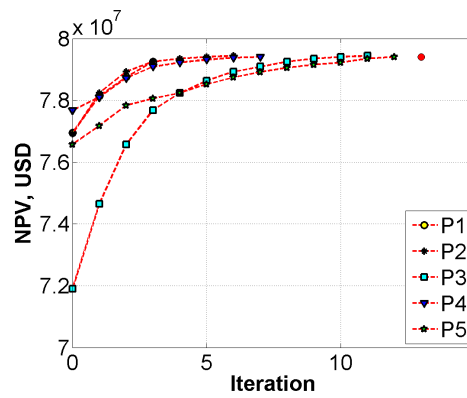
44
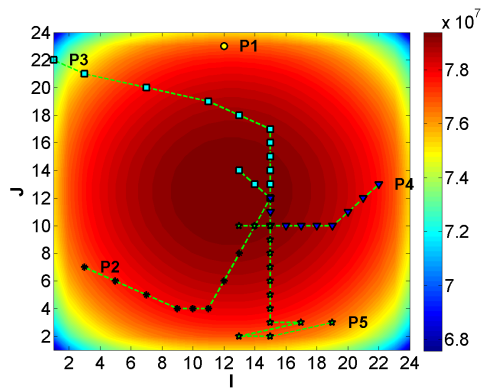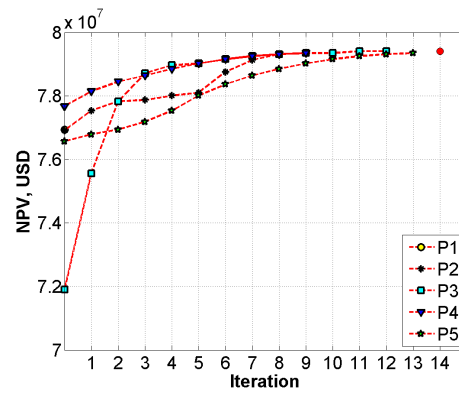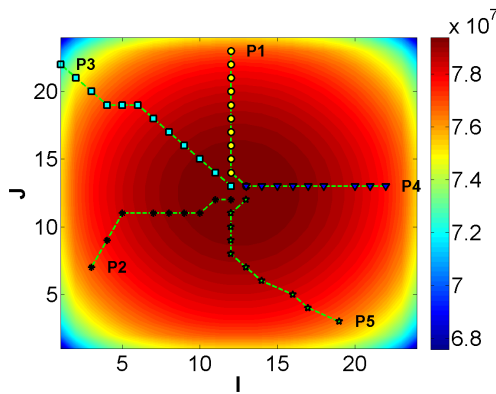
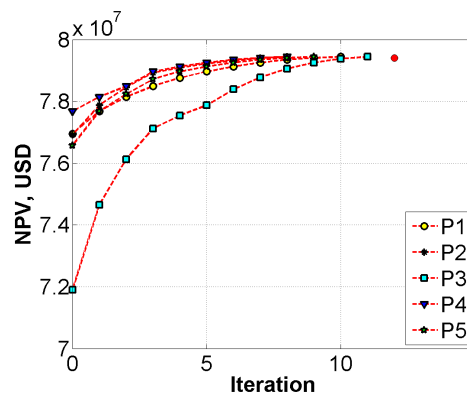(a) Location move ($Ne = 2$)   (b) NPV increase ($Ne = 2$)
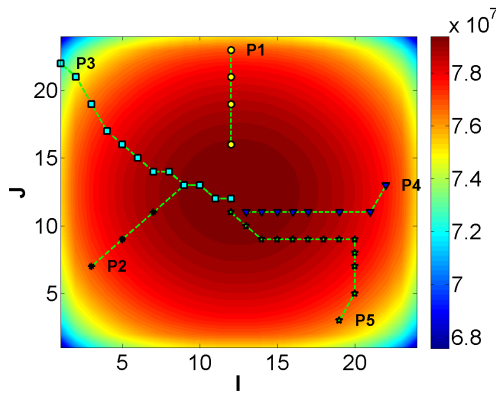
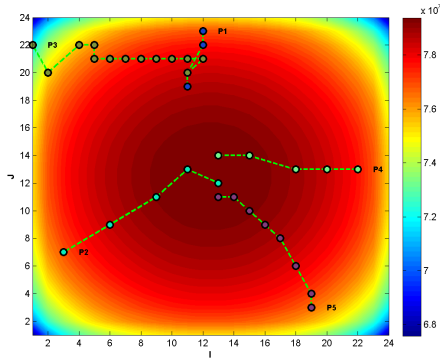(c) Location move ($Ne = 5$)   (d) NPV increase ($Ne = 5$)
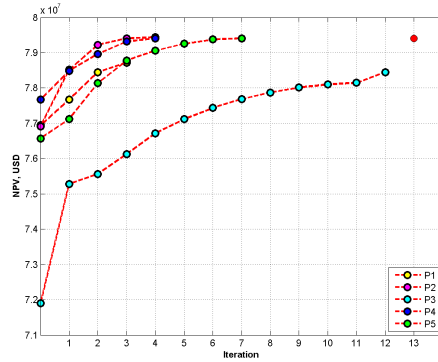
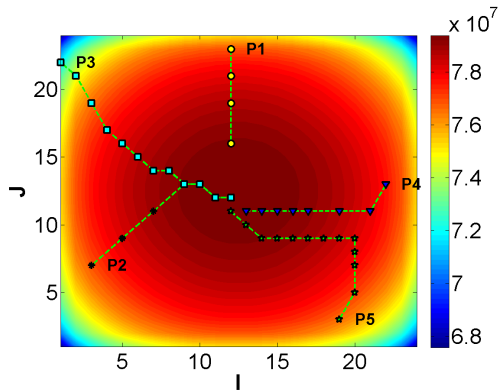(e) Location move ($Ne = 10$)   (f) NPV increase ($Ne = 10$)

Figure 2.7: Impact of ensemble size Ne on EnOpt method. The dots with different colors represent different search path. 'P' represents the starting points.
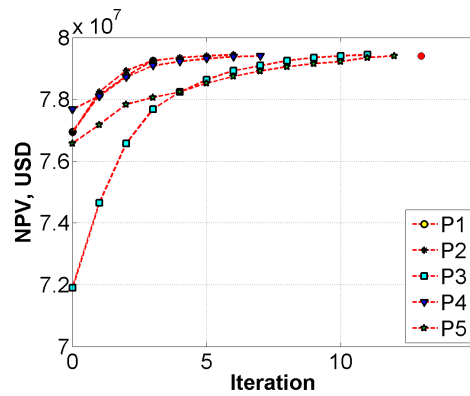
(a) Location move ($Ne = 5$, test 1)

(b) NPV increase ($Ne = 5$, test 1)

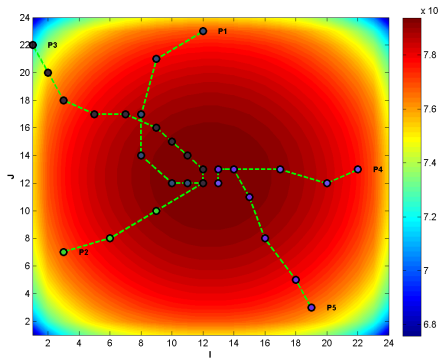(c) Location move ($Ne = 5$, test 2)

(d) NPV increase ($Ne = 5$, test 2)

Figure 2.8: Impact of perturbed realizations on well placement using EnOpt. The dots with different colors represent different search path. 'P' represents the starting points.

Figure 2.9 shows optimization results using different variance of the ensemble. In this study, I set the variance as a constant for the first three steps, and progressively decrease the ensemble variance for the subsequent steps. This is to study the impact of ensemble variance to the optimal results. As shown in Figure 2.9(a), if the variance is initially too large, the estimated search direction might be incorrect, which consequently reduces the convergence rate of the algorithm. Even though I can obtain the optimal solution in Figure 2.9(c), it requires many iterations as well as the computation time to obtain the optimal solution (Figure 2.9(d)). Thus, there is a trade-off between the variance value and the computation time. It is important to select a suitable variance based on the properties of the reservoir. In general, if the heterogeneity of the reservoir is large, a greater value of the ensemble variance may be used (and vice versa for the homogeneous reservoir).

However, for the factors relevant to the SPSA algorithm, I consider the starting points, the selection of gain sequence and the perturbation from the Bernoulli distribution. Because SPSA is also a gradient-based algorithm, the optimal solution may be dependent on the starting points. If we start from a point closer to the optimum, the algorithm can converge very fast; otherwise, the algorithm might get trapped at some local optima. Generally, multi-starting points can be used to impair the effect from poor starting points. The gain sequence is the step size to perturb the variables in each iteration. If the gain is too large, the algorithm will diverge. However, if the gain is too small, more iterations may be required to converge, leading to an intensive computation effort. The perturbation is the search direction from the current well location, and this search direction is sampled randomly from the Bernoulli distribution. Different tests generate different search directions, which can then impact the optimization results and the performance of the algorithm.
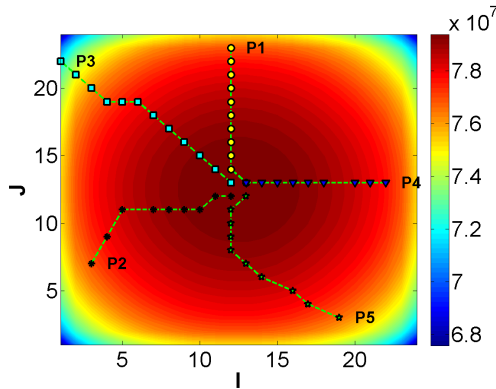
In this study, I compare the performance of SPSA using five different starting points. The performance of the SPSA algorithm is first evaluated with different gains
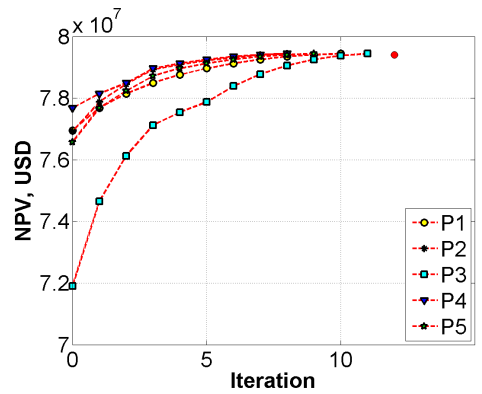
(a) Location move ($Ne = 10$, $\sigma = 4$ & 2)
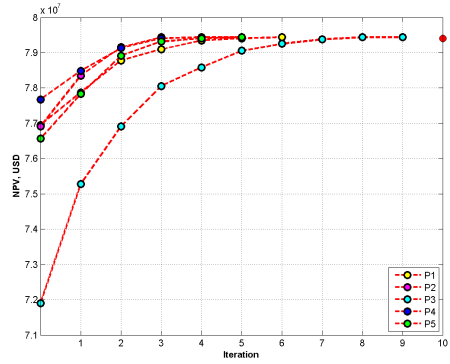
(b) NPV increase ($Ne = 10$, $\sigma = 4$ & 2)

(c) Location move ($Ne = 10$, $\sigma = 2$ & 1)
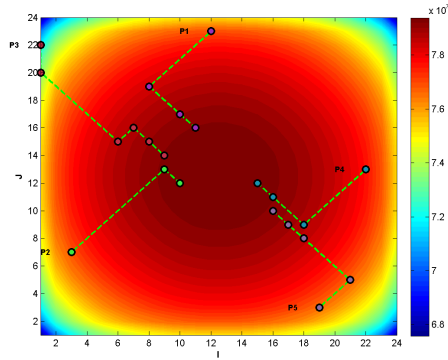
(d) NPV increase ($Ne = 10$, $\sigma = 2$ & 1)

Figure 2.9: Impact of ensemble perturbation variance on EnOpt method. The dots with different colors represent different search path. 'P' represents the starting points.

where the impact of the gain sequence on the optimal solution is shown in Figure 2.10.

In the SPSA algorithm, the step size (gain) decreases with the number of iterations in a manner that is suitable for the problem and the convergence conditions. In practical problems, the gain sequence is predefined based on several experiments. However, it is difficult to select the proper gain sequence for the well placement problem. As shown in Figure 2.10(a), if the step size is too small, the maximum number of iterations may be exceeded before the algorithm converges to the optimum. Therefore, a fixed gain SPSA (FSP) is proposed in this work. The performance of the algorithm for different gain sizes is evaluated using the gain size $u = 2$ in Figure 2.10(c), $u = 4$ in Figure 2.10(e), and $u = 1$ in Figure 2.11. The results shown here are based on the update of the well locations and the improvement of the NPV where we see that large gains tend to converge in a few steps. However, if the gain is much larger than the grid dimension, it can result in the dramatic update on well locations, which may not reach the global optimum. On the other hand, a small gain is more stable, although it requires more iterations to converge as it generally leads to a solution with a higher NPV than the one obtained from a large gain. Therefore, the selection of a suitable gain value is an important step for this optimization algorithm.

In general, the performance of SPSA depends on the step size and searching directions. On average, over repeated tests, SPSA can converge to the optimal value, but in the interest of practicality, SPSA may only be applied once or twice with several starting points. Figure 2.11 shows the impact from the searching direction generated from the Bernoulli distribution. For example, in test 1 (Figure 2.11(a)), from starting point 2, the solution can reach the optimum directly, but in test 2 (Figure 2.11(c)), because a different perturbation changes the search direction, it therefore requires more iterations to converge.
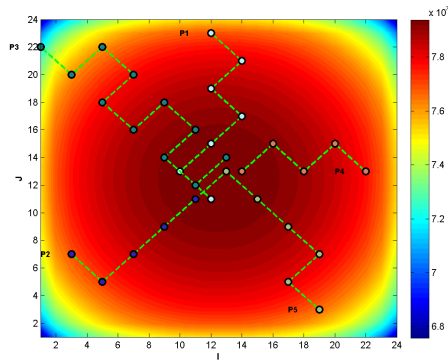
After analyzing the factors that impact both EnOpt and SPSA algorithms, these
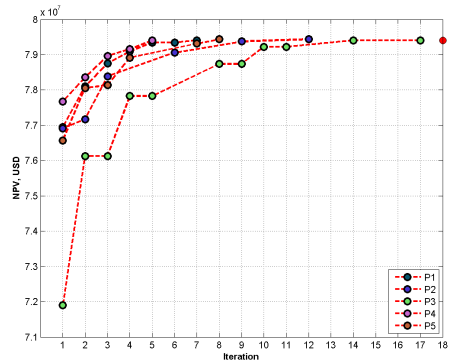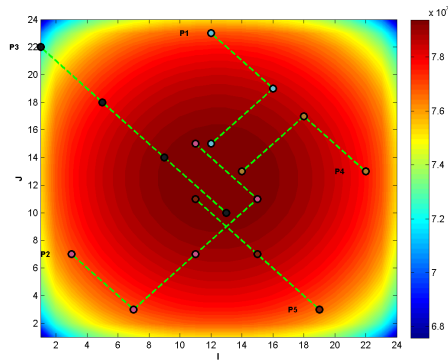
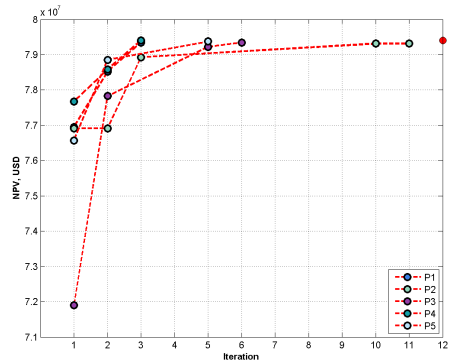(a) Location move (u decreasing)
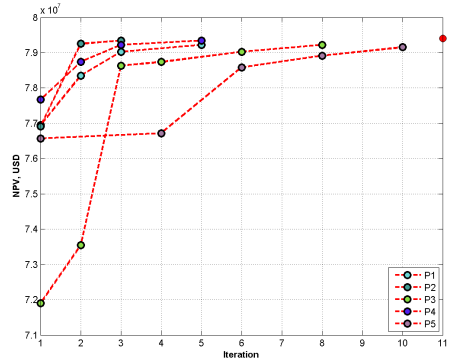
(b) NPV increase (u decreasing)

(c) Location move ($u = 2$)

(d) NPV increase ($u = 2$)

(e) Location move ($u = 4$)

(f) NPV increase ($u = 4$)

Figure 2.10: Impact of gain size u on SPSA algorithm. The dots with different colors represent different search path. 'P' represents the starting points.

(a) Location move ($u = 1$, test 1)

(b) NPV increase ($u = 1$, test 1)

(c) Location move ($u = 1$, test 2)
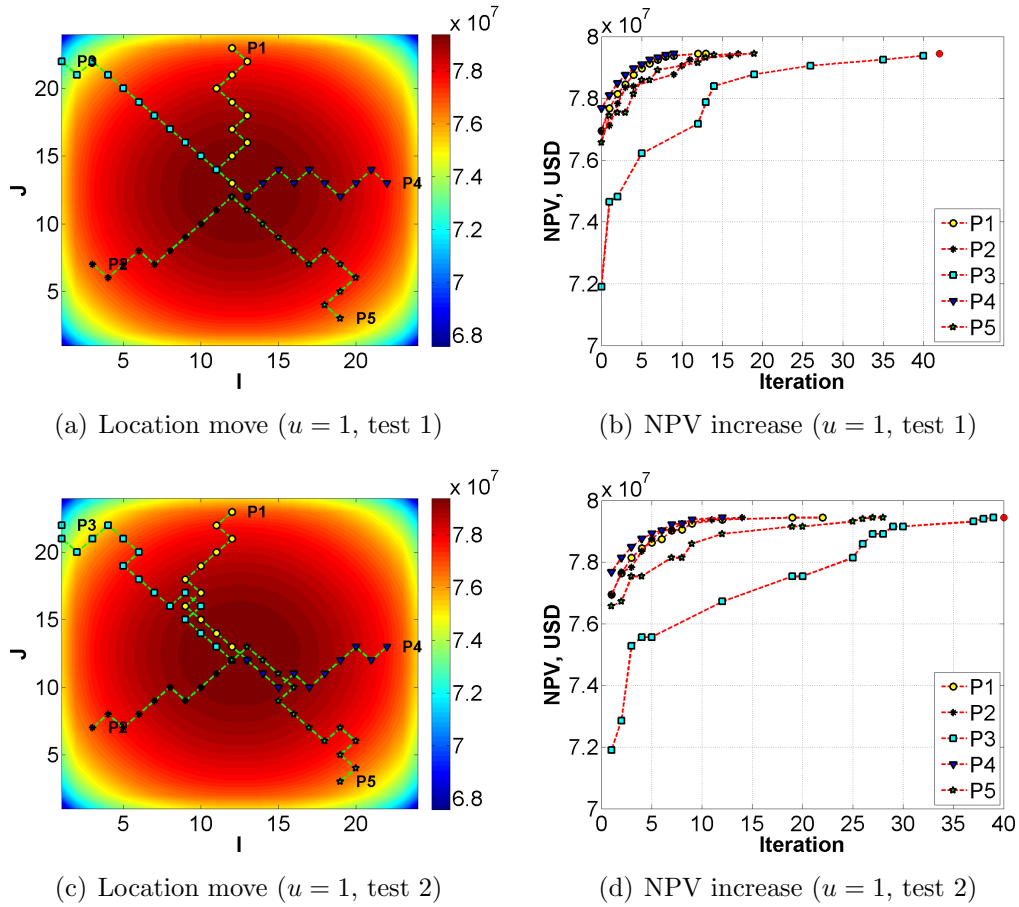
(d) NPV increase ($u = 1$, test 2)

Figure 2.11: Impact of the Bernoulli sampling on SPSA algorithm. The dots with different colors represent different search path. 'P' represents the starting points.

two methods are applied on a 2-D and a 3-D synthetic reservoir model. The description of the reservoir is provided at the beginning of each case study, followed by the results of the optimization algorithms.

2.4.2 Two-Dimensional Heterogeneous Reservoir Model

I use two-dimensional heterogeneous reservoir in this study with the size of 2400 ft $\times$ 2400 ft $\times$ 30 ft. The reservoir model was discretized on a 24×24 grid lattice. The size of each grid block is 100 ft $\times$ 100 ft $\times$ 30 ft. The thickness of the reservoir is 30 ft. The permeability is heterogeneous, as shown in Figure 2.12. The reservoir properties are summarized in Table 2.3. The optimization algorithms are applied to search for the optimal well location of a single vertical producer. The other reservoir parameters are shown in Table 2.2. An exhaustive search is also performed in order to determine the optimal well location and to assess the performance of each algorithm.

Table 2.3: 2-D heterogeneous reservoir properties

Description	Properties
Number of grid blocks	$24 \times 24 \times 1$
Number of layers	1
Grid Block size	100 ft $\times$ 100 ft $\times$ 30 ft
Reservoir thickness	30 ft
Reservoir top depth	9000 ft
Water oil contact	9035 ft
Porosity	0.30
Initial reservoir pressure	3600 psia
Production time	5 years
BHP	500 psia

As stated in Section 2.4.1, the performance of the EnOpt algorithm depends on the ensemble size and its variance. For this study, an ensemble size of 20 is selected, and two groups of variance values are chosen to generate the ensembles (Figure 2.14). I choose 5 different starting points in the experiments. In Figures 2.14(a) and 2.14(b), the variance chosen for EnOpt are 2 and 1, and in Figures 2.14(c) to 2.14(d), the variance values are 5 and 2. We see from these plots that the choice variance significantly
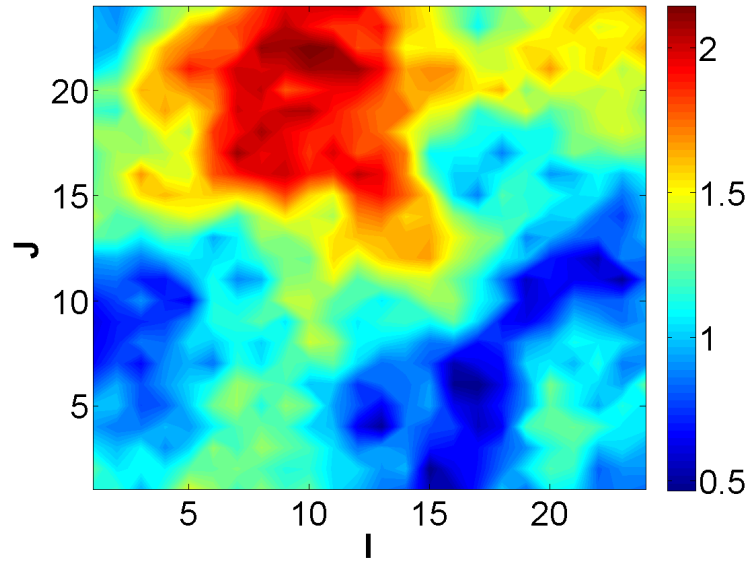
Figure 2.12: Logarithm permeability contour for 2-D heterogeneous reservoir model (unit: mD)

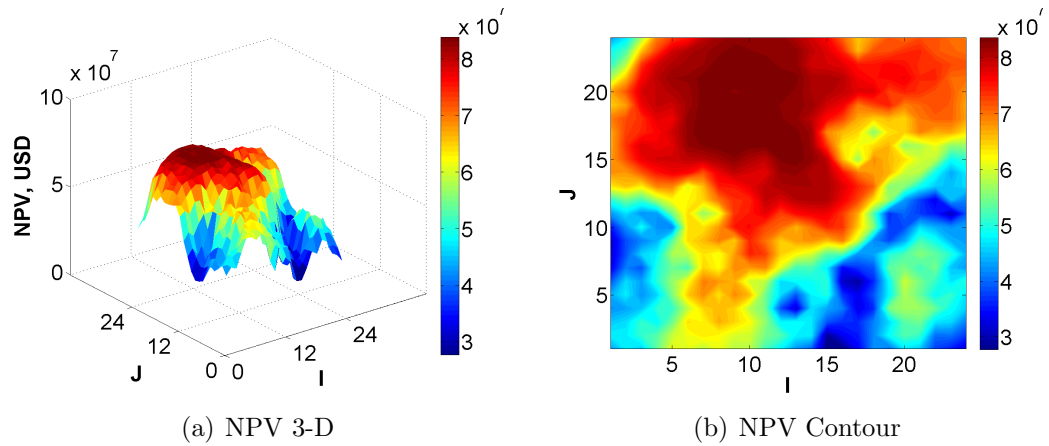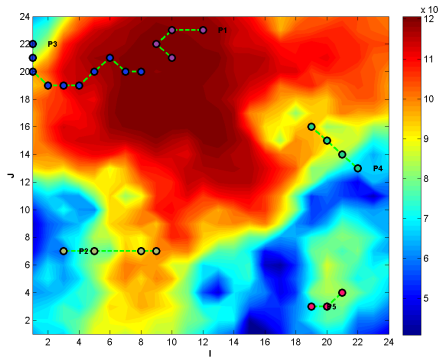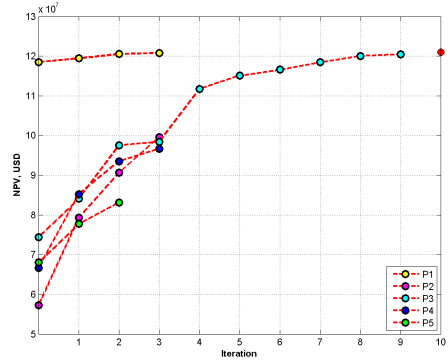

(a) NPV 3-D

(b) NPV Contour

Figure 2.13: NPV 3-D and NPV contour plot for 2-D heterogeneous reservoir model (unit: USD)
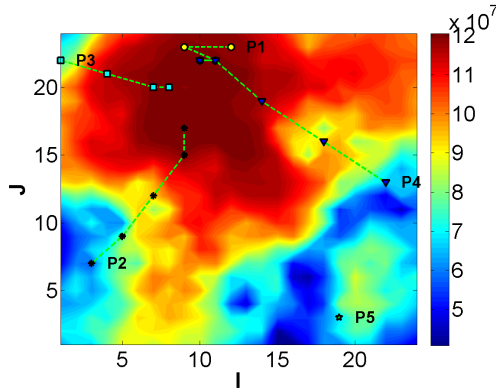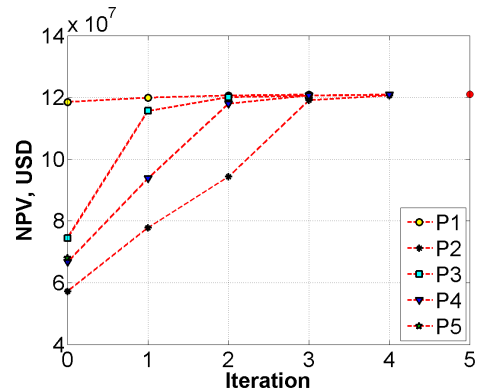
impacts the optimal solution.

(a) Location move ($\sigma = 2$ & 1)

(b) NPV increase ($\sigma = 2$ & 1)

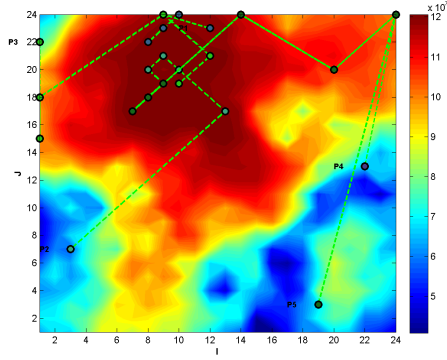(c) Location move ($\sigma = 5$ & 2)

(d) NPV increase ($\sigma = 5$ & 2)

Figure 2.14: Application of EnOpt on 2-D heterogeneous reservoir model

Figure 2.15 shows the results from the application of SPSA on the 2-D heterogeneous reservoir. We see that SPSA tends to converge to the global optimum in this example. Figure 2.15(a) shows the results obtained from all 5 starting points while Figures 2.15(c) and 2.15(l) show the same optimal result for different starting points.

2.4.3 Three-Dimensional Heterogeneous Reservoir Model

The size of three-dimensional heterogeneous reservoir is 2400 ft × 2400 ft × 90 ft. It has three production layers. This reservoir model is discretized on a 24 × 24 × 3 grid lattice. The size of each grid block is 100 ft × 100 ft × 30 ft. The thickness of the reservoir is 90 ft, with 10 ft of water occupying the bottom of the reservoir.

(a) Location move (Summary)
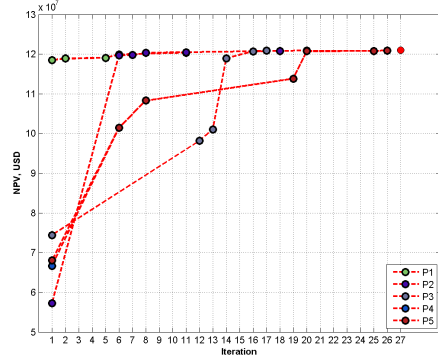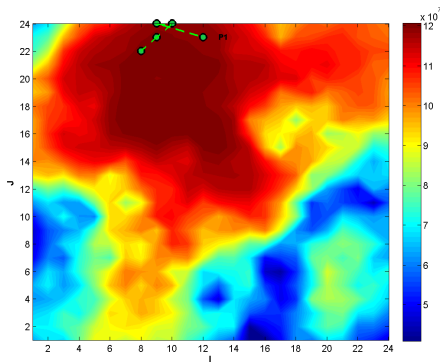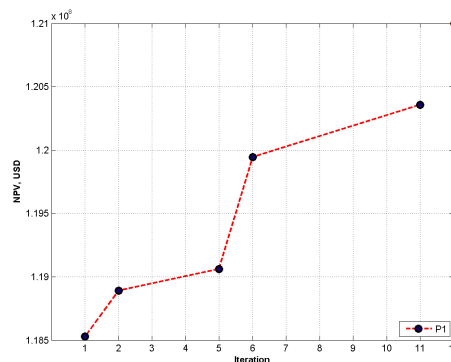
(b) NPV increase (Summary)

(c) Location move (Point 1)

(d) NPV increase (Point 1)

(e) Location move (Point 2)

(f) NPV increase (Point 2)

55

(g) Location move (Point 3)

(h) NPV increase (Point 3)
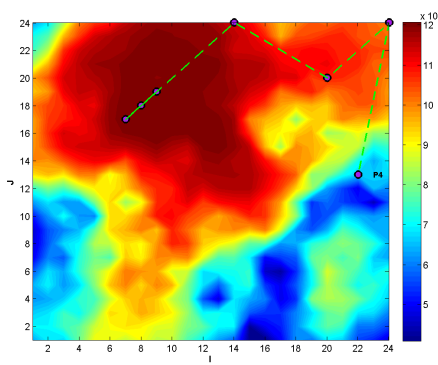
(i) Location move (Point 4)
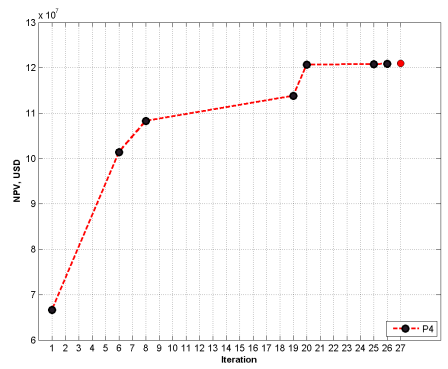
(j) NPV increase (Point 4)
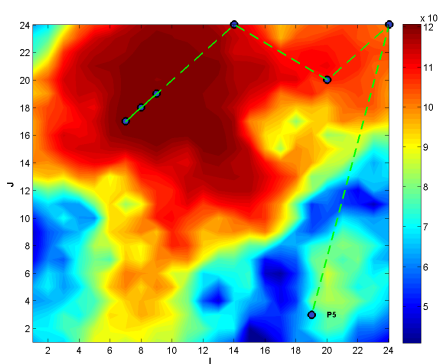
(k) Location move (Point 5)
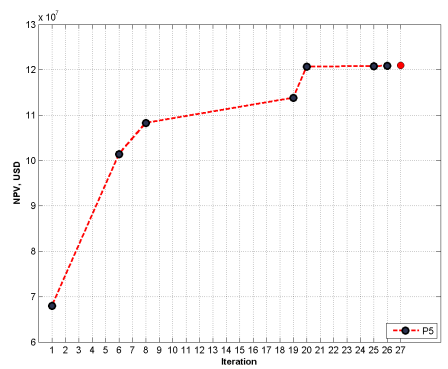
(l) NPV increase (Point 5)

Figure 2.15: Application of SPSA on 2-D heterogeneous reservoir model

The permeability is heterogeneous, as shown in Figure 2.16. The reservoir properties are summarized in Table 2.4. One vertical producer will be placed in the reservoir by applying the optimization algorithms to find the optimal well loca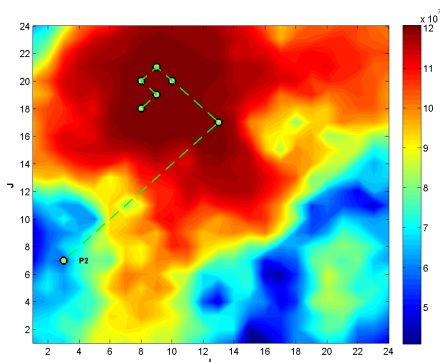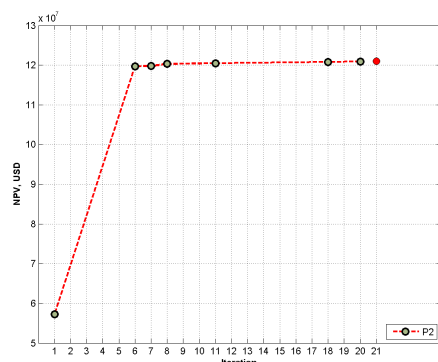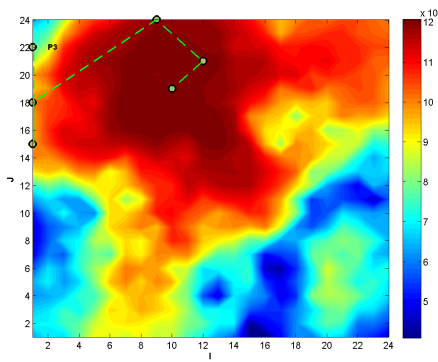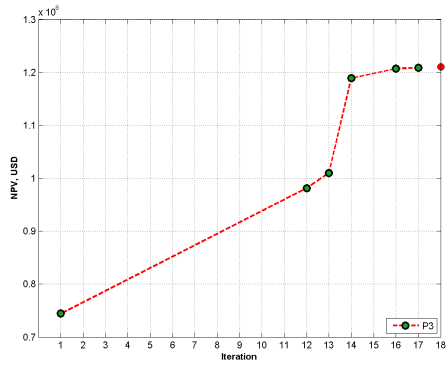tion. The parameters used for NPV function are shown in Table 2.2. The NPV 3-D surface and contour plot in Figure 2.17 are obtained from the exhaustive search by repositioning a single producer in the reservoir, and running the simulator to obtain the NPVs for each gird block.

Table 2.4: 3-D heterogeneous reservoir properties

Description	Properties
Number of grid blocks	$24 \times 24 \times 3$
Number of layers	3
Grid Block size	100 ft $\times$ 100 ft $\times$ 30 ft
Reservoir thickness	90 ft
Reservoir top depth	9000 ft
Water oil contact	9095 ft
Porosity	0.30
Initial reservoir pressure	3600 psia
Production time	5 years
BHP	500 psia

(a) Layer 1   (b) Layer 2   (c) Layer 3
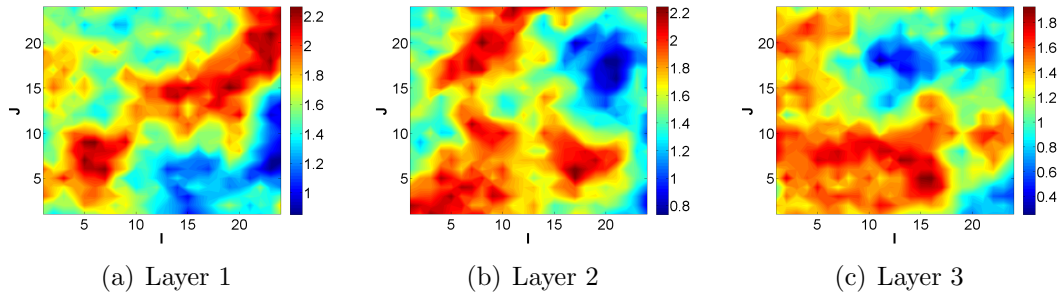
Figure 2.16: Logarithm permeability contour for 3-D heterogeneous reservoir model (unit: mD)

The application of EnOpt on 3-D heterogeneous reservoir case is shown in Figure 2.18. In order to test the performance for different ensemble sizes, the ensemble size of 20 and 50 are selected and the variance of well locations is set as 5 for the first 2 successful steps and as 2 for the following steps. From the results, we see the

(a) NPV 3-D   (b) NPV contour
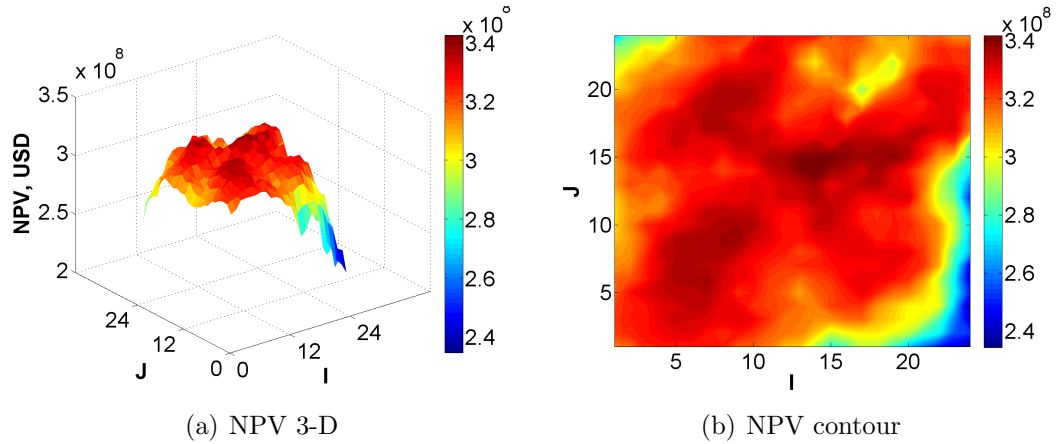
Figure 2.17: NPV 3-D and NPV contour plot for 3-D heterogeneous reservoir model (unit: USD)

ensemble size of 50 shows approximately the same performance as with an ensemble size of 20. In order to compare EnOpt and SPSA, the results from the best scenario (Ne = 20) are selected, where N_e denotes the ensemble size.

The optimization results from SPSA algorithm are shown in Figure 2.19. From the plot in Figure 2.19(a), it is difficult to distinguish the results obtained from different starting points, so the location of solutions from different starting points are illustrated in separate figures. The algorithm converges to an optimal solution with a few iterations. It should be noted that the results are dependent on the predefined starting points.

Based on all the experiments for the application of EnOpt and SPSA algorithms on the 2-D homogeneous, the 2-D heterogeneous and the 3-D heterogeneous models, the optimization results are summarized in Table 2.5 and Table 2.6. The data shown in the tables are the average values from different cases. From the summary of the number of function evaluations recorded in these two tables, we see the number of function evaluations that EnOpt requires is more than three times as that of SPSA. Therefore, we can conclude that for obtaining a similar level of accuracy, SPSA might be more beneficial for practical field case studies.

In order to compare the results, the NPV is shown in Figure 2.20 where we see

(a) Location move ($Ne = 20$, $\sigma = 5$ & 2)

(b) NPV increase ($Ne = 20$, $\sigma = 5$ & 2)

(c) Location move ($Ne = 50$, $\sigma = 5$ & 2)

(d) NPV increase ($Ne = 50$, $\sigma = 5$ & 2)
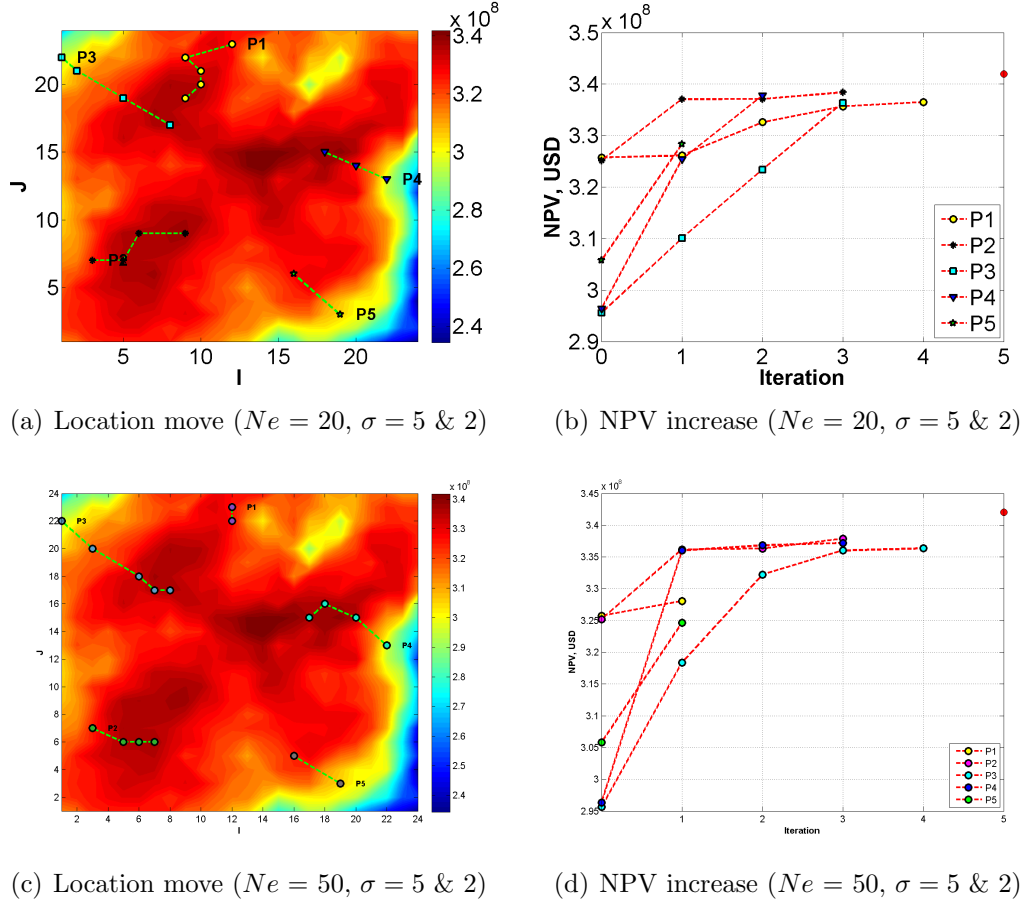
Figure 2.18: Application of EnOpt on the 3-D heterogeneous reservoir model

Table 2.5: Summary of EnOpt optimization results

Items	2D homo	2D hetero	3D hetero
Total function evaluations	127.7	158.8	145.8
Initial NPV, USD	7.60E+07	7.70E+07	3.10E+08
Maximum NPV, USD	7.94E+07	1.07E+08	3.35E+08
NPV increase percentage, %	4.53	40.27	8.31

Table 2.6: Summary of SPSA optimization results

Items	2D homo	2D hetero	3D hetero
Total function evaluations	31.85	41.3	40.9
Initial NPV, USD	7.60E+07	7.70E+07	3.10E+08
Maximum NPV, USD	7.94E+07	1.15E+08	3.36E+08
NPV increase percentage, %	4.43	49.38	8.58
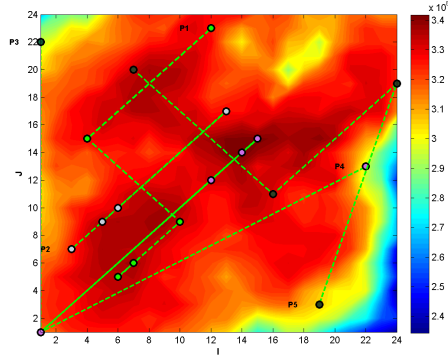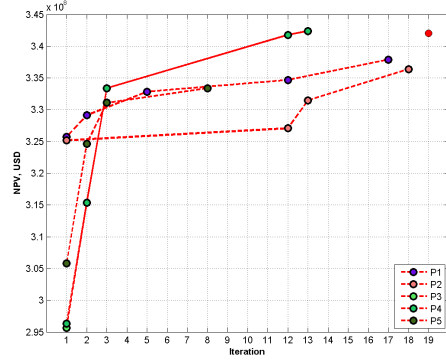
59

(a) Location move (Summary)

(b) NPV increase (Summary)
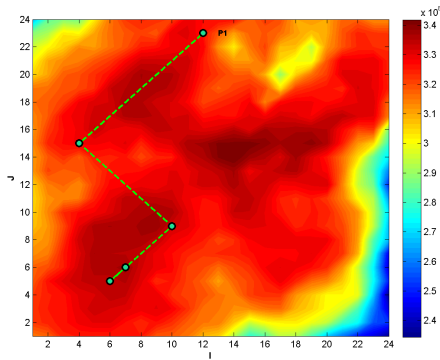
(c) Location move (Point 1)
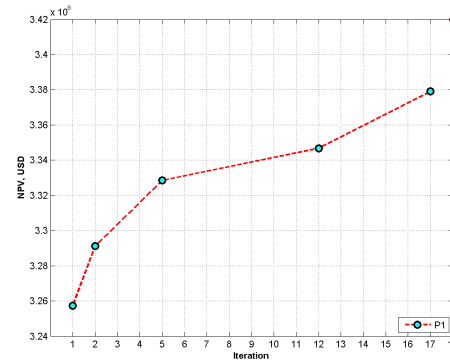
(d) NPV increase (Point 1)
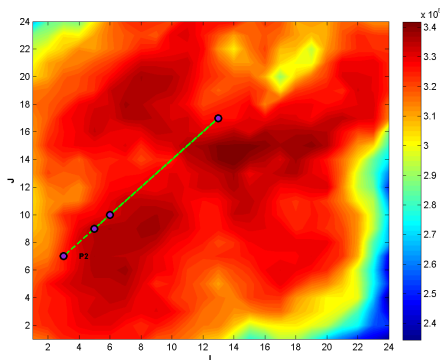
(e) Location move (Point 2)
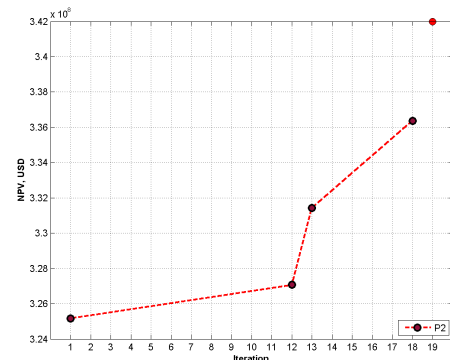
(f) NPV increase (Point 2)
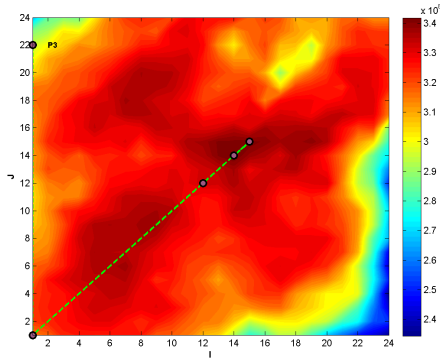
(g) Location move (Point 3)
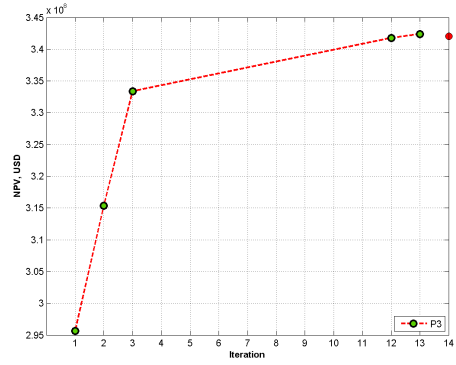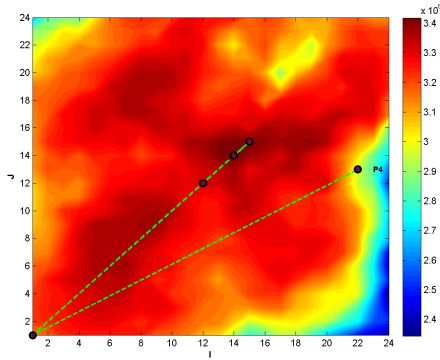
(h) NPV increase (Point 3)

(i) Location move (Point 4)
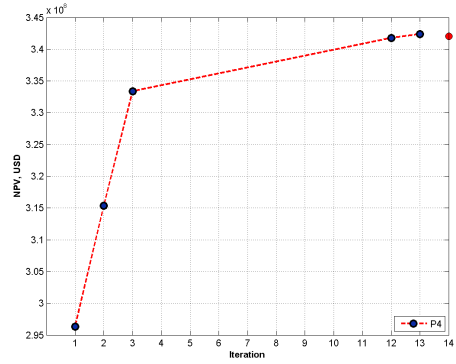
(j) NPV increase (Point 4)
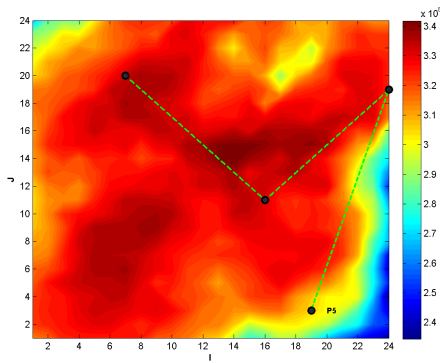
(k) Location move (Point 5)
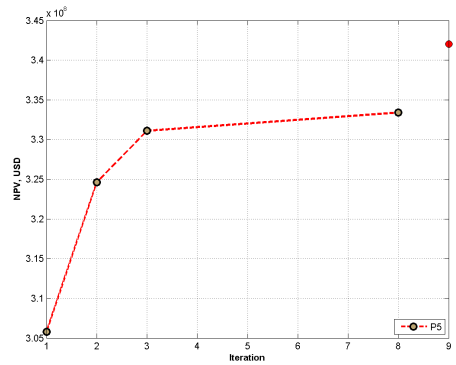
(l) NPV increase (Point 5)

Figure 2.19: Application of SPSA on 3-D heterogeneous reservoir model

that both EnOpt and SPSA can make improvements in maximizing the NPV values. Moreover, the percentage of NPV increase and the number of function evaluations are also plotted in Figure 2.21. From Figure 2.21(b), we see that SPSA requires fewer function evaluations compared to EnOpt, thus this implies a significant decrease in the computation time,making it more applicable to field studies.
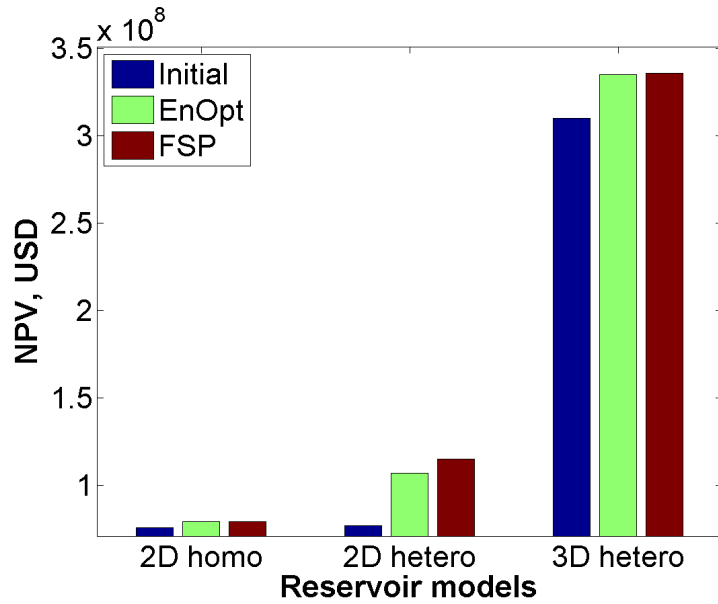
Figure 2.20: Summary of NPV increase from EnOpt and SPSA algorithms for three reservoir models

(a) NPV increase percentage

(b) Number of function evaluations
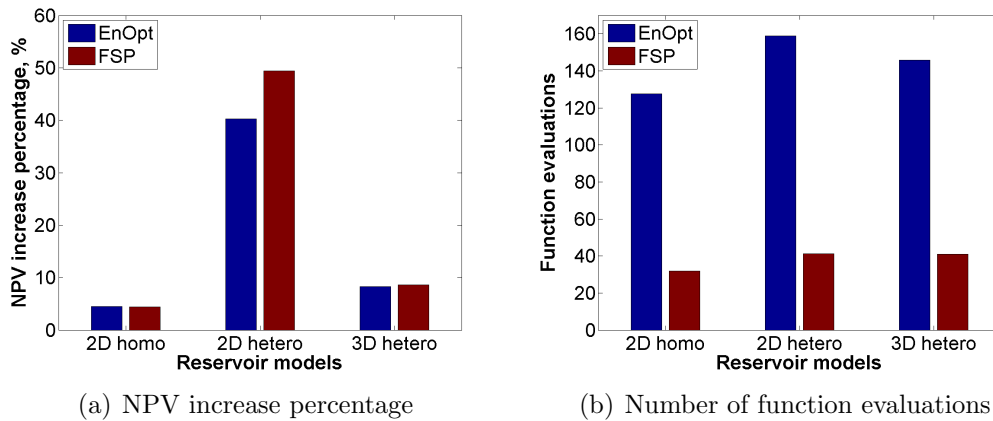
Figure 2.21: NPV increase percentage and number of function evaluations from EnOpt and SPSA algorithms for three reservoir models

2.5 Summary

This chapter develops the formulations of two stochastic approximate gradient methods: Ensemble-Based Optimization (EnOpt) and Fixed-Gain SPSA (FSP) method. Because FSP requires only 2 function evaluations per iteration, FSP tends to be more computationally efficient in comparison with EnOpt for similar accuracy. Since EnOpt and FSP are essentially guided by the approximated gradient, practical application would dictate the choice of several starting points in order to increase the chances of reaching the global optimum. The discussion presented in the case studies highlights the capabilities, suitability and challenges associated with EnOpt and FSP for optimal well placement. It should be noted that for simple case studies, the application of the proposed optimization methods in this dissertation may not be the only solution for making decisions, however, the mathematical optimization can be beneficial when the optimization problems involve large scale highly heterogeneous fields. In the next chapter, I will focus on optimization for multiple well placement.

CHAPTER III

WELL PLACEMENT WITH QUALITY MAPS

3.1 Introduction

The application of EnOpt and FSP was introduced in the previous chapter. The premise for the application of these two algorithms is that the number of wells is fixed. Even though the application is only tested for the placement of a single vertical producer, it is feasible to extend the application to multi-well placement when the number of wells is known. However, if the number of wells is not known *a priori*, the problem becomes more challenging. In the formulation of NPV (Eq. 2.1), we see that the discount rate tends to reduce the contributions from oil production at later stages in the reservoir life, so at the initial stage of the reservoir development, the more wells, the higher total oil production rate. However, the increase in the number of wells also increases the drilling costs. Therefore, a balance should be maintained between the oil production rate and the drilling cost for the new wells.

Generally in the development and appraisal phase of reservoir management, the number of wells to be drilled is dependent on the operational budget. This might lead the operator to drill a limited number of wells, say 4 or 5. Now, this is based entirely on the available operating budget and may not necessarily be optimum. It's possible that we may obtain superior performance with a fewer number of wells or it even might be necessary to drill additional wells. Traditionally, reservoir engineers perform their optimization studies with a fixed number of wells and progressively increase the number of wells until they reach an optimum. For instance, with FSP or EnOpt, they would have to place one well optimally with the maximum NPV, then place two wells with the maximum NPV and continue doing this until they reach the

scenario when the increase in the number of wells does not improve the NPV further. This is extremely time consuming and inefficient.

In this chapter, I propose to use quality maps to determine the optimal number of wells before proceeding to the optimization. A quality map is a 2-D map evaluated from specified parameters that serve as an indicator of reservoir productivity. In connection to the previous chapter (Figure 2.2), the simplified workflow of this chapter is illustrated in Figure 3.1. In the case studies, the quality map approach (QM) will be used to guide the decision of number of wells, followed by the fixed-gain SPSA method (FSP) to decide the optimal well locations. The combination of these two approaches is referred as the QM-FSP method. It provides a framework to determine both the optimal number of wells and the optimal well locations simultaneously.
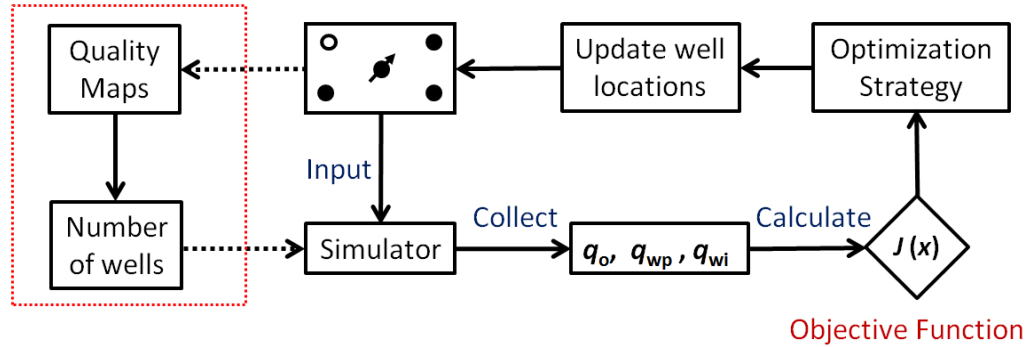
Figure 3.1: Quality map assisted well placement optimization workflow

3.2 Quality Map Assisted Fixed-Gain SPSA Method (QM-FSP)

The concept of quality map has been introduced in other literatures listed in Section 1.3. But most of those studies generated quality maps based on the assumption that multiple wells may be placed based on the single well experiments, so they rely on exhaustive simulation runs to calculate NPVs for each single well location, and plot the NPVs on a 2-D map which is referred as a quality map. This is inefficient

and may not work well for multiple well placement.

The quality map proposed here is very fast to calculate. Because we aim at mapping reservoir regions of high connectivity and high oil production potentials, I select the parameters that can reflect these objectives. For connectivity, it can be easily quantified through the use of inter-block transmissibilities in numerical reservoir simulation, and for oil production potential, it can be indicated by relative oil permeability, therefore, the quality map calculation incorporates the transmissibility and relative oil permeability, which can be obtained through the reservoir model initialization, but does not require any simulation runs.

The advantage of utilizing transmissibility to generate quality maps is the following: Firstly, every commercial simulator formulation is rooted in the use of transmissibilities which is stored in memory and obtained during model initialization. Consequently, even for large reservoir models, the computational effort required is on the order of a few seconds. Secondly, the transmissibility is directly linked to the underlying heterogeneity and does not require interpolation or generation of response surfaces. Because interpolation response surfaces are essentially smooth functions derived from a limited sampling of the reservoir, they may not be entirely appropriate when the scale of heterogeneity is small.

Now, I show how to quantify the connectivity by transmissibilities. In reservoir simulation, the reservoir properties are usually evaluated at the center of the grid block, but transmissibility reflects the connectivity between grid blocks, so the transmissibility can be defined at the boundary of the grid block. For example, given three grid blocks of a 1-D reservoir model shown in Figure 3.2, the connectivity at the grid block i consists of two parts: the connectivity between grid block $i-1$ and i which is represented by the transmissibility $T_{x_{i-\frac{1}{2}}}$ at the left boundary; and the connectivity between grid block i and $i+1$, which is represented by the transmissibility $T_{x_{i+\frac{1}{2}}}$ at the right boundary.
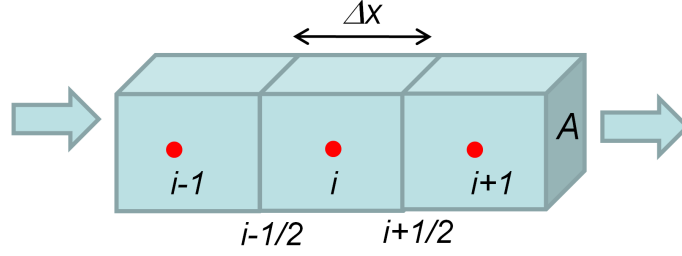
Figure 3.2: Three grid blocks in a 1-D reservoir model

If the transmissibilities T_i and T_{i+1} at the grid centers can be calculated as

$$T_i = \frac{K_i A_i}{\Delta x_i / 2}, \tag{3.1}$$

$$T_{i+1} = \frac{K_{i+1} A_i}{\Delta x_{i+1} / 2}, \tag{3.2}$$

where A_i is the cross-sectional area; K_i and K_{i+1} are the effective permeability in the x- direction for grid block i and $i+1$ respectively; Δx_i and Δx_{i+1} are the grid size in the x- direction for grid block i and $i+1$ respectively, then $T_{x_{i+\frac{1}{2}}}$ can be obtained from

$$T_{x_{i+\frac{1}{2}}} = \frac{T_i T_{i+1}}{T_i + T_{i+1}}. \tag{3.3}$$

If the dimensions of all the grid blocks are equal, the simplified equations for the transmissibility at the boundary of grid blocks are,

$$T_{x_{i+\frac{1}{2}}} = \frac{2 K_i K_{i+1}}{K_i + K_{i+1}} \cdot \frac{A_i}{\Delta x_i}, \tag{3.4}$$

$$T_{x_{i-\frac{1}{2}}} = \frac{2 K_i K_{i-1}}{K_i + K_{i-1}} \cdot \frac{A_i}{\Delta x_i}. \tag{3.5}$$

The initial values for the transmissibility in the x-, y- and z- directions can be obtained from the initialization of the reservoir models without the need for a simulation run. In this study, considering the transmissibility in all the directions, the total transmissibility at grid block (i, j, k) is calculated as

$$T_{r,i,j,k} = \sqrt{T_{x,i,j,k}^2 + T_{y,i,j,k}^2 + T_{z,i,j,k}^2}. \tag{3.6}$$

67

However, simple grid connectivity is not likely to reflect oil production potential, because the oil relative permeabilities at each grid cell are indicative of the oil production potential, a new term called the total quality is defined as

$$T_{q,i,j,k} = T_{r,i,j,k} \cdot K_{ro,i,j,k}. \tag{3.7}$$

This definition works well for the 2-D reservoir cases. However, for 3-D fields, a 2-D representation of regional connectivity is required by computing the average connectivity over all the layers. And a 2-D quality map can be obtained by defining

$$
\begin{aligned}
T_{q,i,j} &= \sum_{k=1}^{N_{layer}} T_{q,i,j,k} \\
&= \sum_{k=1}^{N_{layer}} \left(\sqrt{T_{x,i,j,k}^2 + T_{y,i,j,k}^2 + T_{z,i,j,k}^2} \cdot K_{ro,i,j,k} \right).
\end{aligned} \tag{3.8}
$$

The assumption of applying this approach for 3-D reservoirs is that, even if one out of N_{layer} layers has a high productive potential, this should be reflected on the quality map. Now with these quantities computed, the most productive regions can be identified by selecting the top quality map values, and then define productive regions of high connectivity. In this approach, I treat each of these regions as a potential reservoir volume for well placement.

3.3 Application on Multiple Well Placement

In this section, the idea of quality map assisted well placement is demonstrated on a 2-D and a 3-D reservoir model. The 2-D reservoir model is a new reservoir model but the 3-D model is the same model as introduced in the previous chapter. The number of wells and the corresponding locations are optimized on these two cases.

For the purpose of research comparison, I first perform an exhaustive search to get the optimal number of wells and the corresponding locations as a reference. The *exhaustive search* refers to the number of wells. For the scenarios with fixed numbers of wells starting from 1 well, 2 wells, 3 wells and on, I randomly generate the numerous

well configurations with a certain number of wells, and obtain the maximum NPVs for each scenario tabulated in Table 3.1 and Table 3.2. From the tables, we can see that the scenario with 2 wells achieves the maximum NPV, so it is the optimal case for the 2-D heterogeneous reservoir model, and the one with 3 wells is the optimal case for the 3-D heterogeneous reservoir model.

Table 3.1: Exhaustive search results for the optimal number of wells in 2-D heterogeneous reservoir model

Number of wells	1	2	3
Function evaluations	576	2000	5000
CPU time, hours	0.5	2	4.8
NPV max, USD	8.25E+07	8.50E+07	8.47E+07

Table 3.2: Exhaustive search results for the optimal number of wells in 3-D heterogeneous reservoir model

Number of wells	1	2	3	4
Function evaluations	576	2000	5000	10000
CPU time, hours	0.5	2	6.7	12.75
NPV max, USD	3.41E+08	3.46E+08	3.47E+08	3.46E+08

3.3.1 Two Dimensional Heterogeneous Reservoir Model

The size of the 2-D reservoir model is the same with the 2-D heterogeneous model introduced in Section 2.4.2. But the permeability field is generated differently. The logarithm permeability contour is shown in Figure 3.3, where red color represents high permeability and blue color represents low permeability. The NPV plot is obtained by exhaustive simulation runs of a single well placed in each of the grid blocks through parallel computing. The NPV 3-D surface and the contour plot are shown in Figure 3.4. Although the exhaustive runs of a single well may not indicate the placement of multiple wells, they are prepared to provide an overview for the reservoir productive potentials.
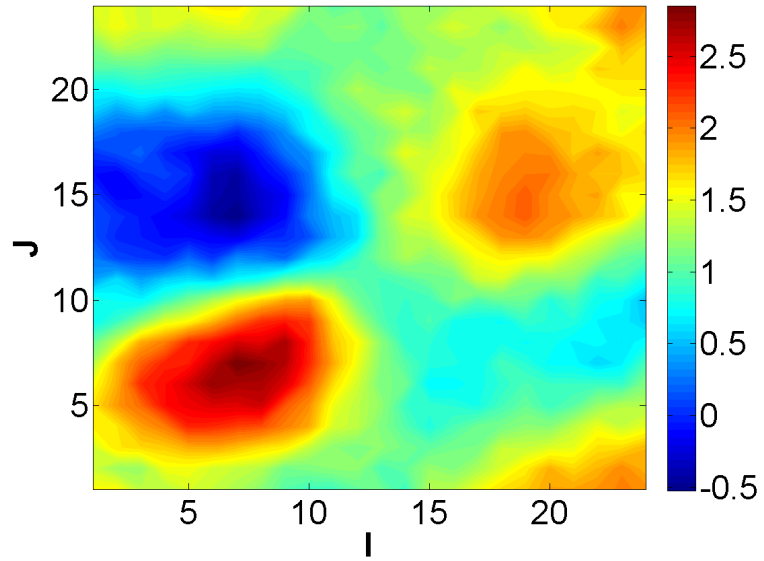
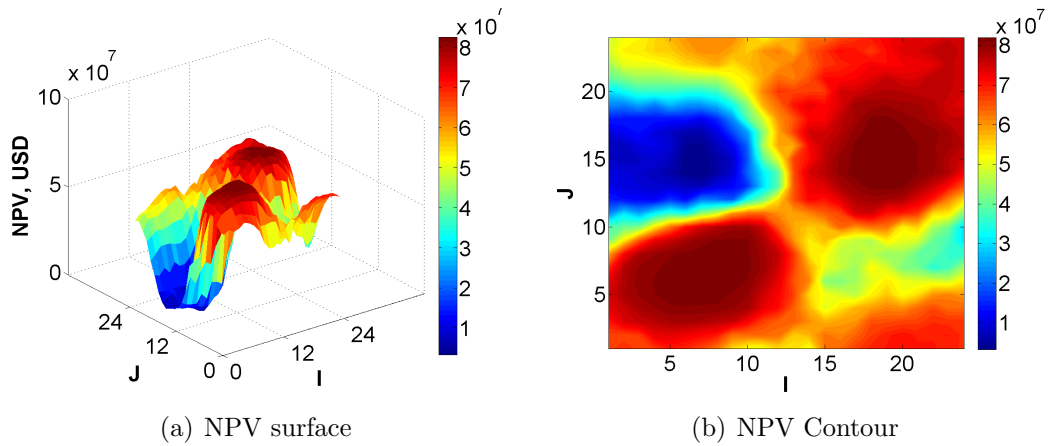**Figure 3.3:** Logarithm permeability contour for 2-D heterogeneous reservoir model (unit: mD)

(a) NPV surface

(b) NPV Contour

Figure 3.4: NPV surface and NPV contour plot for 2-D heterogeneous reservoir model (unit: USD)

3.3.1.1 Application of FSP

If the number of wells is not known *a priori*, exhaustive experiments are needed in terms of the number of wells. Then, the scenario with the highest NPV will be selected as the optimal number of wells. In this case, since FSP can only solve the optimization problem with fixed number of variables, I assume the optimal number of wells is known and constant, and FSP will be applied to decide the optimal well locations for 1 well, 2 wells, 3 wells, and so on. Six different multiple starting points are also used to increase the probability of finding the global optimum. These starting points are randomly selected to cover the whole reservoir.

I show how the algorithm search for the optimal location of two wells from the six starting points in Figure 3.5. The left column of figures show the well location movement on top of the NPV contour map, which indicates the productive regions as a reference background. The right column of the figures show the increase of NPVs during the iterations. We see that some randomly selected starting point, Point 4 (Figure 3.5(g)) for instance, can be very far from the optimal solution, so they get trapped at the local optima even after 18 iterations. Some starting points, Point 5 (Figure 3.5(i)) for instance, starts very close to the productive regions (dark red areas), and the optimization converges within 9 iterations.

Similar procedures are also adopted for the placement of 1 well and 3 wells. Here I will not show the detailed movement from all the starting points, but I select the experiment from the best starting point (the one yields to the maximum NPV) and summarize the results in Figure 3.6. From the maximum NPVs obtained at the end of the iterations, we see 2 wells give the best NPV at 8.31×10^7 USD (Figure 3.6(d)).

3.3.1.2 Application of QM-FSP

Instead of using the traditional exhaustive FSP to search for the optimal number of wells, I now demonstrate how to apply QM-FSP to search for the optimal solution.
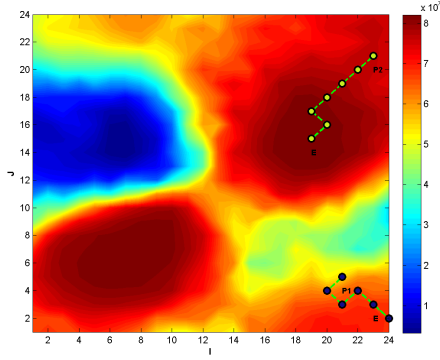
(a) Location move (Point 1)
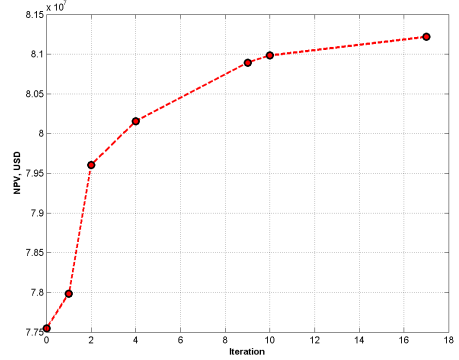
(b) NPV increase (Point 1)
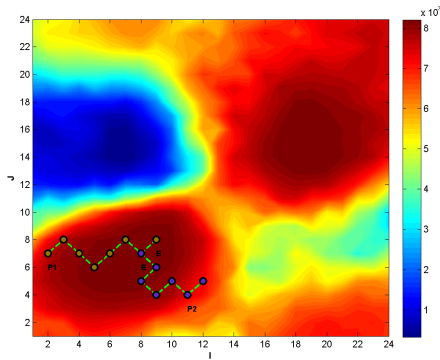
(c) Location move (Point 2)
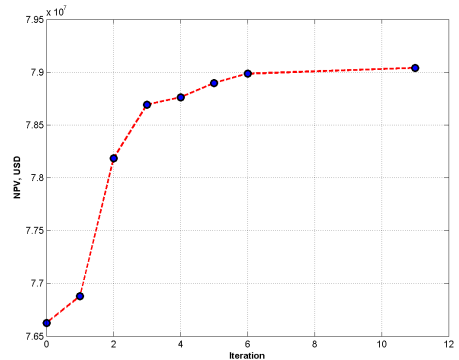
(d) NPV increase (Point 2)
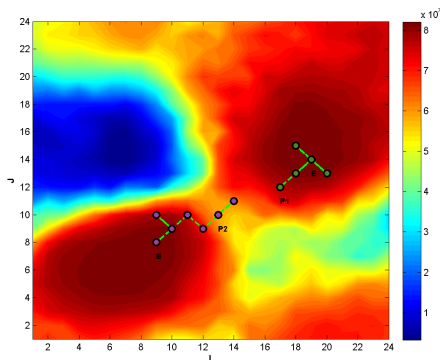
(e) Location move (Point 3)
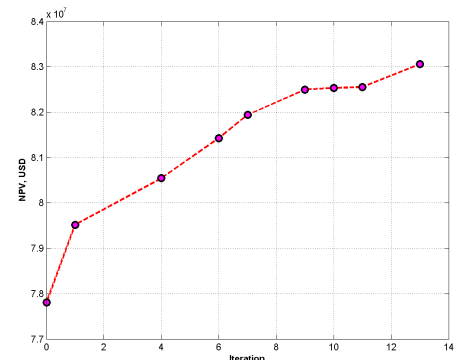
(f) NPV increase (Point 3)
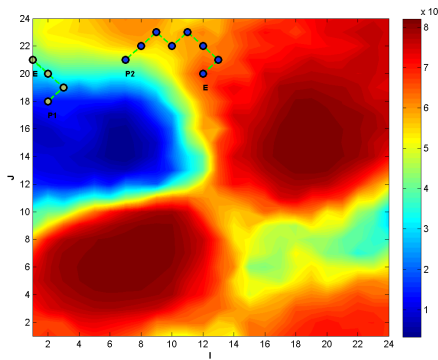
(g) Location move (Point 4)
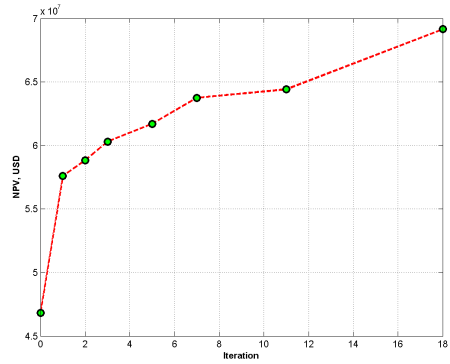
(h) NPV increase (Point 4)
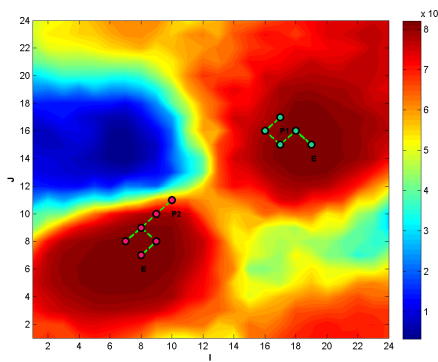
(i) Location move (Point 5, optimal)
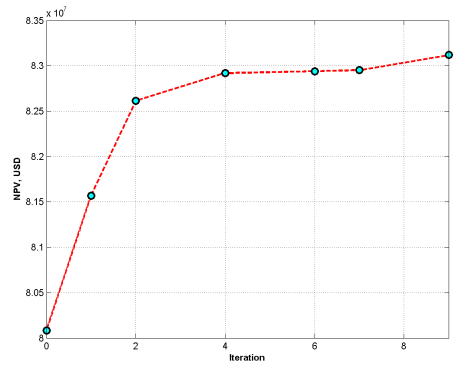
(j) NPV increase (Point 5, optimal)
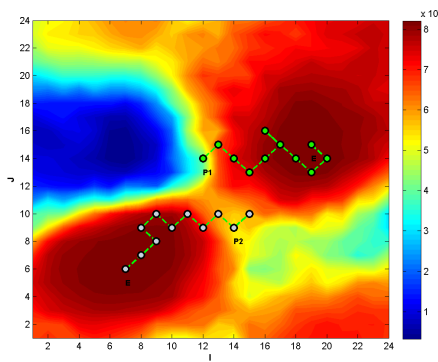
(k) Location move (Point 6)
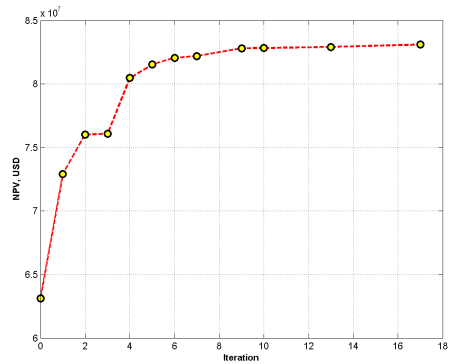
(l) NPV increase (Point 6)

Figure 3.5: FSP for 2 wells' locations from multi-starting points on 2-D heterogeneous reservoir model
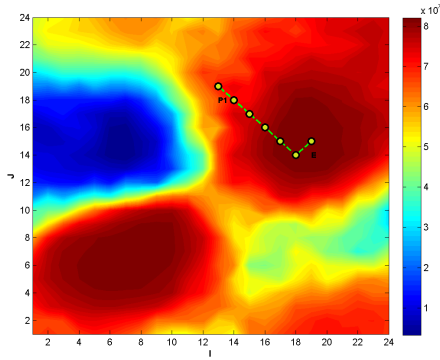
(a) Location move (1 well)
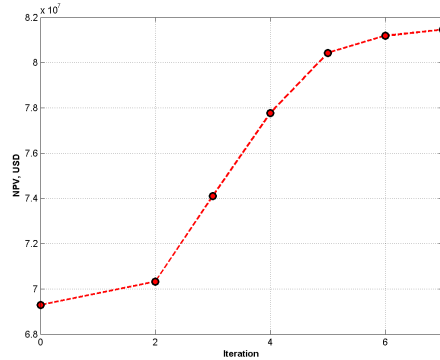
(b) NPV increase (1 well)
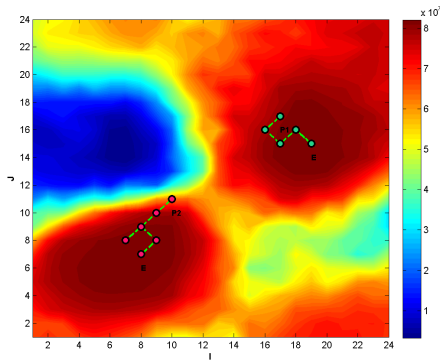
(c) Location move (2 wells)
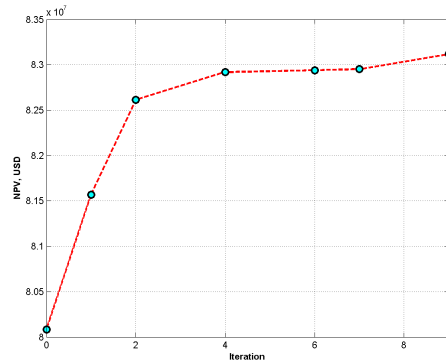
(d) NPV increase (2 wells)
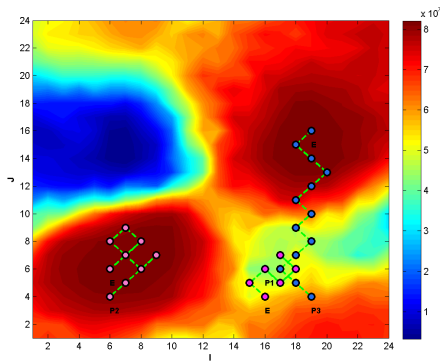
(e) Location move (3 wells)
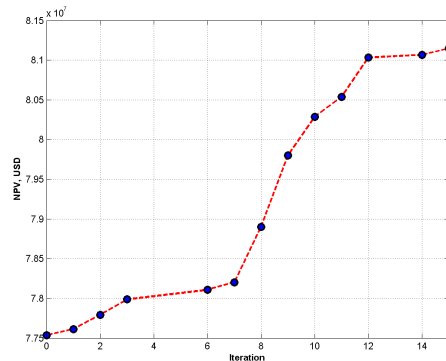
(f) NPV increase (3 wells)

Figure 3.6: Best scenarios from multi-starting points for the number of wells and locations on 2-D heterogeneous reservoir model. P1, P2, . . ., P5 denote the initial locations, and 'E' denotes the locations at the end of the optimization process.

First, prepare for the calculation of the connectivity quality map by the initialization of the reservoir model. Then, obtain the transmissibilities T_x, T_y and T_z, and apply Eq. 3.8 to calculate the values of the total quality at each grid block. The contour map of these values is shown in Figure 3.7(a). The cumulative distribution function of the total quality values is also shown in Figure 3.7(b), which is used to decide the following quality percentiles.

(a) T_q (b) The CDF of T_q
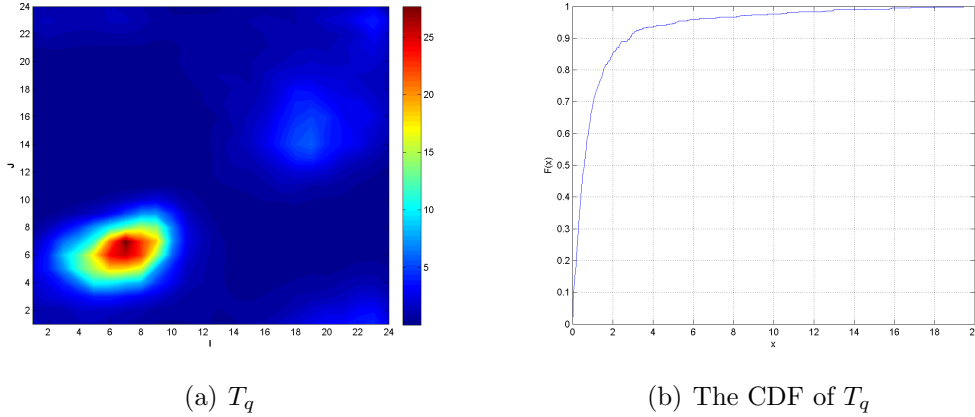
Figure 3.7: Quality map contour and cumulative distribution function (CDF) plot for 2-D heterogeneous reservoir model

From the cumulative distribution function (CDF), I obtain the values for 30th, 60th and 90th percentiles. Then the grid blocks can be colored based on which percentile range their quality values are belong to. The percentile map is plotted in Figure 3.8(a). In this plot, the integer values on the color bar simply show the percentile range each color corresponds to. From low to high, 1 represents the range between 0 and 30th percentile, 2, 3 and 4 represent the ranges of $30^{th} \sim 60^{th}$, $60^{th} \sim 90^{th}$ and $90^{th} \sim 100^{th}$ percentile, respectively. In the color map (Figure 3.8(a)), the dark blue areas have the cells where the total quality is below 30th percentile, and the light blue areas contain cells with the quality value between 30th percentile and 60th percentile. Similarly, the yellow areas are between 60th percentile and 90th percentile, and the red areas are above 90th percentile. Usually, for both of the two reservoir models, 60th percentile is selected to screen the productive regions. This choice is subjective, but it appears to

75

be suitable for the screening purpose in the study cases. In this reservoir model, the potential regions which have the cells with the quality values above 60th percentile are plotted in Figure 3.8(b). Because there is a lower limit in terms of the number of grid cells that consist a candidate region for well placement, we have Figure 3.8(c) where smaller reservoir volumes at the upper left corner and the lower right corner are screened out.

(a) Percentile map   (b) Potential regions   (c) Effective regions
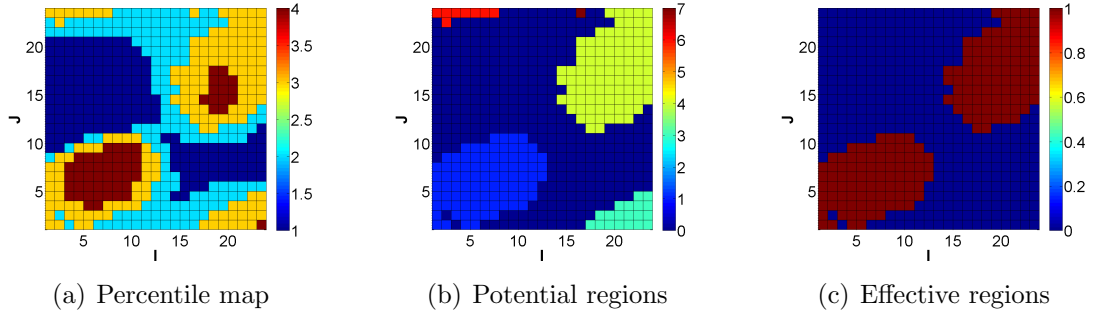
Figure 3.8: Quality maps for 2-D heterogeneous reservoir model

Based on the fact that Figure 3.8(c) shows the two effective regions, it may indicate two productive potential regions, so two will be selected as the optimal number of the new wells. In each region, a random location is sampled to be the starting point for each well in the fixed-gain SPSA (FSP) algorithm. The FSP algorithm is then applied to decide the two optimal well locations, and it only needs 8 iterations to converge to the optimum (Figure 3.9(b)), which is computationally very efficient.

3.3.1.3   Comparison of FSP and QM-FSP

We can compare the performance based on the optimization results obtained from FSP and QM-FSP. The results are tabulated in Table 3.3. The performance of the two methods is compared in terms of the function evaluations, the computation time, and the maximum NPVs. We see the NPV decreases when the number of wells increases from 2 to 3, so clearly 2 is the optimal number of wells for this study.

For the ease of visualization, the results in Table 3.3 are plotted in bar plots in

(a) Well location move

(b) NPV increase
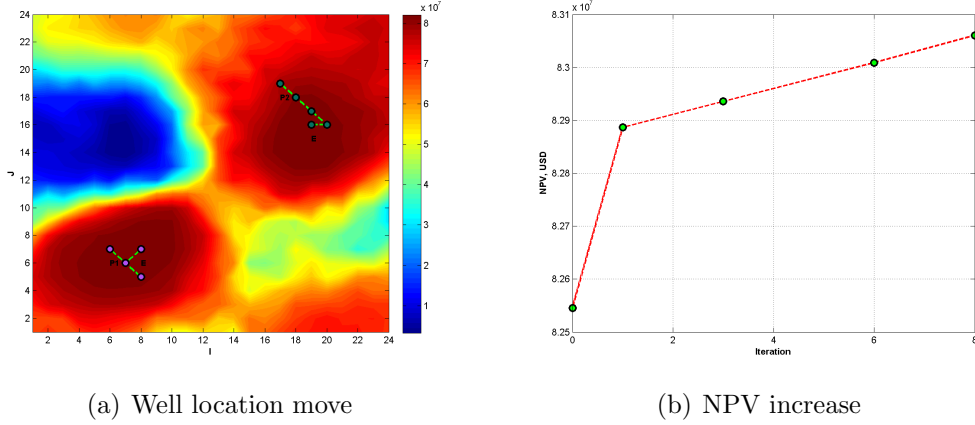
Figure 3.9: Optimization results from QM-FSP for the 2-D heterogeneous reservoir model

Table 3.3: Comparison of FSP and QM-FSP for 2-D heterogeneous reservoir model

Number of wells	1	2	3	QM-FSP
Function evaluations	297	358	159	46
CPU time, minutes	16	19.3	10	2.5
NPV max, USD	8.15E+07	8.31E+07	8.11E+07	8.31E+07

Figure 3.10. Because the computation time is proportional to the number of function evaluations, I only show the plots for computation time here.

Figure 3.11 shows the comparison of FSP and QM-FSP. I show the improvement of NPV from QM-FSP and the NPVs during the iterations of FSP with different starting points. In this figure, the dash lines with red dots are the FSP results with 6 random starting points, and the solid line with blue dots is the QM-FSP results using quality map. From the figure, we see the solid curve from QM-FSP starts with a high NPV and converge within a few iterations. However, most of the dash lines from FSP do not have high NPVs at the starting points and they take more iterations to converge. This is because the starting point for QM-FSP are placed inside the effective regions, which is close to the optimal solution. From this figure we see the capability of quality maps that enable the direct placement of productive wells based on engineering considerations.

The results of FSP and QM-FSP are also compared in the box plot in Figure 3.12.

77

(a) NPV
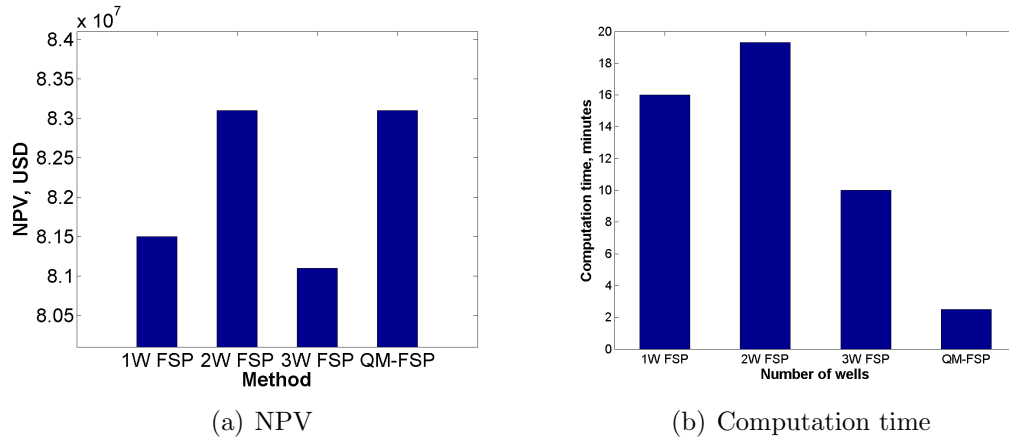
(b) Computation time

Figure 3.10: Comparison of the maximum NPV and the computation time from FSP and QM-FSP for the 2-D heterogeneous reservoir model
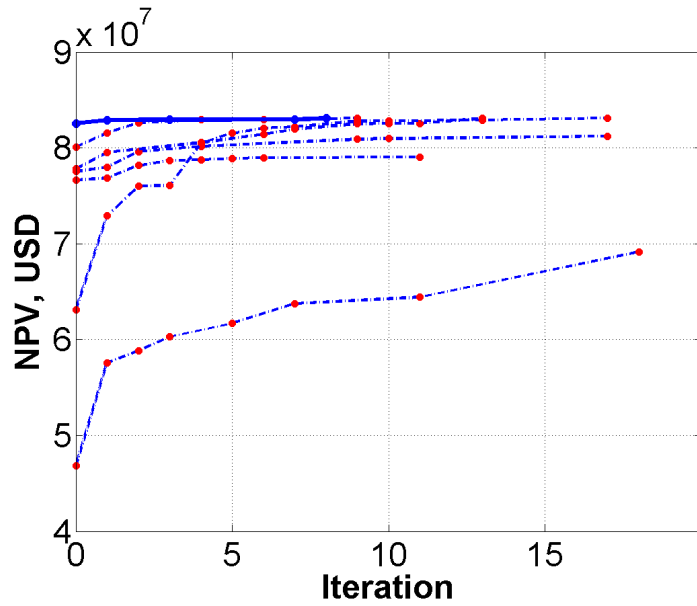
Figure 3.11: Comparison of FSP and QM-FSP optimization in number of wells and locations for 2-D heterogeneous reservoir model. The dash lines with red dots are the FSP results with 6 random starting points over the whole reservoir, and the solid line with blue dots is the QM-FSP results with 1 random sampling in the effective quality map regions.

We can see that QM-FSP provides a greater maximum NPV compared to all the other experiments using FSP. Moreover, for the same number of wells (2 wells), QM-FSP achieved even higher NPV than the traditional FSP method. The comparison of the total computation time between these two methods is also shown in Figure 3.13. We see that the QM-FSP only requires 2.5 minutes of CPU time, while FSP requires over 40 minutes. The reason is that the total computation time for FSP is the summation of the computation time for each scenario with a fixed number of wells.
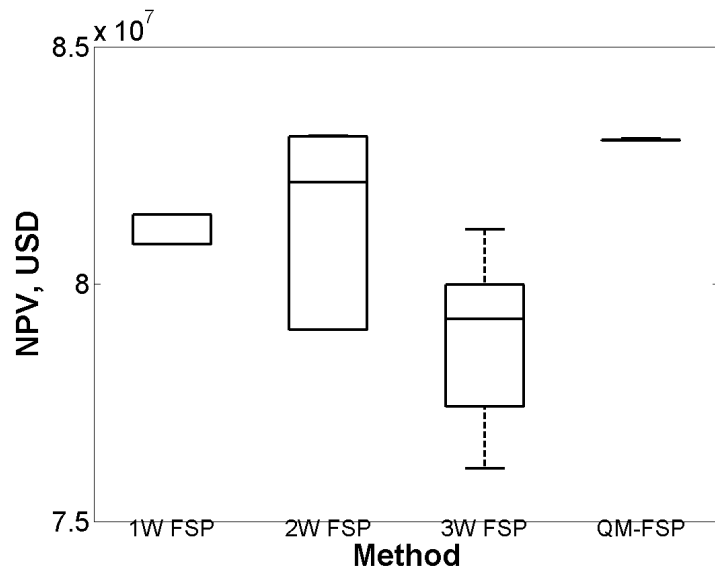
Figure 3.12: Box plot for the results of FSP and QM-FSP for 2-D heterogeneous reservoir model

3.3.2 Three Dimensional Heterogeneous Reservoir Model

3.3.2.1 Application of FSP

The 3-D heterogeneous reservoir model used here is the same as what was used in Chapter 2.4.

When the number of wells is not known *a priori*, exhaustive experiments are needed to decide the optimal number of wells. The scenario with the highest NPV will be selected as the optimal number of wells. In this case, FSP is applied to
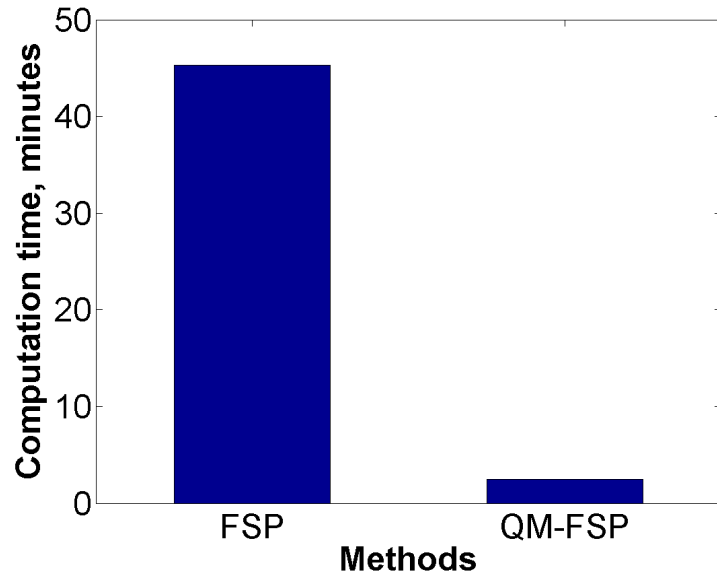
Figure 3.13: Comparison of the total computation time for FSP and QM-FSP method to optimize the number of wells and locations for 2-D heterogeneous reservoir model

determine the optimal well locations for 1 well, 2 wells, 3 wells and so on, until the maximum NPV is reached. Multiple starting points are used to enable FSP to find the global optimum. The starting points are randomly selected to cover the whole reservoir. The results are selected from the best starting points of each scenario and show the well location movement and the NPV improvement in Figure 3.14.

The efficiency of FSP is compared with the exhaustive search method for the optimal number of wells. The maximum NPVs from all the scenarios (numbers of wells) are shown in Figure 3.15(a). In both exhaustive search and FSP experiments, we see a decrease of NPV when the number of wells is increased from 3 to 4, so it clearly shows that 3 wells is the optimum. These two methods provide similar maximum NPVs for each scenario with fixed number of wells. However, FSP takes much less computation time, as is shown in Figure 3.15(b). These experiments show that with a comparable performance, instead of the exhaustive search, the optimal number of wells obtained from FSP can also serve as a reference for the following
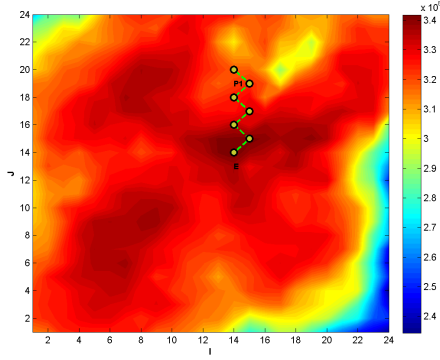
(a) Location move (1 well)
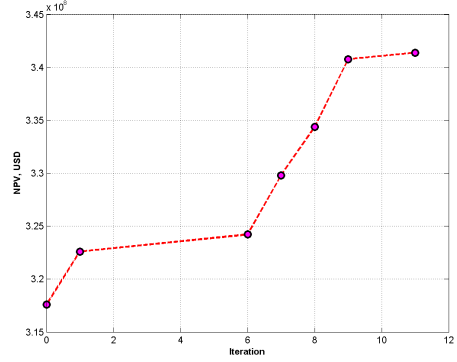
(b) NPV increase (1 well)
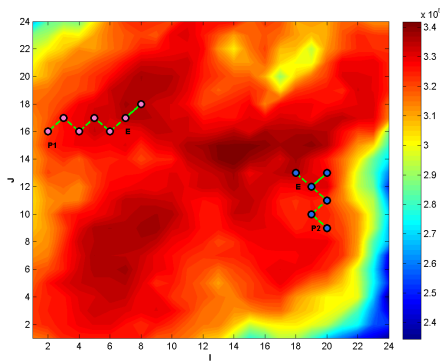
(c) Location move (2 wells)
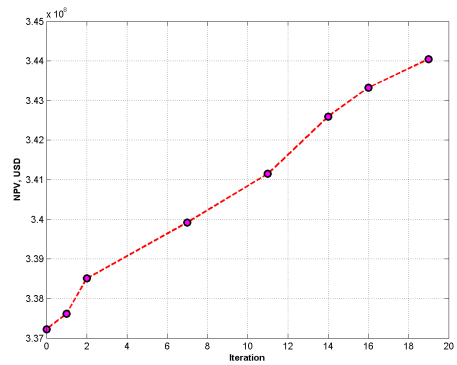
(d) NPV increase (2 wells)
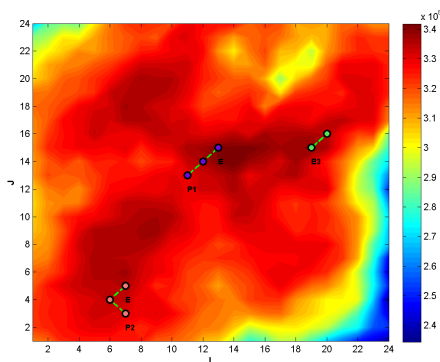
(e) Location move (3 wells)
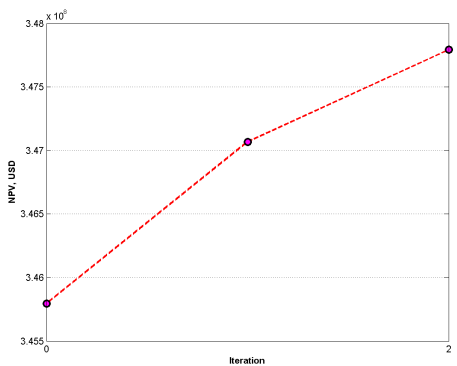
(f) NPV increase (3 wells)
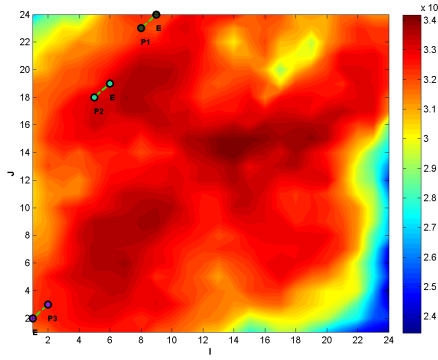
(g) Location move (4 wells)   (h) NPV increase (4 wells)
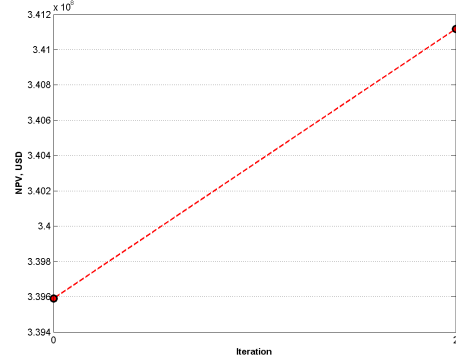
Figure 3.14: Best scenarios from multi-starting points for the number of wells and locations on 3-D heterogeneous reservoir model

QM-FSP method.
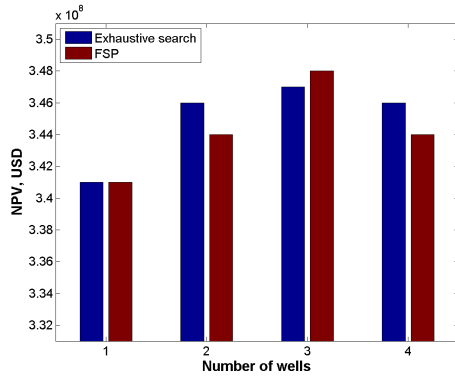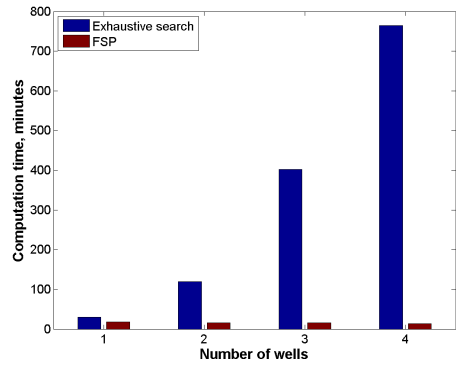
(a) NPV   (b) Function evaluations

Figure 3.15: Comparison of exhaustive search and FSP method for 3-D heterogeneous reservoir model

3.3.2.2   Application of QM-FSP

Now QM-FSP is performed to search for the optimal solution in this reservoir. After the reservoir model initialization, the quality values are calculated based on Eq. 3.7. The contour maps are shown for each layer in Figure 3.16. We see each layer can have a different layer quality map. Also, using Eq. 3.8, the total quality map can be computed as is shown in Figure 3.17(a). It captures the high quality areas from each

layer. I also show the contour map of NPVs obtained from single well placement in each grid block. Although this contour map does not necessarily imply the placement of multiple wells, it provides the potential productive regions.

(a) Layer 1   (b) Layer 2   (c) Layer 3
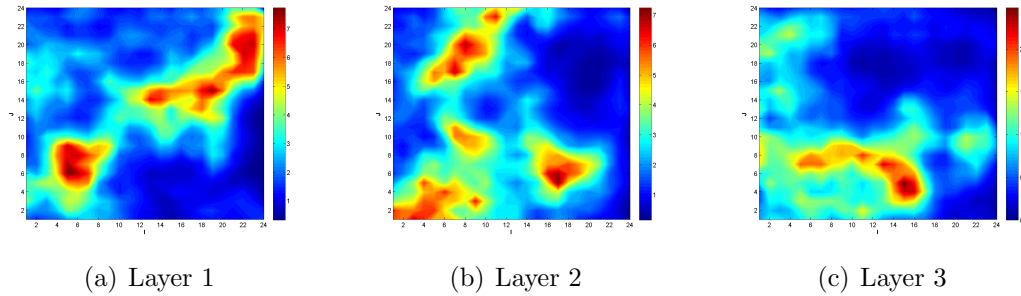
Figure 3.16: The contour plot of the quality values for each layer in the 3-D heterogeneous reservoir model

(a) Total quality contour   (b) NPV contour
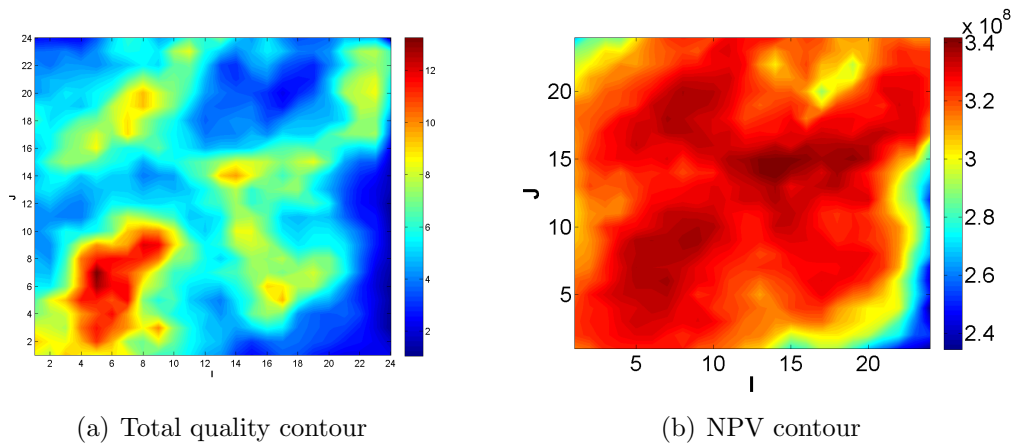
Figure 3.17: Total quality contour and NPV contour for 3-D heterogeneous reservoir model

Based on the cumulative distribution function (CDF) of the quality values, the 30th, 60th and 90th percentile values can be obtained and the colored grid cells are plotted in Figure 3.18(a). In this plot, the dark blue area has the total quality is below 30th percentile, and the light blue area has the quality values between 30th percentile and 60th percentile. Similarly, the yellow area is between 60th percentile and 90th percentile, and the red areas are above 90th percentile. Usually, for both the two reservoir models, 60th percentile will be selected to screen the productive regions.

This choice is subjective, but it appears to be suitable for our case studies. After the quality map screening, the potential regions (Figure 3.18(b)) are identified which consist of the areas that have the total quality values above 60th percentile. Because there is a lower limit in terms of the number of grid cells that in a candidate region for well placement, we have Figure 3.18(c) where smaller reservoir volumes are screened out.

(a) Quality map percentile   (b) Potential regions   (c) Effective regions
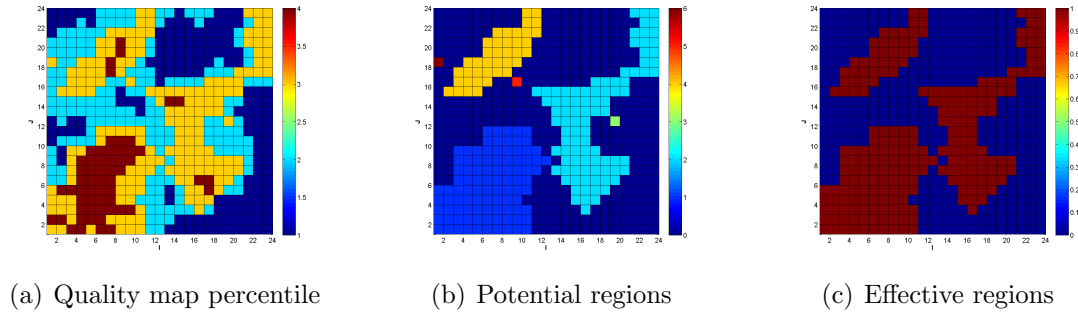
Figure 3.18: Quality map regions in 3-D heterogeneous reservoir model

Based on the fact that Figure 3.18(c) shows three effective regions, three will be selected as the optimal number for the new wells. In each region, a random location is selected to be the starting point for the FSP optimization algorithm. The FSP is applied to search for the locations of the three wells. The well location movement and NPV increase are shown in Figure 3.19. The starting point is selected in the effective quality regions, it is close to the optimal solution. Therefore, it is not necessary to use multiple starting points in this case, and we observe the algorithm quickly converges within 13 iterations.

3.3.2.3 Comparison of FSP and QM-FSP

The performance of the two methods are compared in terms of the function evaluations, computation time, and the maximum NPV. The results are tabulated in Table 3.4. For the ease of visualization, the results from Table 3.4 are plotted in bar plots in Figure 3.20. For FSP, the optimal locations are determined for 1 well, 2 wells,
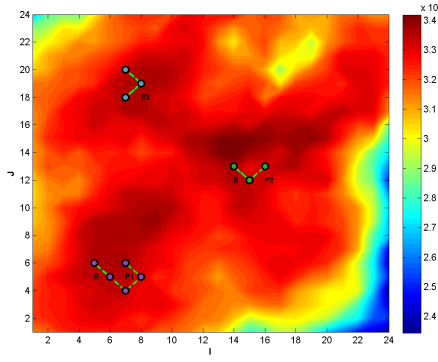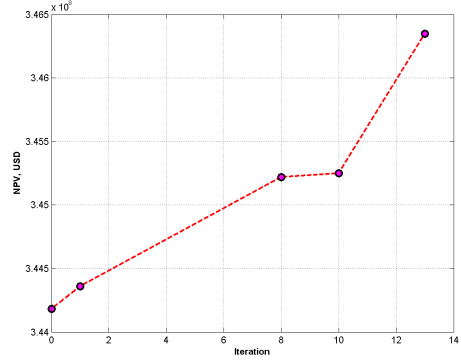
(a) Location move   (b) NPV increase

Figure 3.19: Optimization results from QM-FSP for 3-D heterogeneous reservoir model

3 wells and 4 wells. We see the NPV starts decreasing when we increase the number of wells from 3 to 4, so clearly 3 is the optimal number of wells. It should be noted that the results of QM-FSP are obtained from optimizing the locations of three wells, where the number of wells was determined by the quality map.

Table 3.4: Comparison of FSP and QM-FSP for 3-D heterogeneous reservoir model

Number of wells	1	2	3	4	QM-FSP
Function evaluations	270	222	210	138	36
CPU time, minutes	18	15.6	16.2	13.2	2.2
NPV max, USD	3.41E+08	3.44E+08	3.48E+08	3.44E+08	3.46E+08

The total computation time of each method are summarized and plotted in Figure 3.21. We see that the QM-FSP only requires less than 3 minutes of CPU time, while FSP requires over 60 minutes to reach the optimum solution. This is because in traditional optimization methods, when FSP is applied for multiple well placement, the procedure is based on the exhaustive search for the number of wells. For each scenario, they also require repeating the optimization from multiple starting points. The total computation time for FSP is the summation of the computation time consumed to solve each scenario with a fixed number of wells, until the algorithm finds the scenario that provides the maximum NPV. Consequently, the whole procedure of

(a) NPV   (b) Computation time
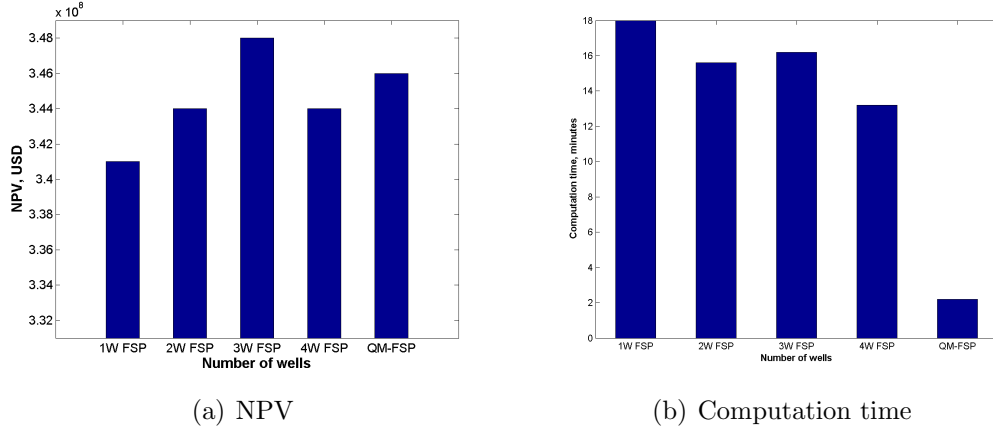
Figure 3.20: Comparison for the NPV and computation time of FSP and QM-FSP for 3-D heterogeneous reservoir model

FSP requires longer computation time.

The performance of FSP and QM-FSP is also compared based on the improvement of NPVs during the optimization iterations and is shown in Figure 3.22. In this figure, the dash lines with red dots are the FSP results with 6 random starting points, and the solid line with blue dots is the QM-FSP results using quality maps. We observe that even though the maximum NPV obtained from QM-FSP is not the highest among all the results including the ones obtained from FSP, the starting point of QM-FSP is fairly good, because it outperforms 80% of the starting points from FSP. Also, the relatively high NPV is obtained with much less computation effort based on the number of iterations required for the convergence.

3.4 Application of QM-FSP on PUNQ-S3 Field Case

After the investigation of FSP and QM-FSP on the 2-D and 3-D synthetic cases from the previous section, the application is now extended to the PUNQ-S3 field case in this section. The PUNQ-S3 geological data and the reservoir model are obtained from the website of Imperial College (Imperial College, 2009).
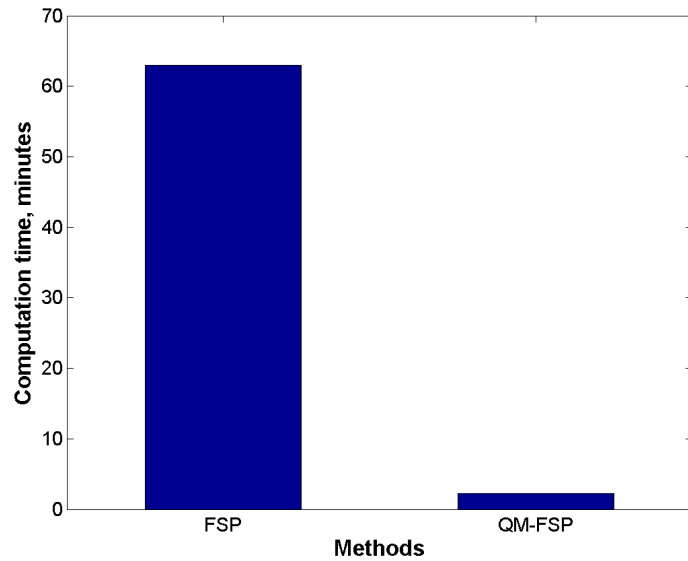
Figure 3.21: Comparison of the total computation time for FSP and QM-FSP method to optimize the number of wells and locations for a 3-D heterogeneous reservoir model.
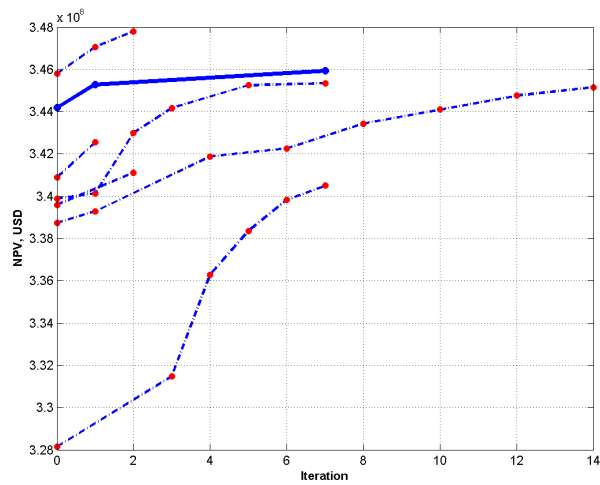
Figure 3.22: Comparison of FSP and QM-FSP optimization in number of wells and locations for 3-D heterogeneous reservoir model. (The dash lines with red dots are the FSP results with 6 random sampling of starting points over the whole reservoir, and the solid line with blue dots is the QM-FSP results with 1 random sampling in the effective quality map regions.)

3.4.1 Reservoir Description
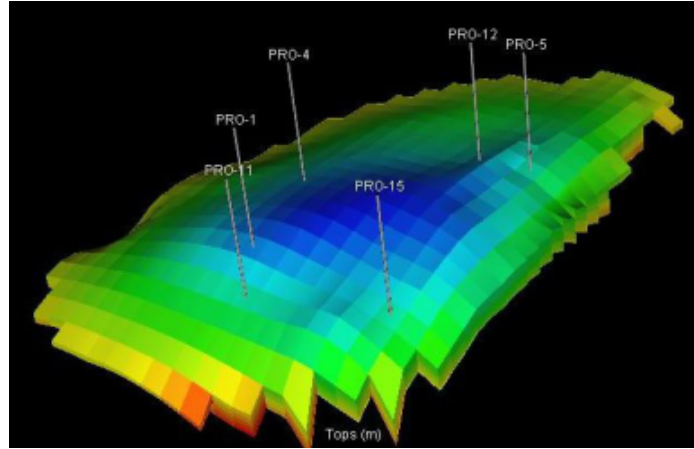
Figure 3.23: The 3-D view of the PUNQ-S3 reservoir model

The PUNQ-S3 case (Figure 3.23) is taken from a real field developed by Elf Exploration Production. The reservoir model contains $19 \times 28 \times 5$ grid blocks, among which 1761 cells are active. The grid sizes in the x- and y- directions are 1800 m, and the grid sizes in the z- direction range from 1.31 m to 8.89 m. As shown in Figure 3.24, there are originally six production wells and five infill wells located in the reservoir. The reservoir is bounded by a fault on the east and south boundary, and a strong aquifer on the north and west boundary. There is a gas cap on the top of the reservoir, located at the center of the reservoir model.

The reservoir has 5 layers, and each layer has different geological properties. The logarithm permeability and porosity of each layer are shown in Figure 3.25. In this study, the reservoir model is modified and the original wells are removed for the application of QM-FSP on well placement optimization.

In order to have an overview on the reservoir productive potentials, the NPVs are obtained by repositioning 1 producer in the reservoir, and running the simulator to get the NPV for each grid block. The NPV 3-D surface and the contour plot are shown in Figure 3.26(a). The color from dark red to dark blue indicates the NPVs vary from high to low.
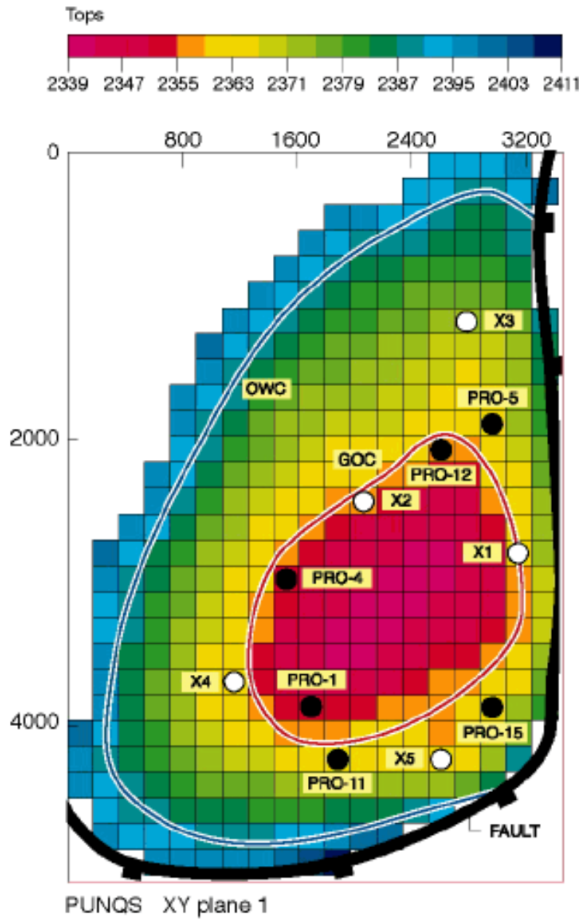
Figure 3.24: The top view of the PUNQ-S3 reservoir model (from Imperial College)

(a) lnK_x (Layer 1) (b) lnK_x (Layer 2) (c) lnK_x (Layer 3) (d) lnK_x (Layer 4) (e) lnK_x (Layer 5)

(f) lnK_z (Layer 1) (g) lnK_z (Layer 2) (h) lnK_z (Layer 3) (i) lnK_z (Layer 4) (j) lnK_z (Layer 5)

(k) ϕ (Layer 1) (l) ϕ (Layer 2) (m) ϕ (Layer 3) (n) ϕ (Layer 4) (o) ϕ (Layer 5)
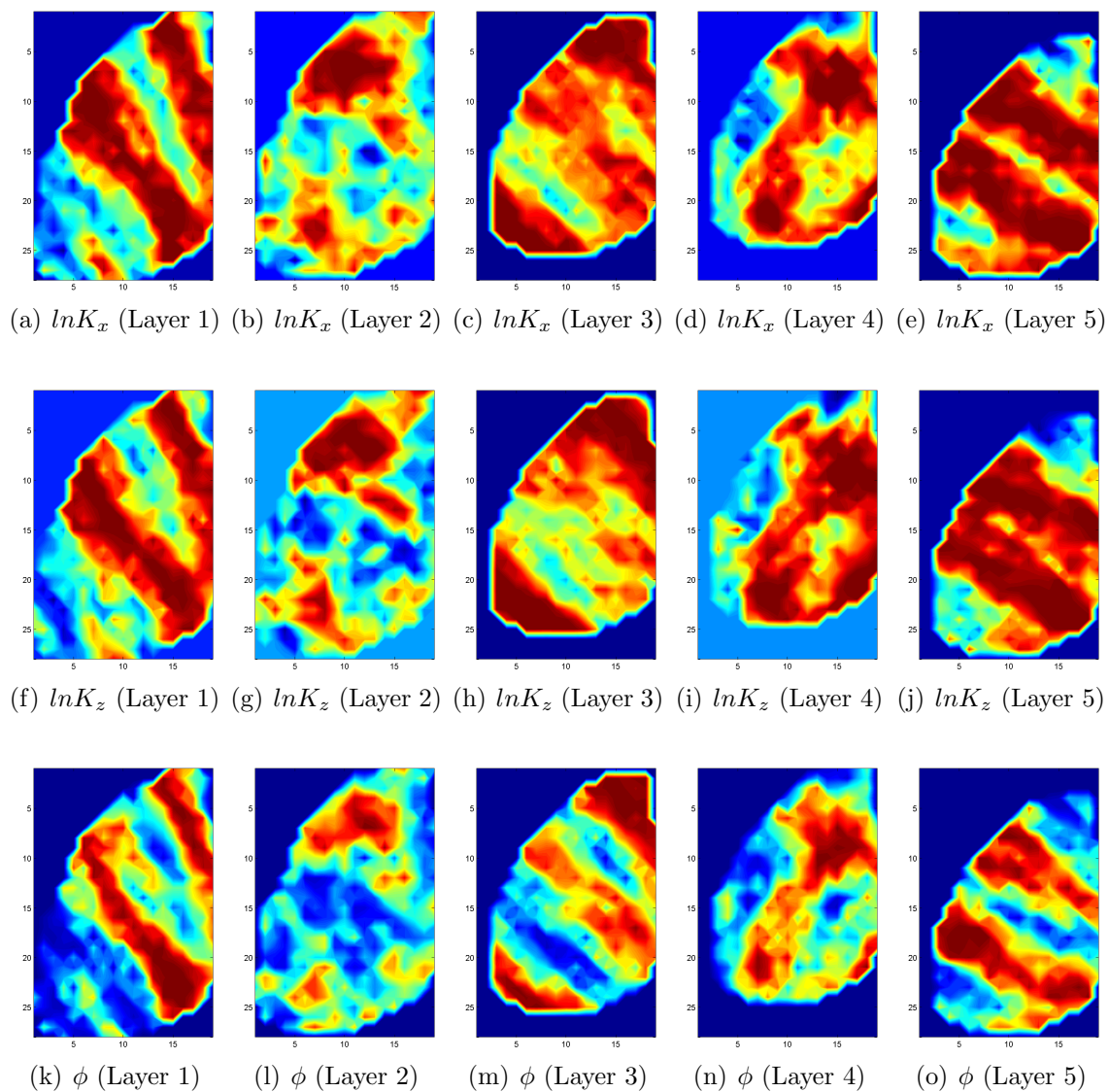
Figure 3.25: Logarithm of permeability and porosity distribution in each layer of the PUNQ-S3 reservoir model (permeability unit: mD)

(a) NPV surface   (b) NPV contour
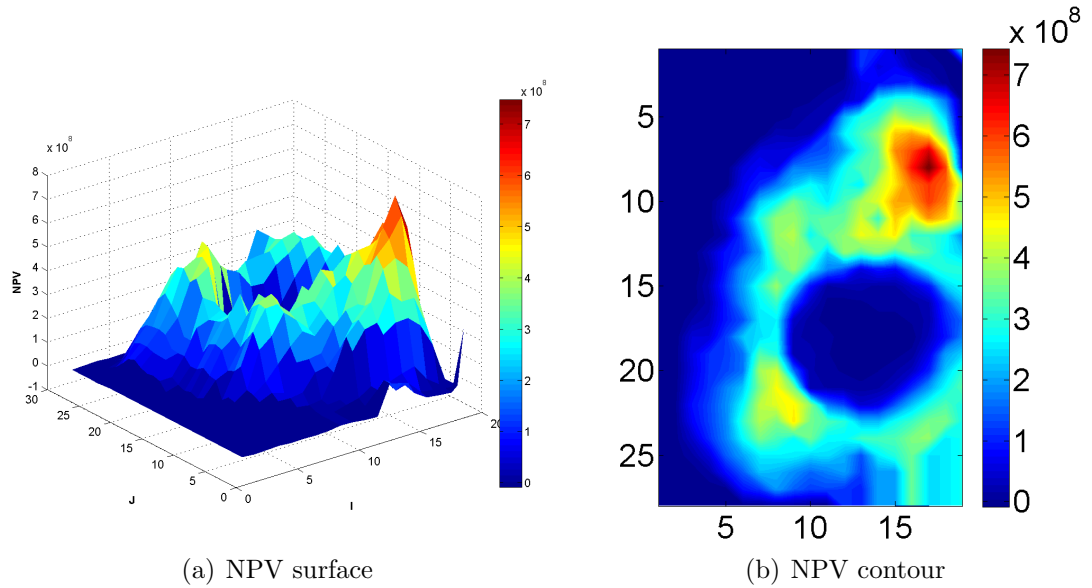
Figure 3.26: NPV surface and contour plots that indicate the high and low NPV areas for PUNQ-S3 field case

3.4.2 Exhaustive Search for Optimal Number of Wells

A test case is conducted using FSP with the exhaustive search for the number of wells. The procedure for the exhaustive search is similar with the studies in the previous section. The FSP is performed to search for the optimal solution in each scenario with a fixed number of wells. Ten starting points are generated for the experiments in each scenario.

In order to demonstrate the search path of the FSP algorithm, the scenario of 7 wells is chosen and the optimization results are shown in Figure 3.27. It also shows the movement of well locations, the optimal locations obtained and the maximum NPV achieved. In Figure 3.27(a), the background is the NPV contour map that indicates the productivity by colors. The values from high to low are represented from dark red color to dark blue color. The dots marked with "P" are the starting points, and the dots marked with "E" are the end points. For clarity, only the end points are shown in Figure 3.27(b), and we see FSP can help the well locations move from the starting points to the high NPV areas.

91

(a) Well location move

(b) Optimal locations
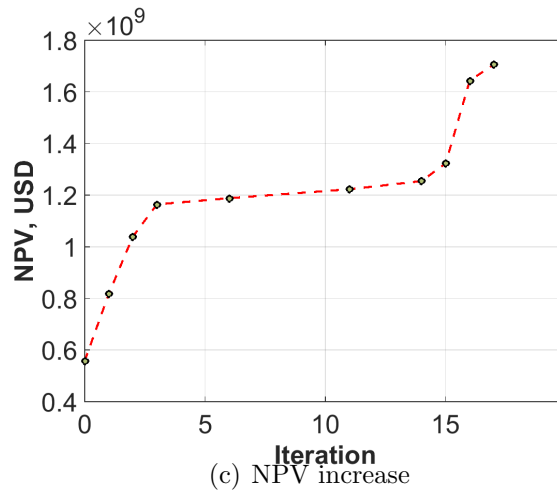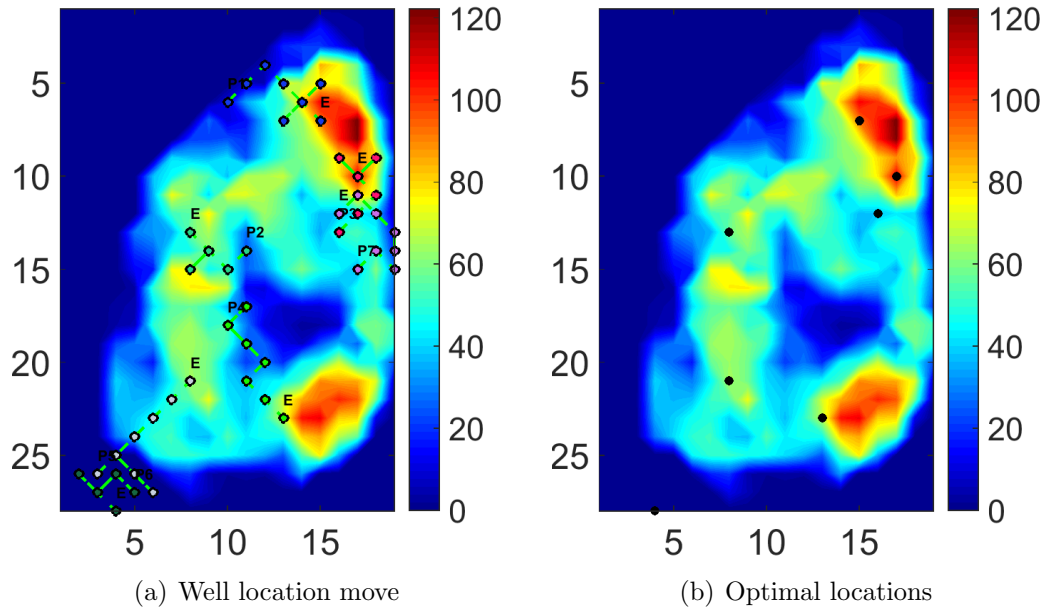
(c) NPV increase

Figure 3.27: Well location move, optimal locations and NPV increase plot for 7 wells using FSP in PUNQ-S3 field case

Similarly, the FSP is performed for other scenarios. The optimal well locations for the first eight scenarios are shown in Figure 3.28 and the results are summarized in Table 3.5. Here, I only show the optimal result with the maximum NPV obtained among the starting points. We can observe that with a fixed number of wells, FSP can move the well locations to the high NPV areas in the first few scenarios. However, if the number of wells keep increasing, there will be high possibility that a few wells will be stuck at the low NPV areas or the boundary of the reservoir model. This also indicates that the random sampling over the whole reservoir increases the possibility of poor samples while the number of wells increases.

Table 3.5: Exhaustive search for optimal number of wells using FSP

Number of wells	1	2	3	4
Maximum NPV, USD	6.72E+08	9.80E+08	1.15E+09	1.22E+09
Computation time, minutes	27.0	21.0	24.2	19.0
Number of wells	5	6	7	8
Maximum NPV, USD	1.38E+09	1.65E+09	1.71E+09	1.66E+09
Computation time, minutes	14.5	21.0	16.5	11.6

In total, the optimization with FSP is performed for the scenarios from 1 well to 11 wells. The bar plots of NPV and computation time are shown in Figure 3.29. We see that when the number of wells increases from 7 to 8, the maximum NPV starts decreasing. Therefore, 7 is the optimal number of wells, with the maximum NPV as 1.71×10^9 dollars. Figure 3.29(b) shows the computation time required for each scenario. When the number of well increases, the FSP stops earlier. This does not indicate that FSP behaves faster or more efficient, but because the more wells in the reservoir, the easier the algorithm gets trapped.

3.4.3   Quality Map Calculation

Based on the introduction and the definition of the total quality map from the previous section, the total quality map is evaluated for this field case in order to identify the high productive regions with good connectivity within the reservoir. Although there

(a) 1 well   (b) 2 wells   (c) 3 wells   (d) 4 wells

(e) 5 wells   (f) 6 wells   (g) 7 wells   (h) 8 wells
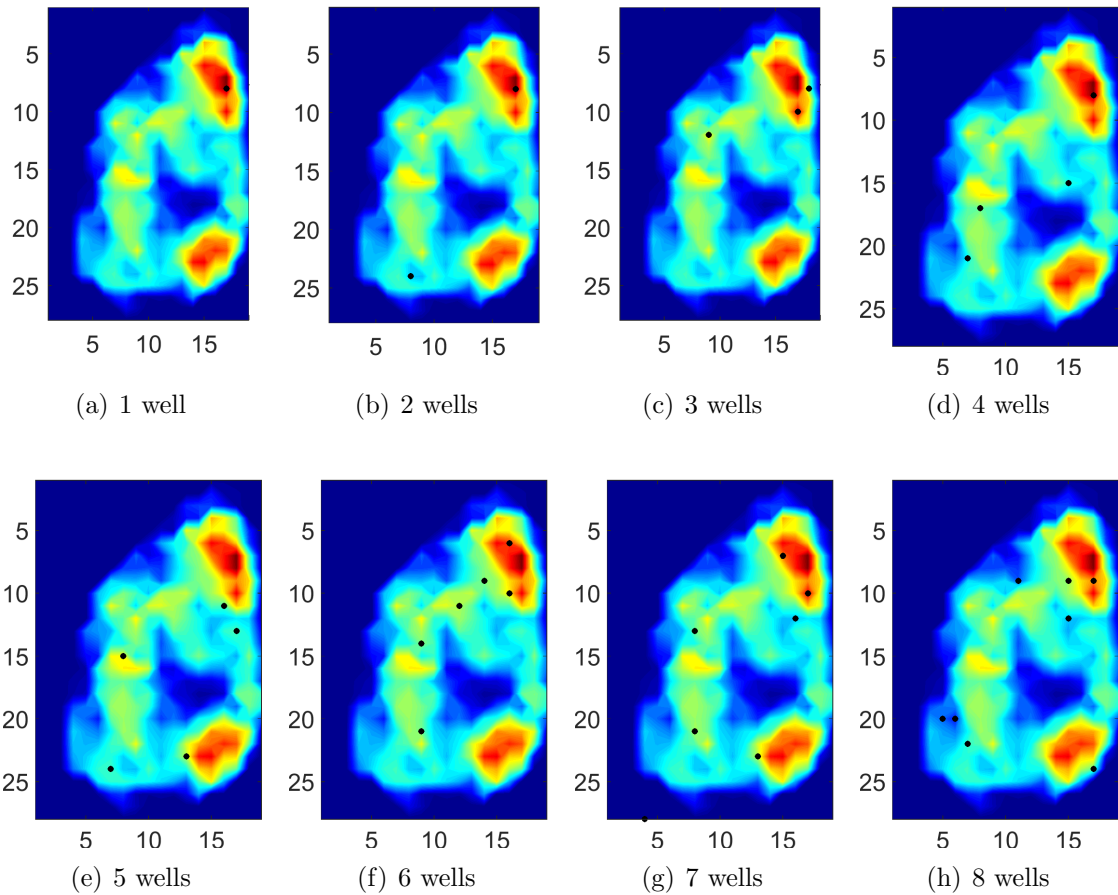
Figure 3.28: Optimal well location for different scenarios (number of wells) using FSP in PUNQ-S3 field case

(a) NPV   (b) Computation time
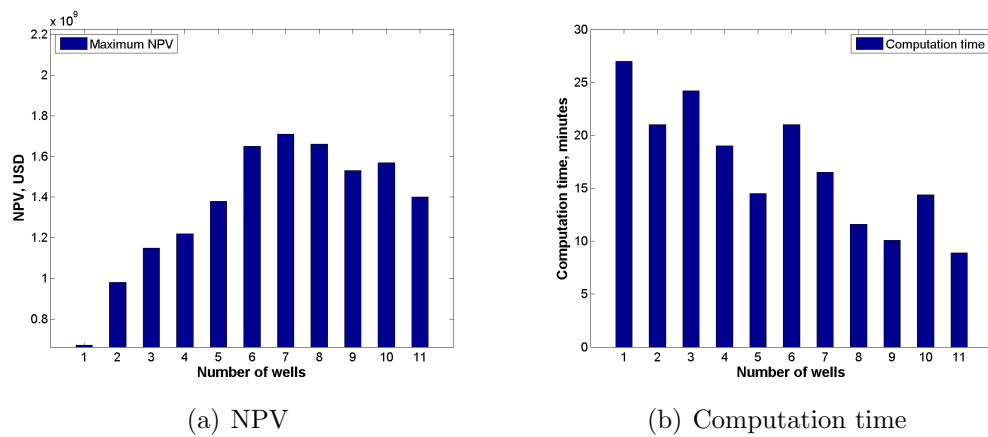
Figure 3.29: Exhaustive search for optimal number of wells using FSP in PUNQ-S3 field case

94

are three phases in this field, including oil, water, and gas, the oil production still accounts for the main revenue of the NPV, and K_{ro} will be used to penalize the total transmissibility to evaluate the regional connectivity and oil production potential. The formulations used to calculate the quality values are shown as follows,

$$T_{r,i,j,k} = \sqrt{T_{x,i,j,k}^2 + T_{y,i,j,k}^2}, \tag{3.9}$$

$$T_{q,i,j,k} = \sqrt{T_{x,i,j,k}^2 + T_{y,i,j,k}^2} \cdot K_{ro,i,j,k}, \tag{3.10}$$

$$T_{q,i,j} = \sum_{k=1}^{N_{layer}} T_{q,i,j,k}$$

$$= \sum_{k=1}^{N_{layer}} \left(\sqrt{T_{x,i,j,k}^2 + T_{y,i,j,k}^2} \cdot K_{ro,i,j,k} \right). \tag{3.11}$$

The values of the transmissibility T_x and T_y used to calculate the total quality are obtained from the reservoir model initialization. Eq. 3.9 is the calculation for transmissibility in each grid block. Eq. 3.10 is the formula to calculate the quality value of each grid block. This includes both the transmissibility and the relative oil permeability. Then the total quality map which indicates the regions of good connectivity is evaluated using Eq. 3.11. It should be noted that T_z is not used for this case, because compared to the grid size in the x- and y- directions, the grid size in z- direction is too small. This causes the small transmissibility in the z- direction, which is negligible in the calculation.

The total transmissibility contours T_r, the relative oil permeability contours K_{ro}, and the quality maps T_q for each layer are shown in Figure 3.30. The use of K_{ro} essentially reflects the presence of mobile oil on the quality map and modifies the transmissibility map to show oil mobility.

The total quality map is then calculated from the results shown in Figure 3.30.

(a) T_r (Layer 1) (b) T_r (Layer 2) (c) T_r (Layer 3) (d) T_r (Layer 4) (e) T_r (Layer 5)

(f) K_{ro} (Layer 1) (g) K_{ro} (Layer 2) (h) K_{ro} (Layer 3) (i) K_{ro} (Layer 4) (j) K_{ro} (Layer 5)

(k) T_q (Layer 1) (l) T_q (Layer 2) (m) T_q (Layer 3) (n) T_q (Layer 4) (o) T_q (Layer 5)
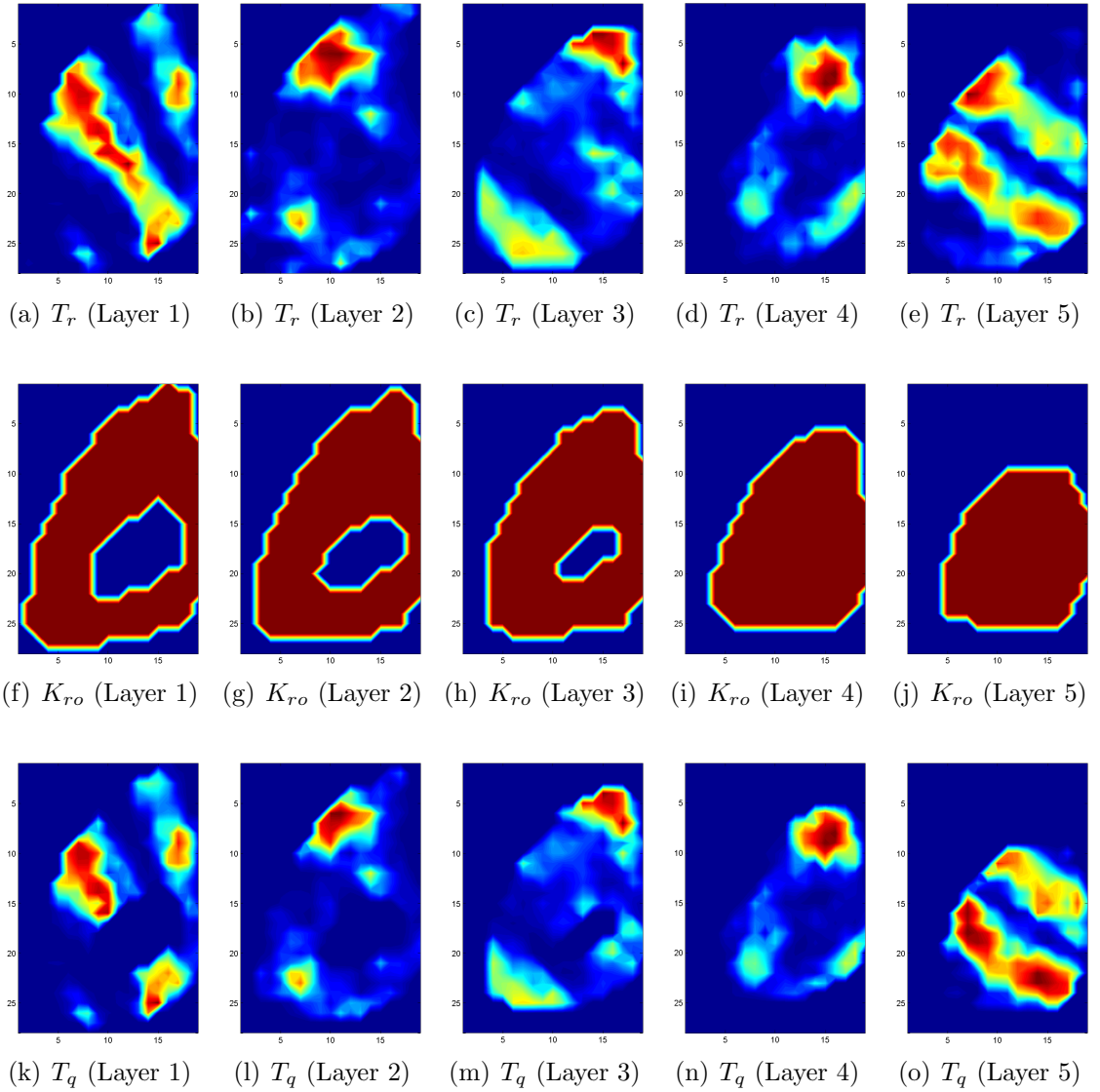
Figure 3.30: Total transmissibility (T_r) contours, relative oil permeability (K_{ro}) contours, and the connectivity (T_q) maps for each layer of the PUNQ-S3 field case

If we compare this total quality map with the NPV contour shown above (Figure 3.26(b)), we see excellent correspondence between the quality map and the productive regions of the reservoir. The NPV contour in Figure 3.26(b), however, is obtained from $19 \times 28 = 532$ simulation runs, which needs approximately half an hour of computation time, the total quality map was obtained in a few seconds. Also, the CDF of the quality values is shown in Figure 3.31(b). This is used to prepare for the following percentile maps.

(a) Total quality map (b) CDF plot
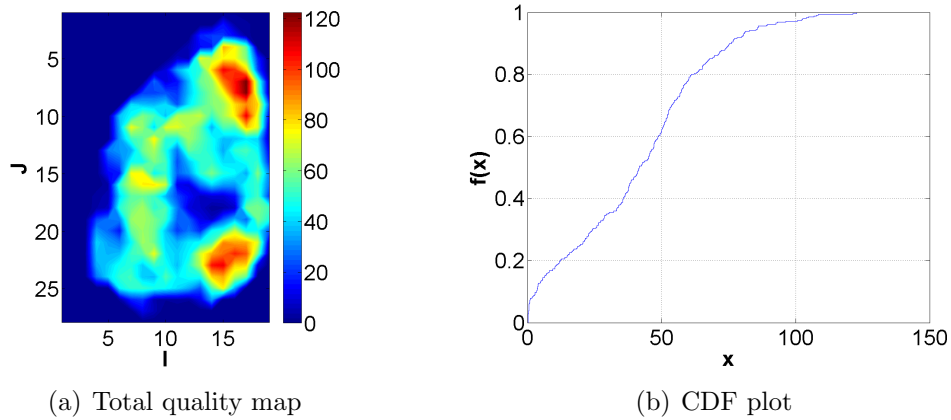
Figure 3.31: Total quality map and the cumulative distribution function (CDF) of the PUNQ-S3 field case

The 30th, 60th, 80th and 90th percentile values of the total quality are obtained from Figure 3.31(b) and are shown in Figure 3.32(a). The quality map shown in Figure 3.32(a) is screened to select regions above 80th percentile (represented by integer "4" in Figure 3.32(a)) of the total quality and other cells are not regarded as reservoir regions of interest. The results are shown in Figure 3.32(b). As stated above, the grid block sizes in the x- and y- directions are very large, and one grid block covers an area of 3 million square meters, which is 800 acres of the reservoir. Therefore, even one grid with the good connectivity can indicate high oil production drainage areas. So only one grid is used as the cut off to define the effective regions (Figure 3.32(c)) in this case. The optimal number of wells and the well locations can then be determined based on this effective region quality map.
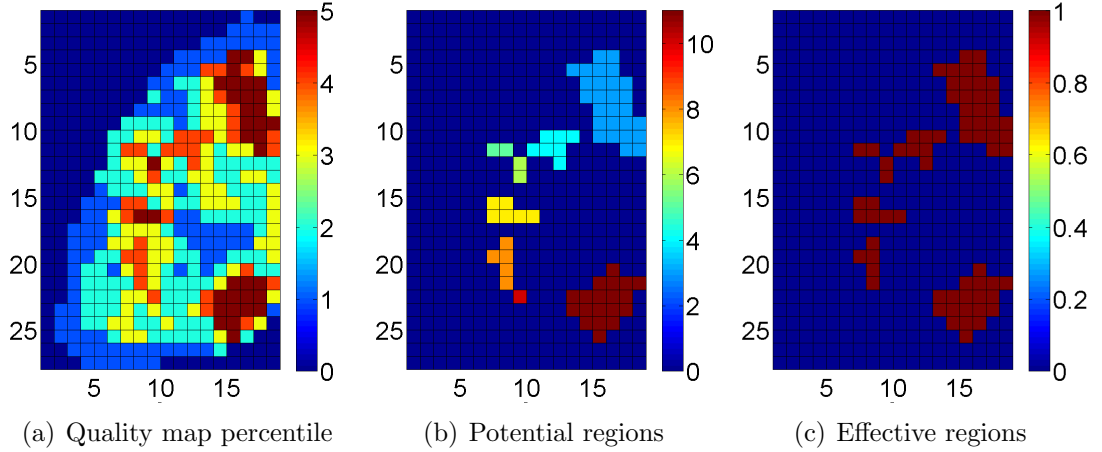
Figure 3.32: Quality map regions in the PUNQ-S3 field case

3.4.4 QM-FSP Application and Results

Theoretically, if the size of each grid cell of the reservoir model is relatively small, the effective regions in the quality map directly allow us to determine the optimal number of wells, as previously shown in the 2-D and 3-D synthetic case studies. However, in the PUNQ-S3 field case, the grid sizes are very large in horizontal directions (1800 m). Therefore, it may be possible to have more than 1 well in the regions demonstrated in Figure 3.32(c). In this situation, the area of 4 grid cells is chosen as the maximum drainage area for each well. In the large upper right region of Figure 3.32(c) which consists of 27 cells, 6 wells are placed randomly, and the lower right region with 19 cells will be placed 4 wells randomly as the starting point. For the other small regions, only 1 well will be placed in each region. Therefore, 16 wells in total will be placed in the reservoir. It is worth mentioning that the choice of a maximum drainage area for each well introduces an element of subjectivity to this approach.

Given the uncertainty of the quality map approach, it is possible that other optimal solutions for the number of wells also exist. Therefore, the experiments for 15, 17 and 18 wells are also performed in the same manner as the experiment of placing 16 wells. The optimal well locations for these scenarios are shown in Figure 3.33.

The results for the maximum NPV achieved and the required computation time of these scenarios are shown in Table 3.6 and are plotted in Figure 3.34. From the table we see either 16 wells or 17 wells achieve the same NPV at 2.22×10^9 dollars. Since the well locations in the quality map effective regions are already very close to the optimal solution, when the FSP method is applied to optimize the well locations, they converge in one or two iterations, or in some test, the starting points are already the optimal solution, so they are not showing the search path and NPV increase for these scenarios.

(a) 15 wells   (b) 16 wells   (c) 17 wells   (d) 18 wells
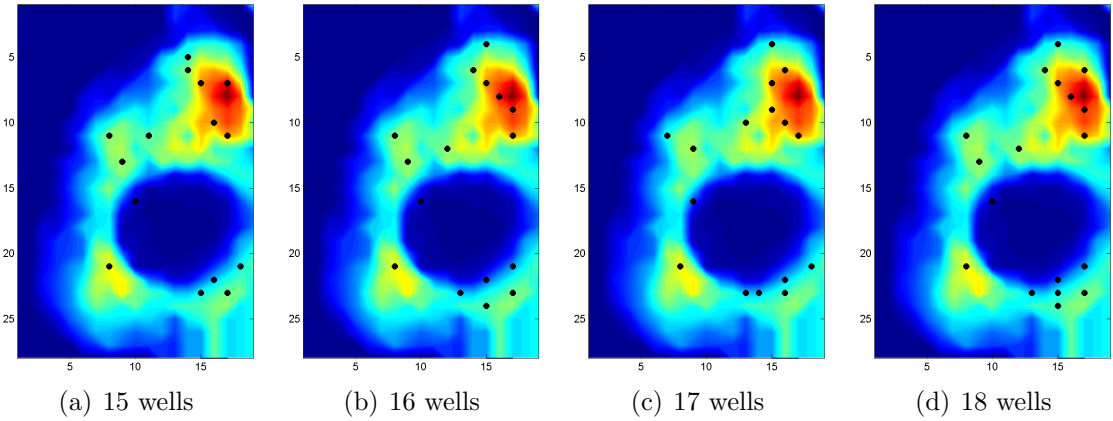
Figure 3.33: Optimal well locations on the top of NPV contour plot for different scenarios (number of wells) using QM-FSP in PUNQ-S3 field case

Table 3.6: Results for optimal number of wells using QM-FSP in PUNQ-S3 field case

Number of wells	15	16	17	18
Maximum NPV, USD	2.19E+09	2.22E+09	2.22E+09	2.21E+09
Computation time, minutes	2.5	2.1	3.5	2

If we see the maximum NPV achieved in QM-FSP together with the exhaustive searching experiments with FSP (Figure 3.35), we observe that QM-FSP provides a scenario with 16 wells that can achieve a much higher NPV. This solution was missed in the traditional FSP method, even though the exhaustive search was performed.

(a) NPV

(b) Computation time
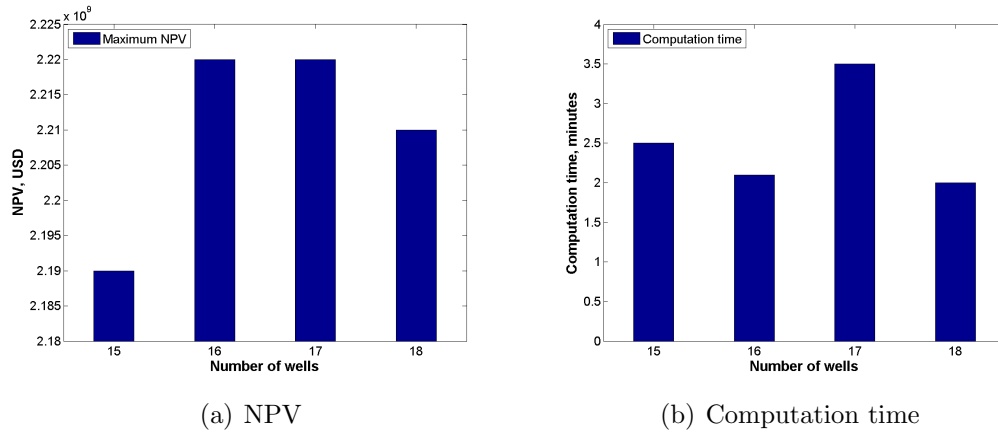
Figure 3.34: Results for optimal number of wells using QM-FSP in PUNQ-S3 field case
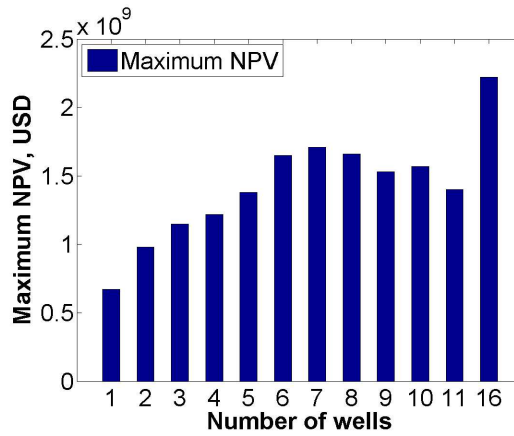
Figure 3.35: Results for optimal number of wells using FSP and QM-FSP in PUNQ-S3 field case. The optimal solutions for scenarios with 1 to 11 wells are obtained from traditional FSP method, and the solution with 16 wells is obtained from QM-FSP method.

The comparison of the maximum NPV values and computation time for the traditional approach and QM-FSP are shown in Figure 3.36. From Figure 3.36(a), we see that the maximum NPV value obtained from QM-FSP increases by 30% compared to the results obtained from the traditional method of using FSP. Moreover, the quality map-guided approach allows rapid determination of the number of wells, while traditional methods require adopting a trial-and-error approach with a changing number of wells. This field case study demonstrates the advantages of QM-FSP again in terms of the quality of the solution obtained and the practical benefits of savings in computation times.

(a) NPV

(b) Computation time
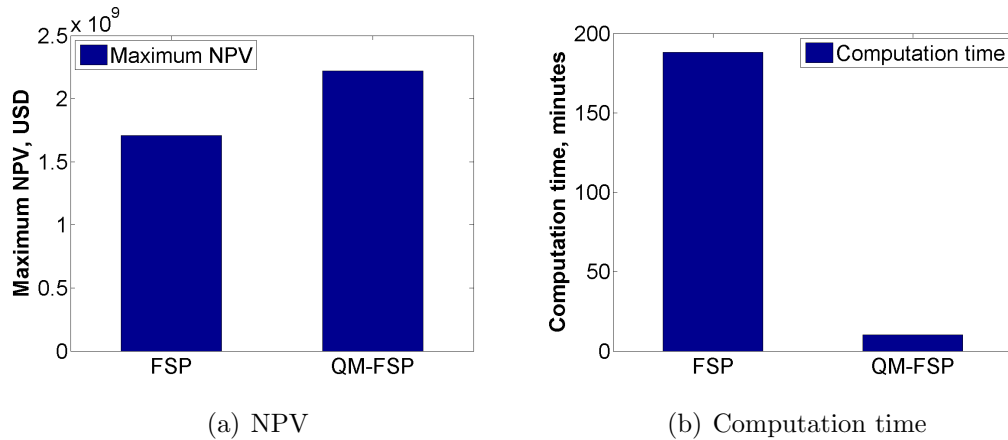
Figure 3.36: Comparison of NPV and optimal number of wells from FSP and QM-FSP in PUNQ-S3 field case

3.5   Summary

In this chapter, I present a promising approach to optimally place multiple wells when the number of wells is not known *a priori*. The method is based on using a quality map-assisted fixed-gain SPSA algorithm (QM-FSP). The basic idea in the use of quality maps is to identify the potential productive regions in a reservoir. The use of quality maps enables the rapid placement of productive wells, and it is rooted strongly in engineering considerations including reservoir connectivity and oil production potential, and can be coupled to any suitable optimization algorithm.

The traditional exhaustive search for the optimal number of wells would require the use of a trial-and-error approach, and the number of function evaluations required are usually very large, so it is very costly. For large fields, the traditional approach may miss the optimal solution even with extensive simulation runs. The multiple well placement using QM-FSP introduced in this chapter has been demonstrated for several case studies and is able to provide a solution with an order of magnitude reduction in computational effort over traditional applications.

CHAPTER IV

MULTI-OBJECTIVE WELL PLACEMENT OPTIMIZATION

4.1 Introduction

With the advent modern drilling techniques, placing wells into more challenging environments becomes technically and economically feasible. Some of these technologies include multi-lateral wells and extended reach wells that are now common in the US especially for unconventional reservoirs.
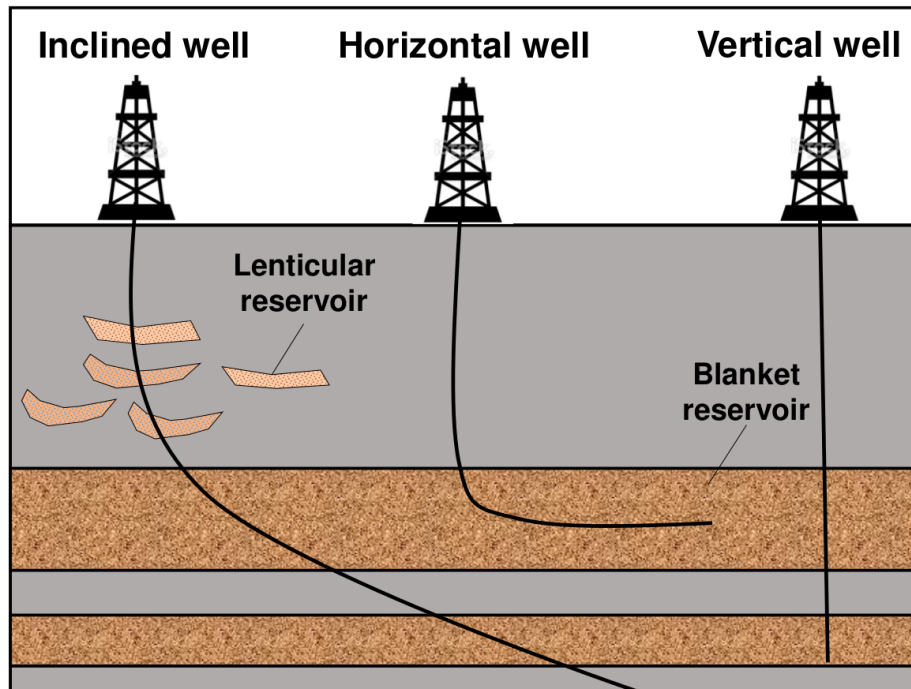
Figure 4.1: Demonstration of different well types.

Hydrocarbon reservoirs may contain multiple hydrocarbon-bearing formations with various depositional environments as shown in Figure 4.1. However, if the subsurface

formation structure is poorly understood, placing wells can be difficult and of high risk. For example, the following two scenarios in Figures 4.2(a) and 4.2(b) demonstrate poor choices of drilling locations that cause the failure of well placement. Both figures illustrate the outcome of poor reservoir characterization that should have been taken into account in the decision-making process.

(a) Anticline   (b) Fault
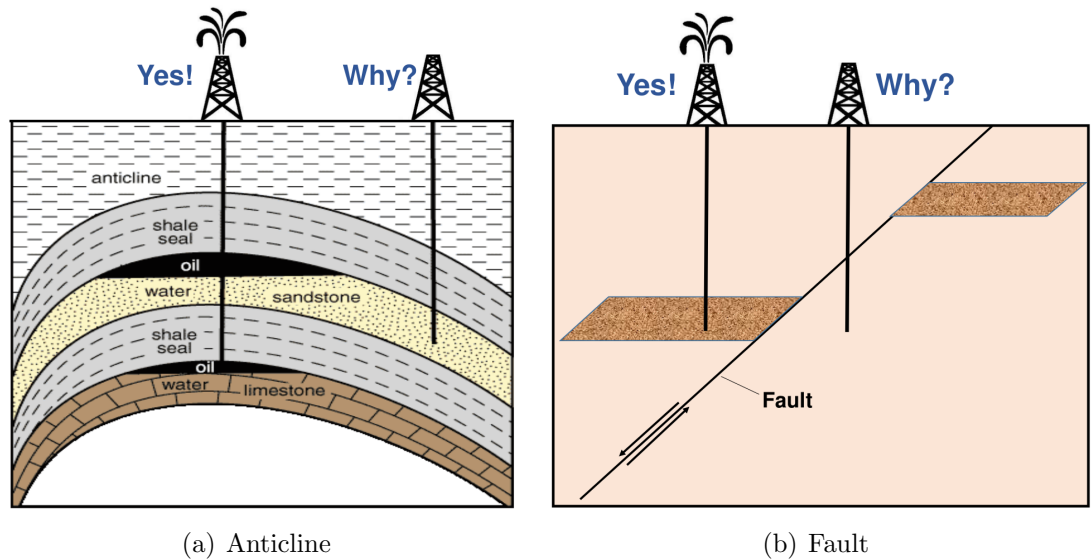
Figure 4.2: Two examples of the unsuccessful well placement.

In reservoir characterization and modeling, the multiple-realization approach has been recognized as an important tool to address the uncertainty estimation (Cottini-Loureiro and Araujo, 2005; Ozdogan and Horne, 2006). For instance, Guyaguler and Horne (2004) consider the reservoir uncertainty in their well placement problem, by carrying out the experiments on 23 history matched realizations with the PUNQ-S3 model. The objective function is the average NPV over 23 realizations. The average NPV provide some information for the uncertainty of the reservoir model, however can not quantify the range of model uncertainty propagated to the objective functions. Therefore, in this work, multi-objective optimization techniques are applied to consider not only the mean but also the variance of the net present value (NPV) for all geological realizations to obtain robust solutions that mitigate the impact of

geological uncertainty.

The objective of this work is to develop a new workflow of well placement optimization process with geological uncertainty to improve decision-making process efficiently and effectively. Specifically, I consider the following problems for well placement optimization:

- How to parameterize and optimize well perforations and inclined wells?

- How to take into account and mitigate the impact of geological uncertainty?

- How to consider the risk attitude of decision-makers in the well placement?

4.2 Problem Formulation

Our goal of the well placement optimization is to maximize the NPV function by optimizing well locations $\mathbf{x}$ for a specified reservoir model. The vector $\mathbf{x}$ contains variables related to well configurations, such as the grid index of well locations, the perforations of vertical wells and the grid index of the heel and toe of inclined wells. For example, the well location of a vertical well is defined with four variables, including $x_{w,i}, x_{w,j}, x_{w,t}, x_{w,b}$, where the indices w and i, j represent the specific well index with its associated lateral coordinates i and j. The vertical coordinates are defined based on perforations. The term $x_{w,t}$ denotes the depth of perforation at the top layer while $x_{w,b}$ denotes the perforation depth at the bottom layer. The depth is represented by grid index in the z-direction. I also assume that all layers between the top and the bottom are perforated. For the total number of N_w wells, $\mathbf{x}$ is defined as

$$\mathbf{x} = [x_{1,i}, x_{1,j}, x_{1,t}, x_{1,b}, \cdots, x_{N_w,i}, x_{N_w,j}, x_{N_w,t}, x_{N_w,b}]^T. \qquad (4.1)$$

If a well is inclined as shown in Figure 4.3, the variables to be optimized are the locations of the heel and the toe of each well, $x_{w,h_i}, x_{w,h_j}, x_{w,h_k}, x_{w,t_i}, x_{w,t_j}, x_{w,t_k}$. For N_w wells, $\mathbf{x}$ is defined as

$$\mathbf{x} = \left[x_{1,h_i}, x_{1,h_j}, x_{1,h_k}, x_{1,t_i}, x_{1,t_j}, x_{1,t_k}, \cdots, x_{N_w,h_i}, x_{N_w,h_j}, x_{N_w,h_k}, x_{N_w,t_i}, x_{N_w,t_j}, x_{N_w,t_k} \right]^T,$$

$$(4.2)$$

where h_i, h_j, h_k are the coordinates of the heel while t_i, t_j, t_k are the coordinates of the toe. The objective function is a scalar valued function of a given well configuration
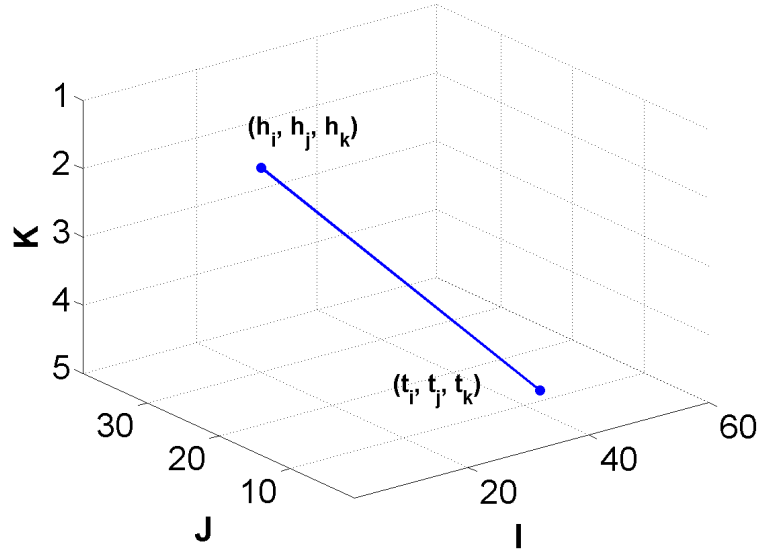
Figure 4.3: 3-D representation of an inclined well

for a given geological realization of the reservoir, as formulated in Eq. 2.1. The NPV formulation is shown as below.

$$J(\mathbf{x}) = \sum_{k=1}^{N_t} \left(\frac{C_o \Delta q_{o,k}(\mathbf{x}) + C_g \Delta q_{g,k}(\mathbf{x}) - C_{wp} \Delta q_{wp,k}(\mathbf{x}) - C_{wi} \Delta q_{wi,k}(\mathbf{x})}{(1+d)^{k\Delta t}} \right) - C_d$$

If the wells are inclined or horizontal, according to Yeten et al. (2003) and Bouzark-ouna (2012), the drilling cost C_d is given as

$$C_d = \sum_{w=1}^{N_w} \left[A \cdot d_w \cdot ln(l_w) \cdot l_w \cdot (2 - \alpha) \right], \tag{4.3}$$

where N_w is the number of wells, A is a user defined coefficient to adjust the drilling cost according to the drilling conditions (Yeten, 2003), d_w is the diameter of the well bore and l_w is the length of the inclined well. Here, the parameter α is a variable that represents the well inclination, defined as

$$\alpha = \frac{h_k - t_k}{l_w}, \tag{4.4}$$

where h_k and t_k are the locations of the heel and the toe in z-direction. Thus, $\alpha = 1$ for vertical wells and $\alpha = 0$ for horizontal wells.

4.3   Multi-Objective Optimization

As indicated earlier, uncertainty in reservoir characterization is often accounted for by the use of multiple geological realizations. Each realization may be individually assessed for optimal well placement. However, from a decision-making point of view, this provides limited utility for well placement.

In this work, I not only optimize the mean of the NPV but also consider the robustness of the solutions that is defined as the spread of NPV acquired from all realizations. I quantify the spread of NPV by the standard deviation. A higher value of the standard deviation of the NPV indicates that the NPV of the proposed well configuration may deviate significantly from its expected value and may result in a higher risk of failure (a lower NPV than expected).

Considering a feasible criterion space of two objectives, the solutions depend on the minimization or maximization of the respective objective functions as shown in Figure 4.4. Given the same variable space, the optimization of objective functions searches for different optimal solutions that depend on the definition of objectives. In this work, both objective functions are formulated as minimization problems. Therefore, I minimize the negative mean NPV which provides the same results as the
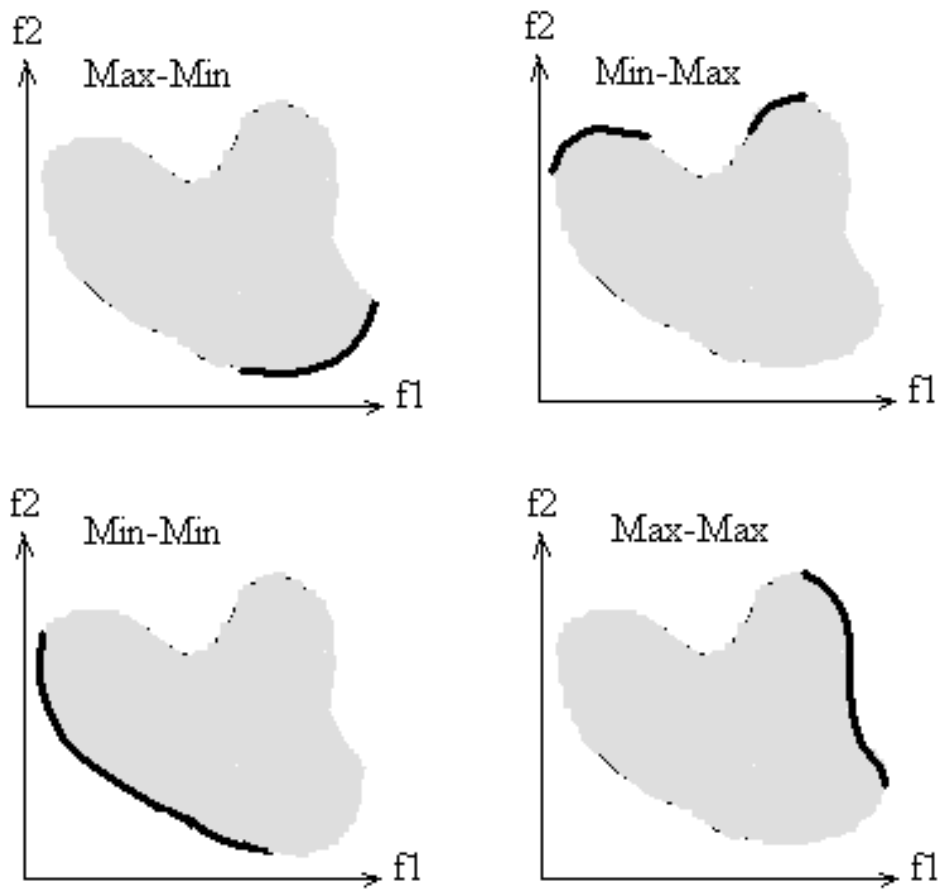
Figure 4.4: Example of the optimal solutions with different objective combinations. (Source: wiki.ece.cmu.edu)

maximization of the positive mean NPV. Equation 4.5 shows the mathematical formulation of the multi-objective optimization problem.

$$
\begin{aligned}
\text{Minimize:} \quad & f_1(\mathbf{x}) = -\mu(J(\mathbf{x})) \\
\text{Minimize:} \quad & f_2(\mathbf{x}) = \sigma(J(\mathbf{x})) \\
\text{Subject to:} \quad & \mathbf{x} \in \mathbf{u}
\end{aligned}
\tag{4.5}
$$

where $\mu(J(\mathbf{x}))$ and $\sigma(J(\mathbf{x}))$ are the mean and standard deviation of NPV evaluated over all geological models. $\mathbf{u}$ is the feasible domain for $\mathbf{x}$.

4.3.1 NSGA-II Algorithm

Although there exist various methods to solve multi-objective optimization problems, NSGA-II has been proven to be one of the algorithms that perform well on different types of objective functions (Zitzler et al., 2003). In this section, I provide an overview of the NSGA-II algorithm.

The workflow of the original NSGA algorithm can be found in Srinivas and Deb (1994). Later, Deb et al. (2002) propose a modified NSGA-II algorithm to address the issues of the original NSGA algorithm: computational complexity and lacking of elitism. Here, elitism is defined as the property of individuals that possess superiority with regard to objective function values.

Before describing the algorithm, I will first introduce the concept of domination. For the minimization problems described in Eq. 4.5, given two feasible solutions $\mathbf{x}_1$ and $\mathbf{x}_2$, $\mathbf{x}_1$ is said to dominate $\mathbf{x}_2$, if

1. $f_i(\mathbf{x}_1) \leq f_i(\mathbf{x}_2)$ for all indices $i \in \{1, 2\}$ and

2. $f_j(\mathbf{x}_1) < f_j(\mathbf{x}_2)$ for at least one index $j \in \{1, 2\}$

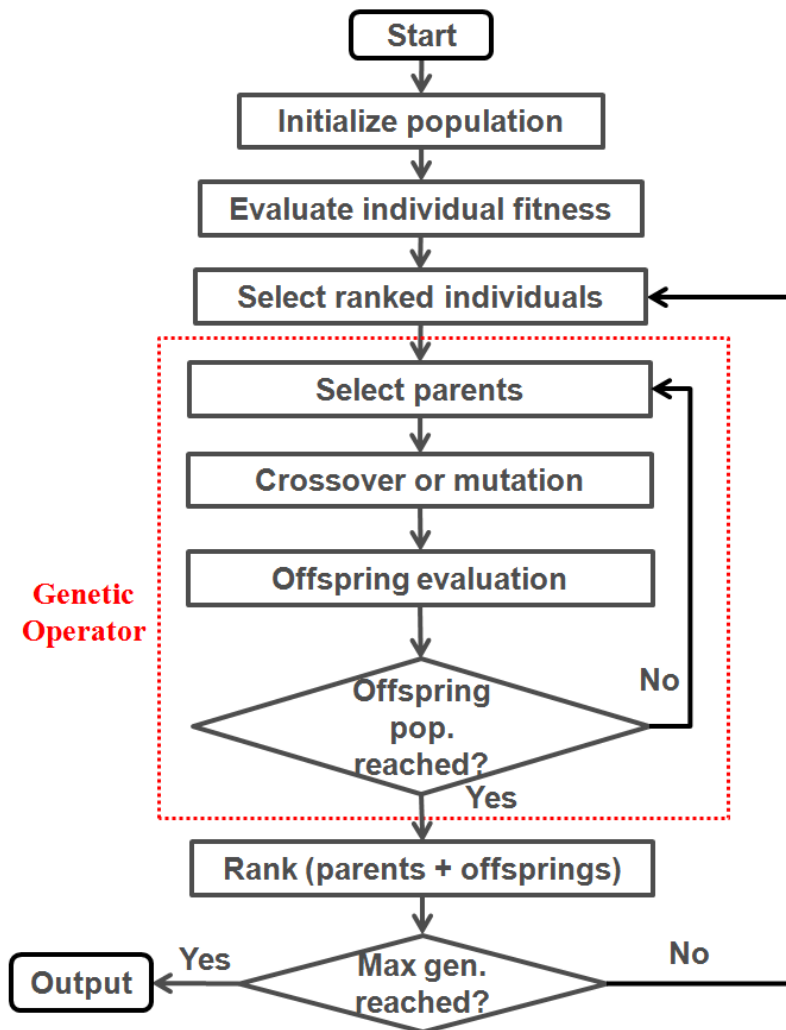The flowchart for NSGA-II is shown in Figure 4.5, followed by a description of each of the steps.

Figure 4.5: NSGA-II algorithm flowchart. 'pop.' stands for population. 'gen.' stands for generation.

1. Population initialization: The initial population of NSGA-II algorithm may be selected depending on the dimension of the variables. In my study, the initial population refers to the set of initial guesses of well locations. I chose a number of initial populations that equals to the number of variables. Without any prior knowledge, the initial population may be generated randomly with the use of constraints, if any. With prior knowledge, the choice of an initial population can be used to accelerate the convergence and save computation time. In this work, I compare the performance of the workflow for the situations with and without prior knowledge.

2. Non-dominated sorting: Following function evaluations of the individuals at each iteration, the individuals are ranked by considering the fitness and crowding distances. Fitness is the ability of an individual to survive and reproduce for the next generation, while crowding distance is a measurement of how close an individual is to its neighbors and it is calculated as the summation of individual distances corresponding to each objective (Deb et al., 2002). In order to seek solutions that result in appropriate values of objective functions and possess good diversity, I rank the individuals based on the objective functions and the crowding distance between every two individuals. For instance, if two locations are to be selected out of three well locations $(1, 1), (2, 2), (4, 4)$ in the same generation, and these locations are non-dominated individuals, based on the crowding distance at each location, $(1, 1)$ and $(4, 4)$ will be selected to keep the diversity of the solutions.

3. Genetic operator: Based on the ranking of individuals, top-ranked individuals are chosen as parents and genetic operator is performed to generate offspring individuals. The genetic operator is described in details below. Objective functions are then evaluated for each individual in the offspring populations. The

genetic operator formulation can be found in Seshadri (2006). Real-coded genetic algorithm uses Simulated Binary Crossover (SBX) (Deb and Agrawal, 1995) and polynomial mutation (Raghuwanshi and Kakde, 2004). Here, the formulation of genetic operator are given according to Seshadri (2006).

(a) Simulated Binary Crossover: Given $p_{1,k}$ and $p_{2,k}$ as the kth elements of selected parents, then the kth element of the ith child $c_{i,k}$ can be generated from the binary crossover as

$$
\begin{aligned}
c_{1,k} &= \frac{1}{2}[(1 - \beta_k)p_{1,k} + (1 + \beta_k)p_{2,k}] \\
c_{2,k} &= \frac{1}{2}[(1 + \beta_k)p_{1,k} + (1 - \beta_k)p_{2,k}]
\end{aligned}
\tag{4.6}
$$

where $\beta_k (\geq 0)$ is a random number sampled from the density

$$
\begin{aligned}
p(\beta) &= \frac{1}{2}(\eta_c + 1)\beta^{\eta_c}, \text{if } 0 \leq \beta \leq 1 \\
p(\beta) &= \frac{1}{2}(\eta_c + 1)\frac{1}{\beta^{\eta_c+2}}, \text{if } \beta > 1.
\end{aligned}
\tag{4.7}
$$

This distribution can be obtained from a random number u that is uniformly sampled between $(0, 1)$.

$$
\begin{aligned}
\beta(u) &= (2u)^{\frac{1}{\eta_c+1}} \\
\beta(u) &= \frac{1}{[2(1 - u)]^{\frac{1}{\eta_c+1}}}
\end{aligned}
\tag{4.8}
$$

where η_c is the distribution index for crossover. $\eta_c = 20$ as suggested in Deb et al. (2002).

(b) Polynomial Mutation: Given p_k as parent population within the bound (p_k^l, p_k^u), the child population c_k can be generated as

$$
c_k = p_k + (p_k^u - p_k^l)\delta_k
\tag{4.9}
$$

where δ_k is a small variation calculated from a polynomial distribution using

$$\delta_k = (2r_k)^{\frac{1}{\eta m+1}} - 1, \text{if } r_k < 0.5$$

$$\delta_k = 1 - [2(1 - r_k)]^{\frac{1}{\eta m+1}}, \text{if } r_k \geq 0.5. \tag{4.10}$$

where η_m is the mutation distribution index and r_k is a uniformly sampled random number between $(0, 1)$. $\eta_m = 20$ as suggested in Deb et al. (2002).

4. Recombination and selection: Both parents and offspring are combined for non-dominated sorting to evaluate their fitness values where the best (top-ranked) individuals will be the parents of the next generation. Two individuals are referred to as the non-dominant if neither individual is superior to the other by comparing different objectives. The rank (fitness) of individuals are assigned so that individuals in the first front (Pareto front) are always the non-dominant while individuals in the second rank are dominated by the individuals in the first rank. This is further illustrated in Figure 4.6. For the selection process, the individuals from the first rank are selected with priority. If the designed population size is not reached, the individuals from the second rank will be considered; this operation is repeated until the number of individuals is satisfied. Then, the selected individuals will become the next generation parents.

A demonstration of the NSGA-II algorithm is shown in Figure 4.6. The colored dots in the objective space represent the values of the objective functions for a given set of candidate well locations. The colors indicate different iterations. In this figure, the algorithm starts from the upper-right corner with the blue dots represent the objective functions for the initial guess of well locations (represented by the black dots in the variable space). After a certain number of iterations N_i, the algorithm stops at the Pareto front presented by the red dots at the lower-left corner. The concept of non-dominated solutions is presented by the points marked with "A" and "B" in this figure. We see point A is a non-dominated solution compared to point

B, because point A is superior compared to point B in terms of both the objective functions.
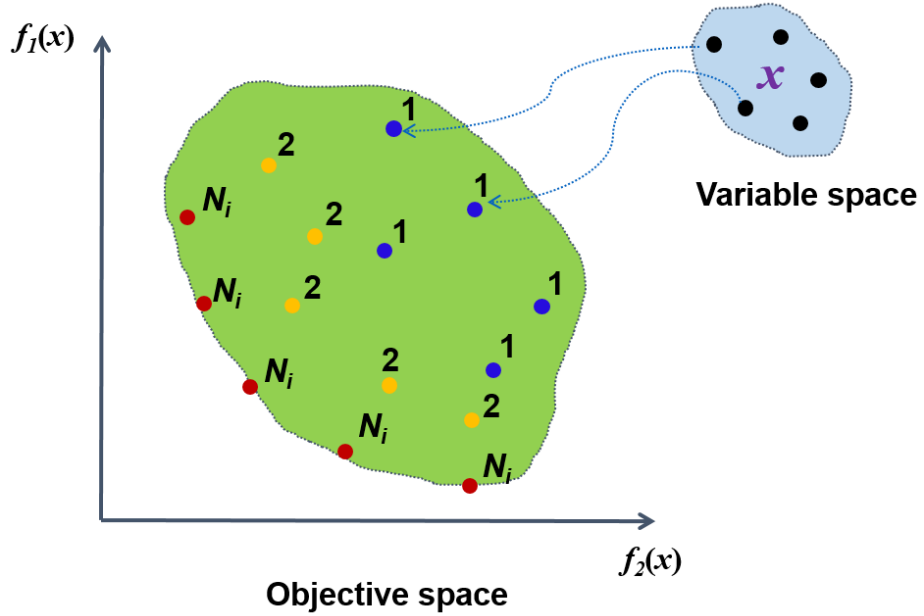

Figure 4.6: A demonstration of the NSGA-II algorithm. The colored dots represent values of the objective functions $f_1(x)$ and $f_2(x)$ at each iteration $1, 2, N_i$ for five candidate well locations.

4.3.2 Accelerating Optimization Process

Since multi-objective optimization requires numerous objective function evaluations and can be time consuming, it may be infeasible for practical applications. One method of accelerating the multi-objective optimization is to use prior knowledge to reduce the size of the search domain for well locations. In this study, an Oil-in-Place (OIP) map is used as a guide for potential well locations in the reservoir. The OIP map is approximated from the value of OIP in each grid defined as

$$OIP_{i,j} \cong \sum_{k=1}^{N_{layer}} (V_{pore} \cdot S_o)_{i,j,k} \tag{4.11}$$

$$\cong \sum_{k=1}^{N_{layer}} (\Delta z \cdot NTG \cdot \phi \cdot So)_{i,j,k}$$

114

where i, j are grid coordinates; S_o represents the oil saturation in each grid cell. V_{pore} represents a corresponding pore volume which are approximated by the reservoir thickness Δz, the net to gross ratio NTG and the porosity ϕ. The search space for well locations is restricted to grid locations (i, j) where the potential oil target is large, as quantified by $OIP_{i,j}$.

Well placement optimization for large fields can also be challenging due to the computational needs associated with modeling fluid flow through reservoir simulation. In order to accelerate the simulation process, a physical surrogate of reservoir models is used which is obtained by upscaling techniques. This will be demonstrated later in a field case study in Section 4.5. A general overview of upscaling is provided in Figure 4.7.
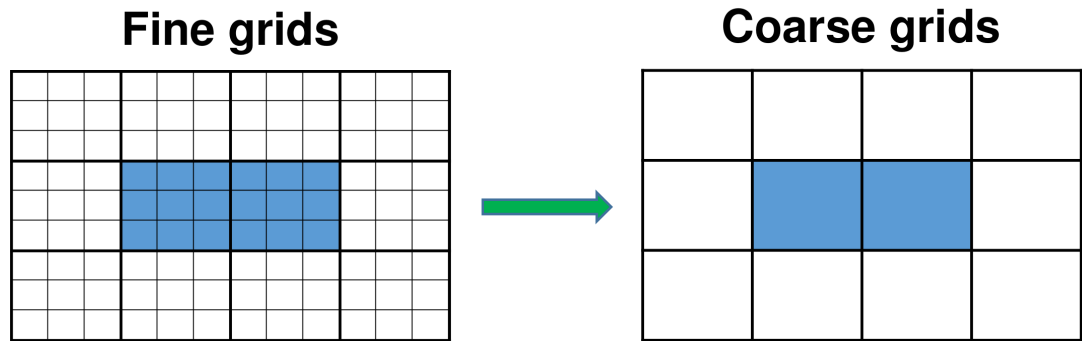

Figure 4.7: Demonstration of reservoir upscaling

For the case studies in the following sections, Figure 4.8 provides an overview of the optimization process. Starting from the variable space $\mathbf{x}$, I first prepare well configurations for simulation. Then, I combine the well configuration with different geological realizations to evaluate the NPV of all the geological models. Parallel computing is used to reduce the total simulation time. After obtaining all the NPV, the mean and standard deviation of the NPV are used as separate objective under multi-objective optimization framework as described above using NSGA-II.
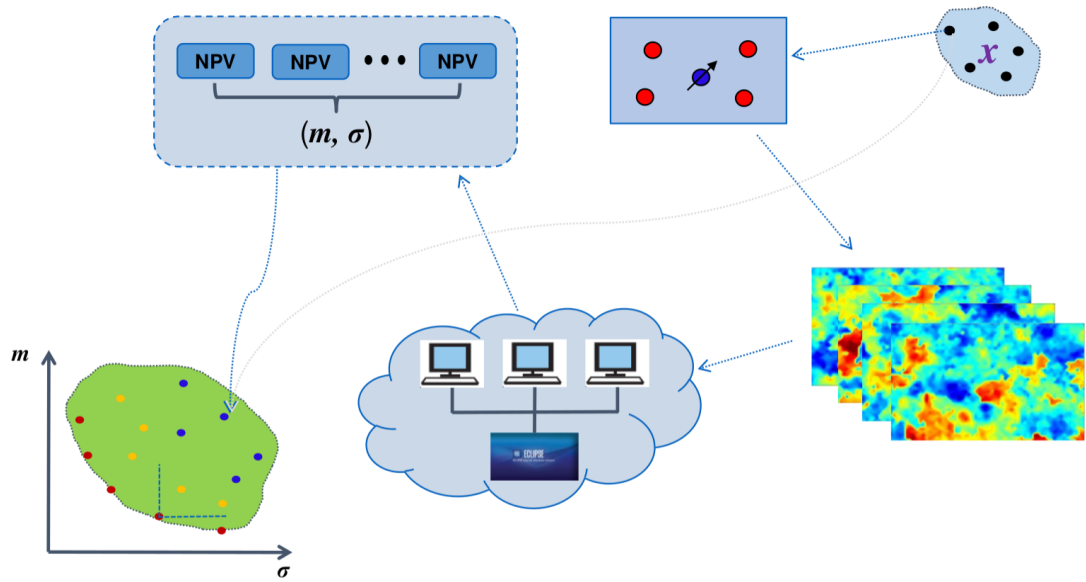
Figure 4.8: A demonstration of the function evaluation and the optimization workflow for reservoir cases.

4.4 Vertical Well Placement on The Sailor Reservoir[1]

4.4.1 Reservoir Description

The Sailor case is a 3-D heterogeneous reservoir model with one fault located in the center of the reservoir (Figure 4.9). The reservoir is supported by two aquifers at the northern boundary. The oil-water-contact is at 3400 meters. The 3-D reservoir model is discretized on a $60 \times 39 \times 5$ grid lattice. In the reference case, 3 producers and 2 injectors are placed in the reservoir with a total production time of 6 years. The producers are controlled by a bottom hole pressure (BHP) of 100 bar and the injectors are controlled by BHP of 500 bar.

In order to evaluate the performance of the optimization algorithm, I first remove all the wells from the reservoir and treat it as a green field. Then 3 producers and

---

[1]**Part of the results in this section has been published in Chang et al. (2014) and Chang et al. (2015).**
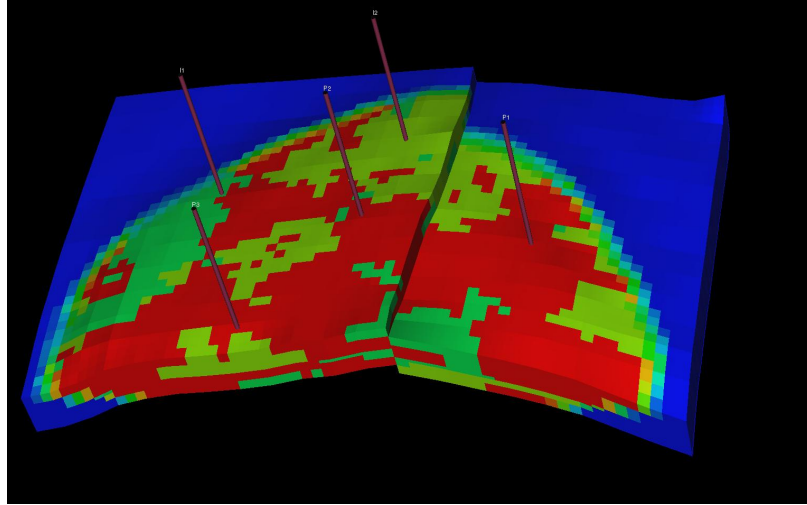
116

Figure 4.9: The Sailor 3-D reservoir model. The colors from red to blue represent the values of oil saturation vary from high to low.

2 injectors are placed simultaneously and compare the well locations from the optimization procedure to the reference case. The NPV is calculated from the constants defined in Table. 4.1.

Table 4.1: Constant parameters for NPV calculation

Oil price, $/SM3	500.0
Gas price, $/SM3	0.15
Water disposal cost, $/SM3	-30
Water injection cost, $/SM3	-50
Discount rate	0.1

35 different reservoir models are generated by geoscientists to capture the geological uncertainty of the Sailor case. I choose 20 representative geological models based on the percentiles of the original oil-in-place (OOIP) values. In Figure 4.10, a crossplot shows the field oil production total (FOPT) and the original oil in place (FOIP) of each reservoir model, and the selected geological models are marked with black dots and the blue numbers indicate the name of each selected model.
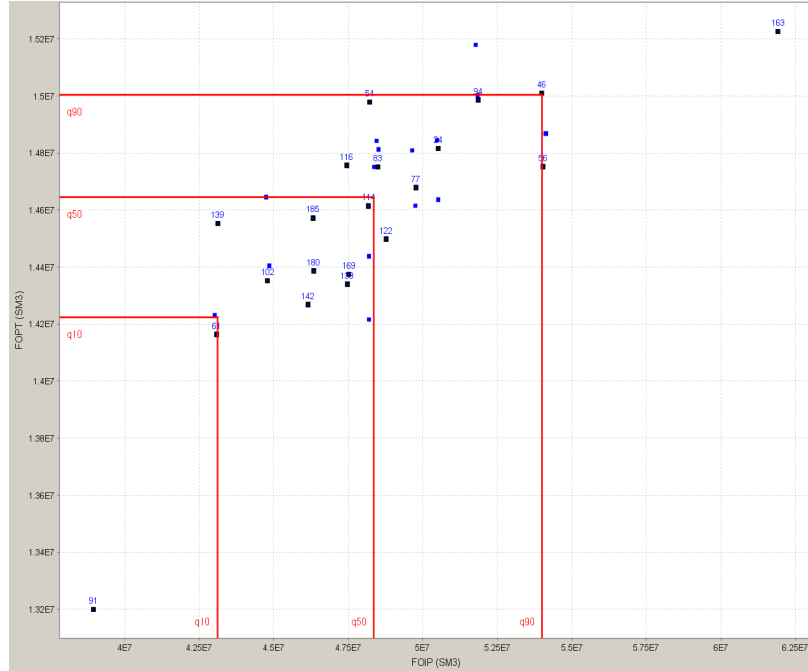
Figure 4.10: Selected 20 geological models of the Sailor case

4.4.2 Performance of NSGA-II

The Sailor reference case has 3 producers and 2 injectors that were determined by experienced reservoir engineers. The selection of these well locations involves a comprehensive analysis of the geological models and testing of around 300 different well placement configurations. In order to evaluate the results from the optimization algorithm, I take the well locations from the Sailor base case as the reference solutions. I then remove all the wells from the reservoir model, and utilize the optimization algorithm described earlier to place an identical number of wells.

The population size is 20 and the algorithm stops when the maximum number of 30 iterations is reached. The solutions obtained are shown in Figure 4.11. Each solid dot represents the mean and standard deviation of NPV calculated from each of the well configurations obtained from the genetic operator. The color of the solid dots represents the top-ranked solutions obtained in each iteration. In each iteration, 20 well configurations are evaluated on all the geological realizations, but only the

118

top-ranked solutions are shown in the figure. From the first to the last iteration, we see that the solutions progressively improve as they move towards the Pareto front (dark red).

The goal of multi-objective optimization is to search for a group of non-dominated diverse solutions in the objective function space so that the decision-makers can make choices based on their risk attitude. From Figure 4.11, we see a diverse Pareto front that contains multiple solutions. Around the reference case (the yellow star), there are four solutions appear which have superior performance in comparison to the reference case. The bottom right corner of the Pareto gives the scenario with the highest mean NPV, that is 2 billion US dollars higher than the NPV of the reference case. But the large standard deviation value at this solution indicates a high decision risk of field development, so decision-makers being risk-averse or risk-neutral may not consider this scenario as their final selection.

The mean and standard deviation of the NPV from top-ranked individuals for each iteration are shown in Figure 4.12(a). We see the improvement of the solutions from the 10th to the 20th iteration. One of the important characteristic of multi-objective problems is that the improvement of one objective function is often accompanied by the degradation of the other objective function in Figure 4.12(b).

The solutions obtained from NSGA-II are shown in Figure 4.13 where the group of diverse and non-dominated solutions allows decision-maker multiple choices for well placement. The yellow star in the figure represents the reference case. We see the optimization approach is able to find a few different solutions that are superior to the reference case. The well configuration scenarios 1, 9 and 12 indicated by the arrows will be evaluated in the following analysis.

The well locations corresponding to scenarios 1, 9 and 12 are shown in Figure 4.14. In Scenario 12, the distances between one injector and two producers are fairly small, while in Scenario 9, one injector is located adjacent to the fault and both injectors
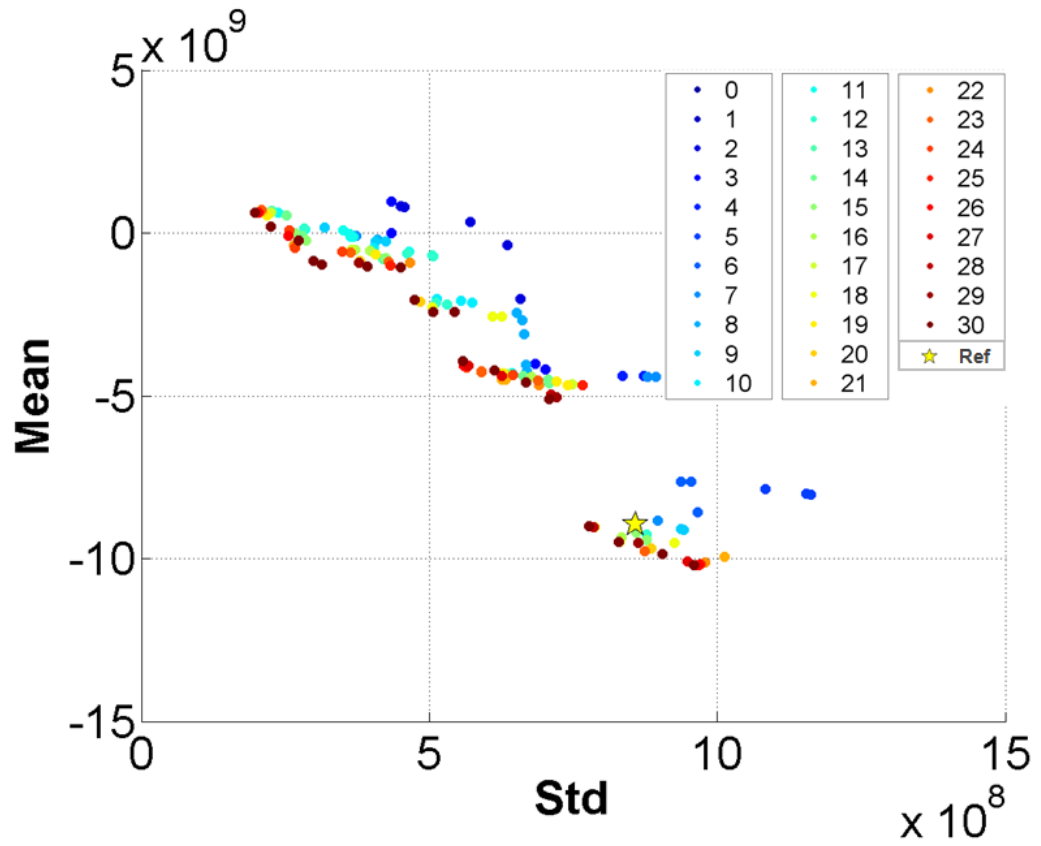
Figure 4.11: Pareto evolutions of top-ranked scenarios from NSGA-II

(a) NPV mean and iterations

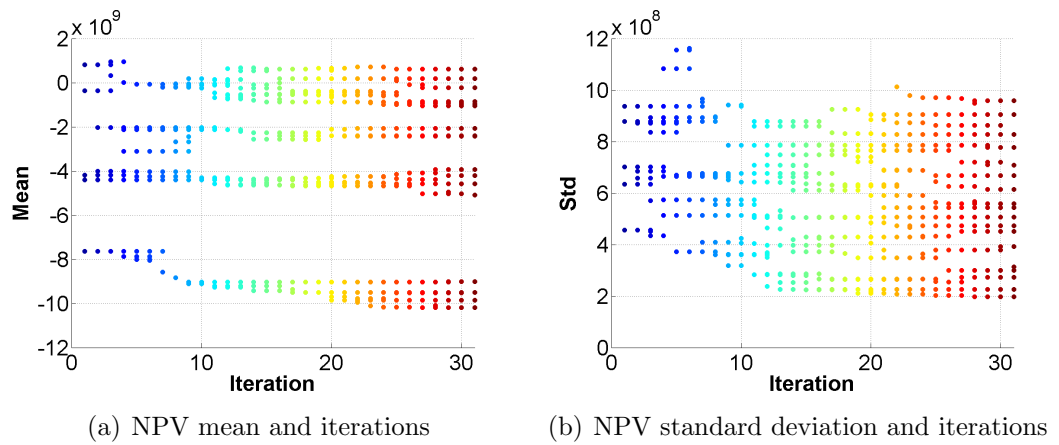(b) NPV standard deviation and iterations

Figure 4.12: Evolutions of the mean and standard deviation of NPV for top-ranked scenarios during the iterations of NSGA-II
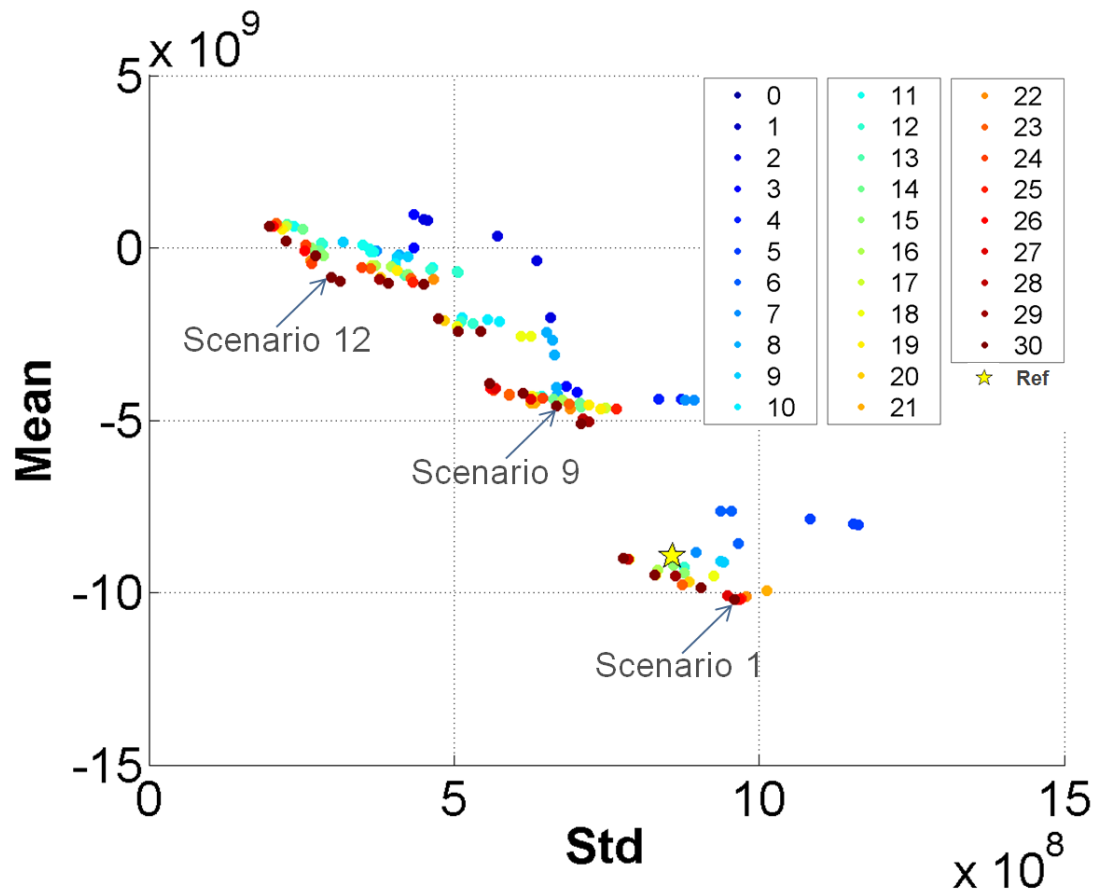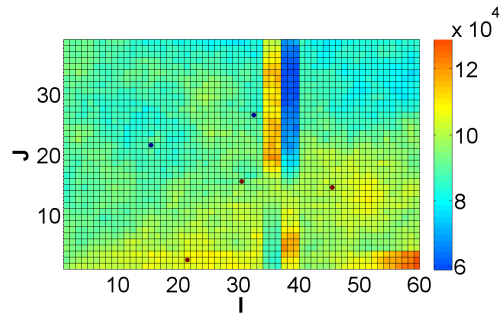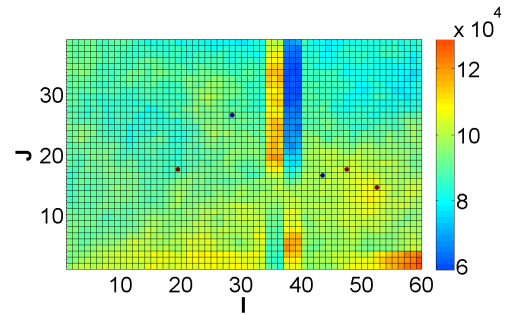
Figure 4.13: Pareto evolutions of top-ranked scenarios from NSGA-II (Unit: USD). The dots represent the top-ranked individuals appear at each generation of the algorithm and the yellow star represent the reference case.

(a) Reference

(b) Scenario 12
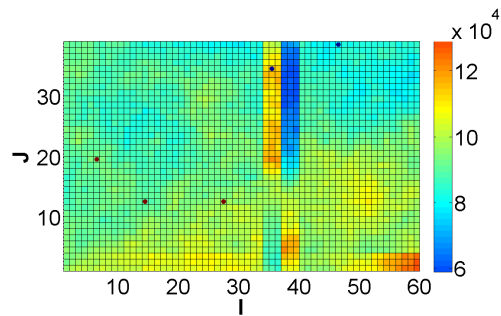
(c) Scenario 9

(d) Scenario 1

Figure 4.14: Comparison of well configurations of reference case and selected scenarios from final Pareto of NSGA-II. Blue dots represent injectors and red dots represent producers. The color bar shows mean oil-in-place values of grid cells (Unit: SM3).

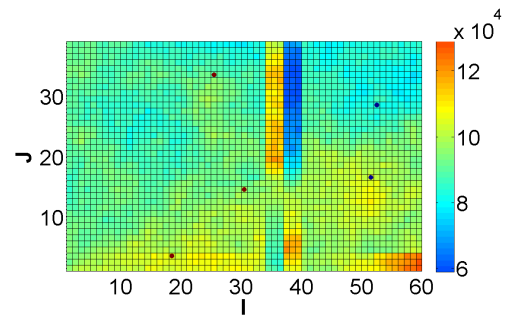are very far from producers. I ran simulations of the selected well configuration scenarios on all the geological realizations to obtain the field liquid production data at each simulation time step. Then I plotted field oil production total (FOPT), field gas production total (FGPT), field water production total (FWPT), and field water injection total (FWIT) in the box plots for each time step to compare the performance of selected scenarios with the reference case.

The results are shown in Figure 4.15. Dark blue boxes show the results from reference case while the red boxes show the results from Scenario 1 which has the highest mean NPV with the highest risk. The reference case has a comparable oil and gas production compared to Scenario 1. However, the reference case is characterized by high water production and high water injection that reduces the NPV. In addition, the reason for the lower NPV obtained from Scenario 12 and Scenario 9 lies in the improper locations of producers and injectors. While the reference case has a good well configuration, the short distances between injectors and producers may lead to water breakthrough when compared to Scenario 1. However, the reference case has a smaller variability leading to a smaller risk in comparison to Scenario 1.

At the end of the simulation steps, I obtained oil saturation data and calculated the residual oil in each grid cell. Then, a 2-D mean residual oil map (Figure 4.16) is obtained after performing vertical averaging of residual oil values. Compared to the reference case, from Scenario 12 to Scenarios 1 and 9, there is a clear shrinking in the residual oil area. This is consistent with the mean NPV increases shown in Figure 4.13.

4.4.3 OIP Map Assisted NSGA-II (OIP-NSGA-II)

4.4.3.1 OIP quality maps

For simulator-based optimization problems, computation costs may be reduced by utilizing any available prior knowledge. Because the goal of maximizing NPV largely depends on oil production, I employ an oil-in-place map (OIP map) to constrain the
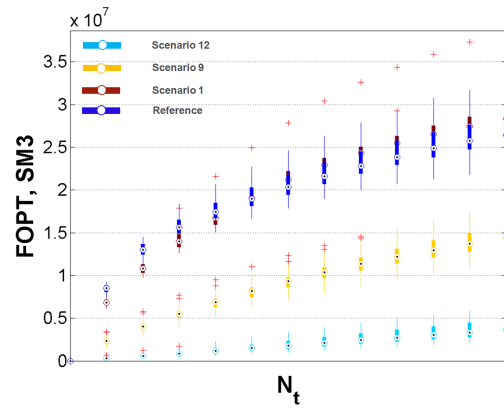
(a) FOPT
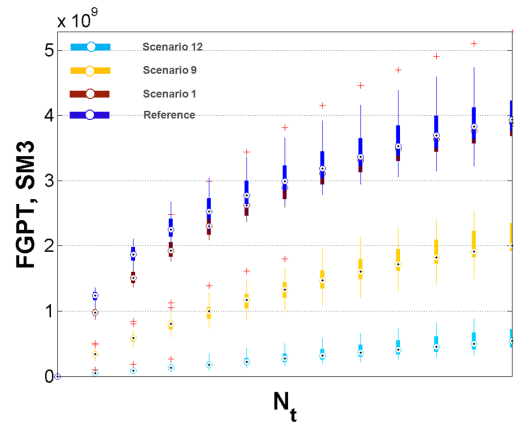
(b) FGPT
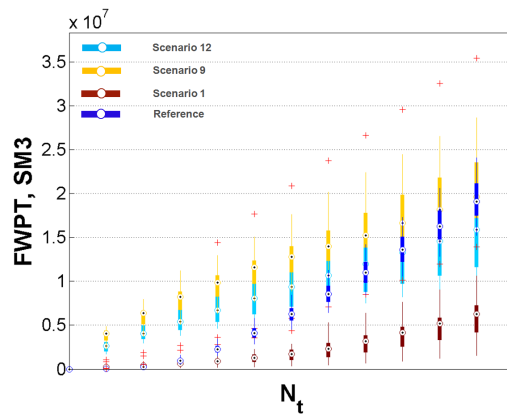
(c) FWPT

(d) FWIT

Figure 4.15: Boxplot comparisons of field production profiles of well configurations in reference case and selected scenarios from NSGA-II

(a) Reference

(b) Scenario 12

(c) Scenario 9

(d) Scenario 1

Figure 4.16: Comparison of mean residual oil maps for reference case and selected scenarios from final Pareto of NSGA-II

locations of the planned wells. This approach essentially accelerates the optimization process by reducing the search domain for feasible well locations.
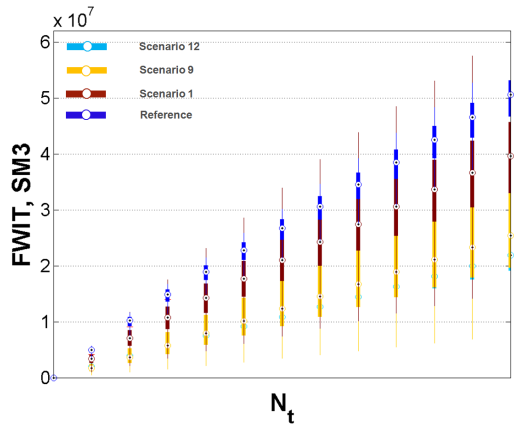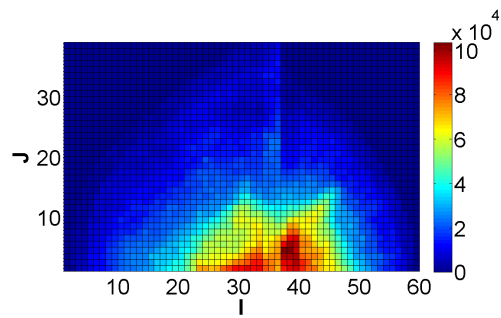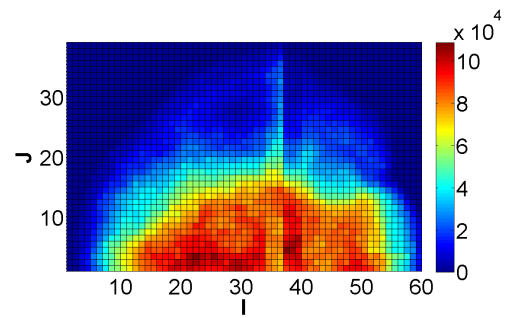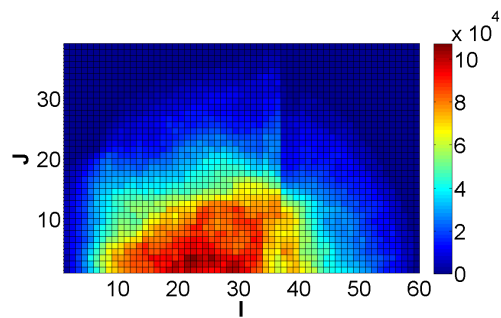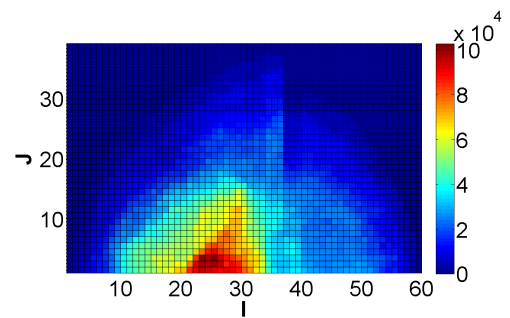
I create this map by first calculating the OIP values of each grid based on the pore volume and initial oil saturation values to obtain a 2-D OIP map for each layer as shown in Figure 4.17). Then, at each grid, the OIP values are summed by layer in a vertical direction to obtain a 2-D OIP map of the entire reservoir model. This process is repeated on all the 20 geological models so that each grid location has 20 OIP values. This step is illustrated in Figure 4.18.

Figure 4.19(a) shows the reservoir regions with cells colored by OIP values where grid cells are ranked based on OIP percentiles; 20th, 40th 60th and 80th percentiles. The grid cells that belong to each of the percentile are colored by integers 0, 1, 2, 3 and 4. In order to allow for several optimal solutions, I set a fairly large range — 40th percentile as the threshold to screen out the less productive reservoir regions with lower OIP values. Thus, all qualified grid cells with OIP values above the 40th percentile are colored with integer 1 as shown in dark red color in Figure 4.19(b). This region provides the constraints to place the wells during optimization process.

4.4.3.2 Performance of OIP-NSGA-II

With the use of OIP region map, I employ the OIP-assisted NSGA-II (OIP-NSGA-II) on the Sailor field case. The Pareto evolutions during each iteration are shown in Figure 4.20. Comparison of the final Pareto of the NSGA-II and the OIP-NSGA-II as shown in Figure 4.22 reveals that the OIP-NSGA-II method is promising in that the solutions are clustered around the reference case.

4.4.4 Comparisons of NSGA-II & OIP-NSGA-II

The comparison of the final Pareto from NSGA-II and OIP-NSGA-II are shown in Figure 4.22. Using the NSGA-II method without employing the OIP map, most of the solutions are clustered around the area with low risk associated with a low
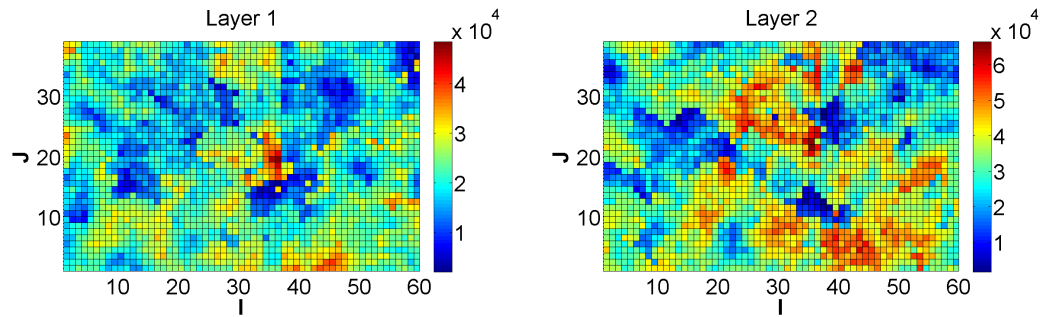
(a) Layer 1

(b) Layer 2
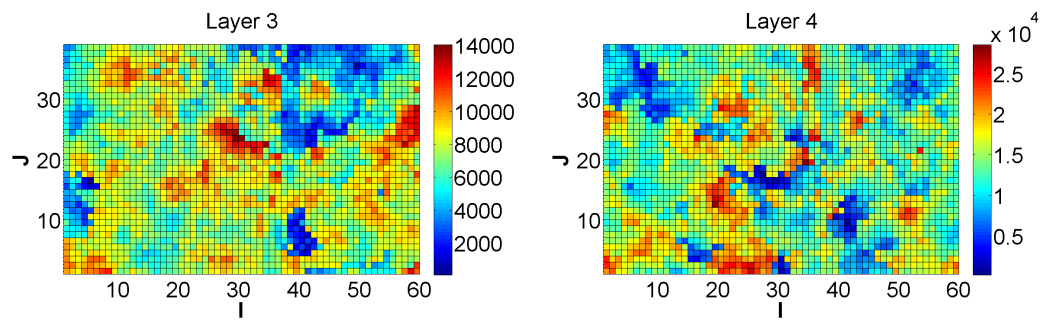
(c) Layer 3

(d) Layer 4
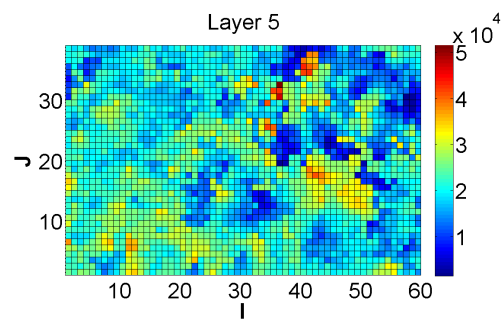
(e) Layer 5

Figure 4.17: OIP maps of each layer in the Sailor case

127
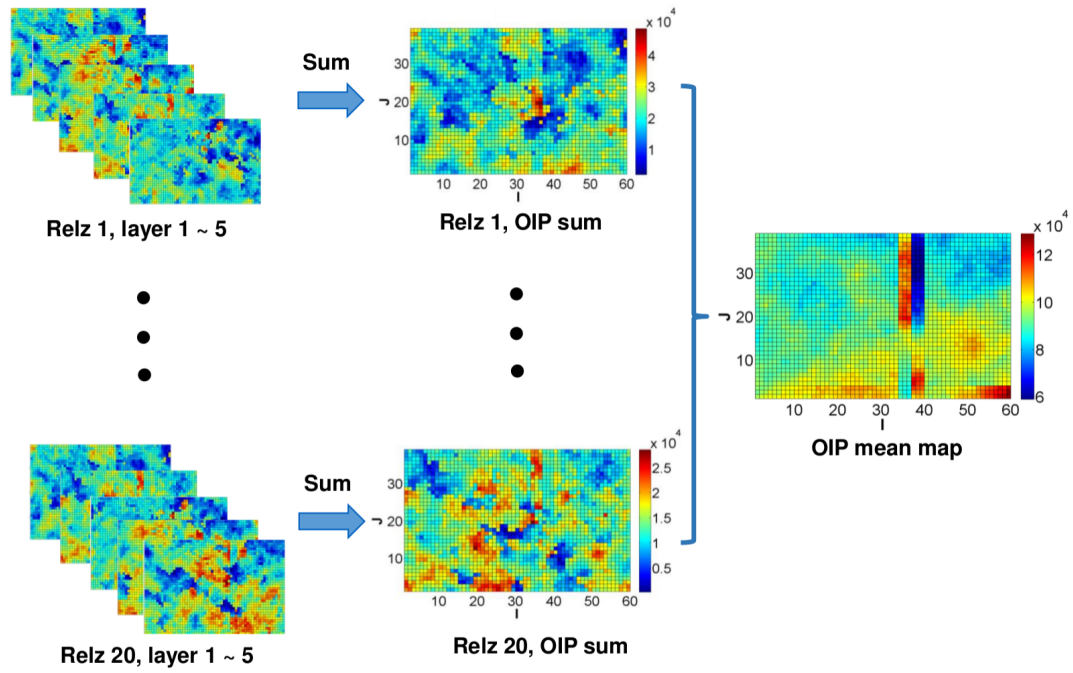
Figure 4.18: An illustration of obtaining the oil-in-place mean map from geological realizations.

(a) OIP percentile map
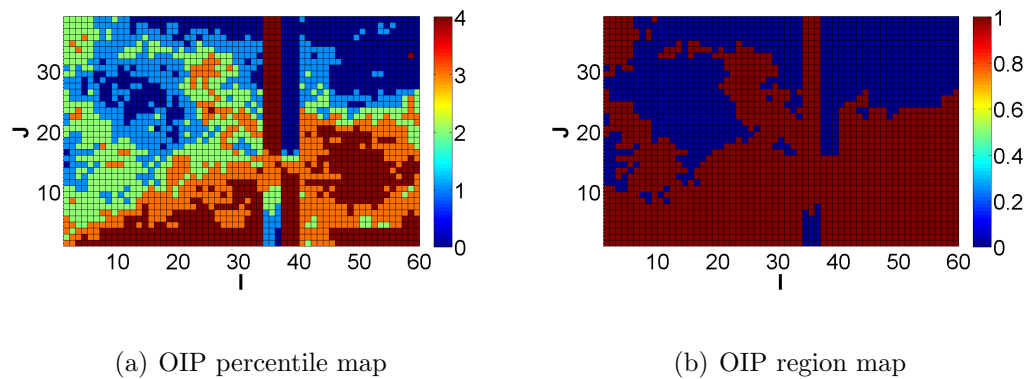
(b) OIP region map

Figure 4.19: OIP contour, percentile and region maps in the Sailor case
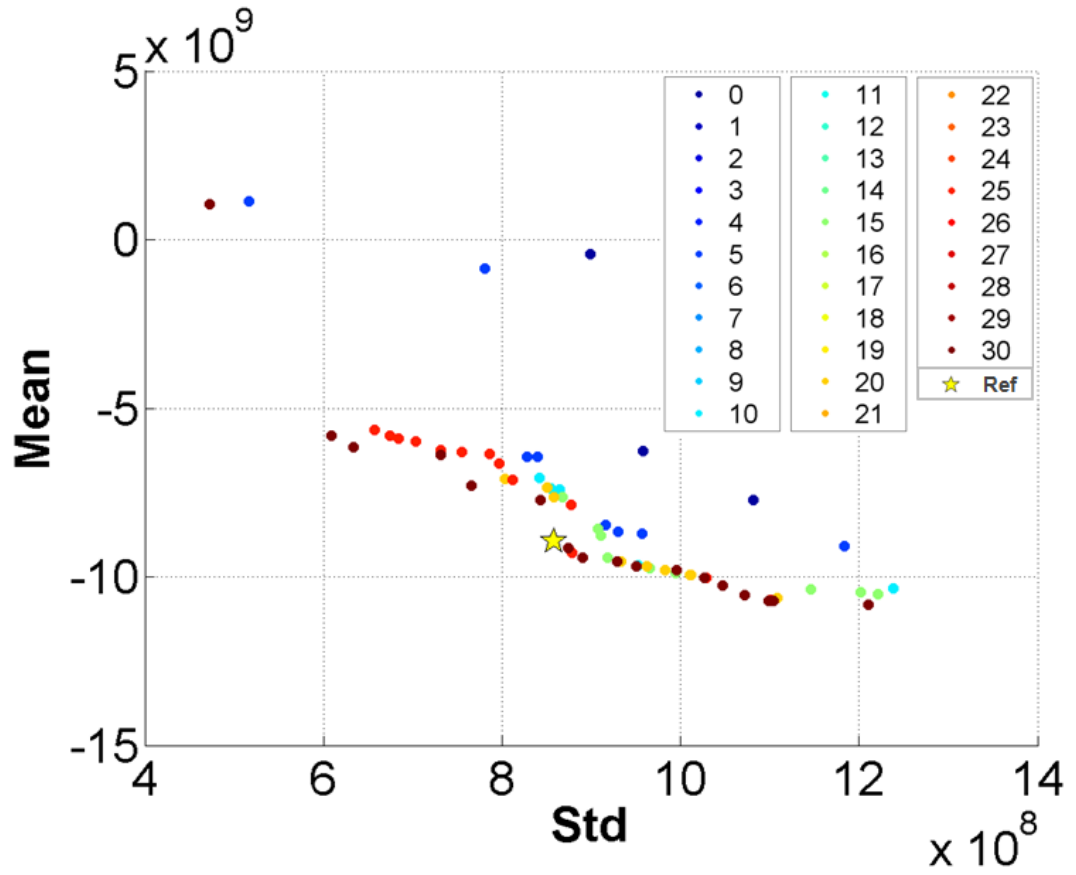
Figure 4.20: Pareto evolutions of top-ranked scenarios from OIP-NSGA-II

(a) NPV mean vs. iteration

(b) NPV standard deviation vs. iteration
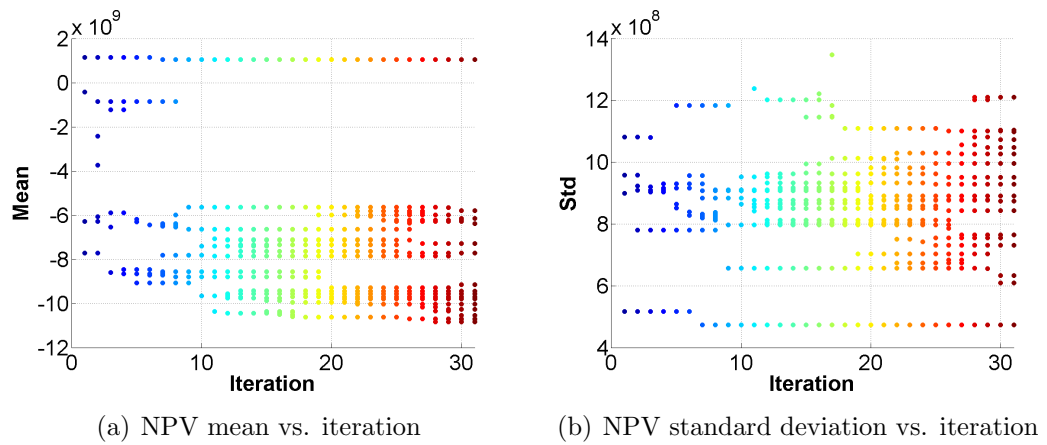
Figure 4.21: NPV mean and standard deviation evolutions of top-ranked scenarios during iterations of OIP-NSGA-II

129

standard deviation of NPV as shown by the large blue dots. Although the goal of multi-objective optimization is to find diverse solutions while maximizing NPV and minimizing the decision risk, these so-called "optimal" solutions however produce large quantities of water. But the OIP-NSGA-II approach avoids such mathematically optimal but practically infeasible solutions by restricting the search to predefined regions based on some prior knowledge.
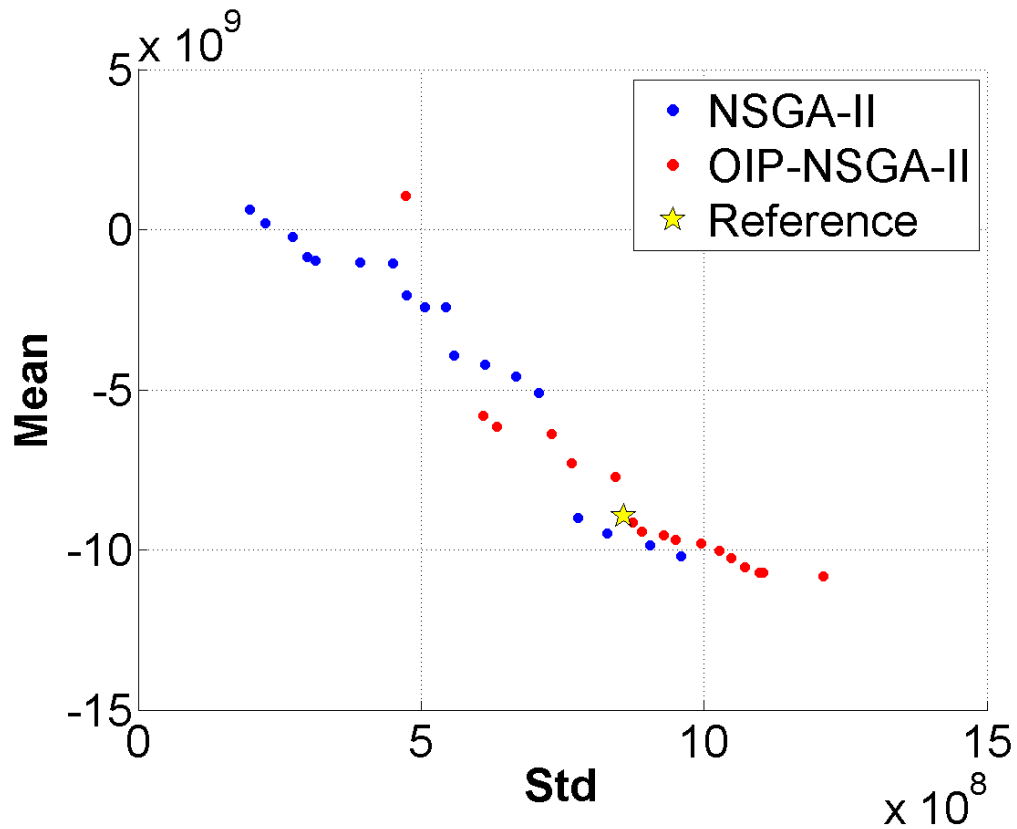
Figure 4.22: Comparison of Pareto at last iteration of NSGA-II & OIP-NSGA-II

A comparison of the computation time of the NSGA-II and the OIP-NSGA-II is shown in Figure 4.23. The OIP-NSGA-II requires only half of the computation time of the NSGA-II by limiting the search space to the constrained area from the OIP method and therefore provide more practical and meaningful solutions for field development strategies.
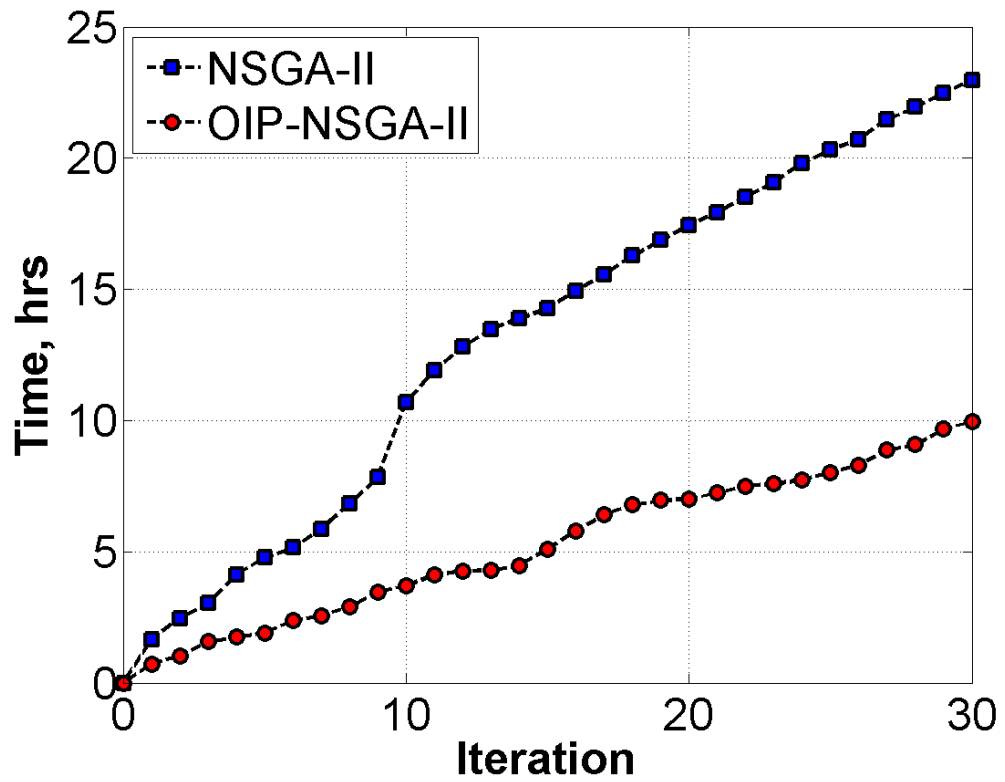
Figure 4.23: Comparison of computation time for NSGA-II & OIP-NSGA-II

4.4.5 OIP-NSGA-II Solution Analysis

The production profiles and residual oil in place for the final Pareto using the OIP-NSGA-II method for the 4th, 9th and 19th scenario are compared with the reference case in this study. From Figure 4.24, we see that the mean of the NPV increases from scenarios 4, 9 and 19 as does the standard deviation.
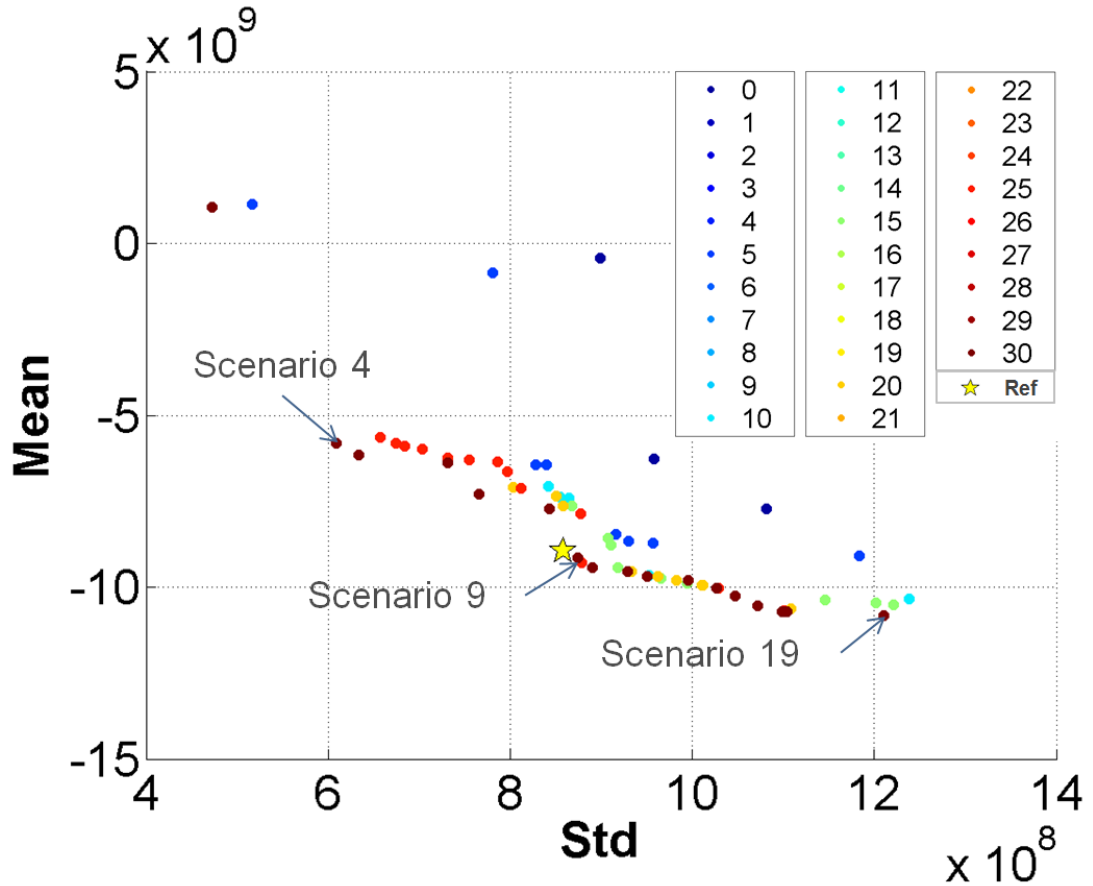
Figure 4.24: Selected scenarios from the final Pareto of OIP-NSGA-II

Figure 4.25 shows the well configurations of 3 producers and 2 injectors in the reference case and the selected scenarios. Red dots represent the producer locations and blue ones represent the injector locations.

I run simulations of the selected well configuration scenarios on all selected geological models to obtain the field liquid production data at each simulation time step,
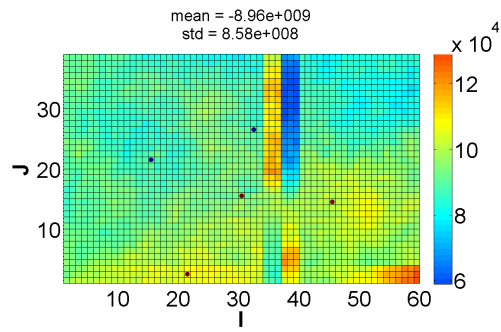
(a) Reference
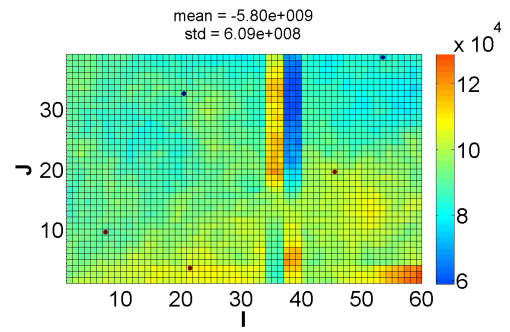
(b) Scenario 4
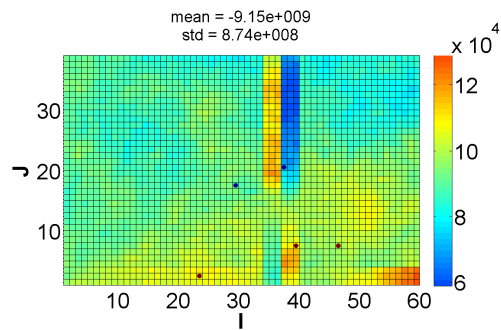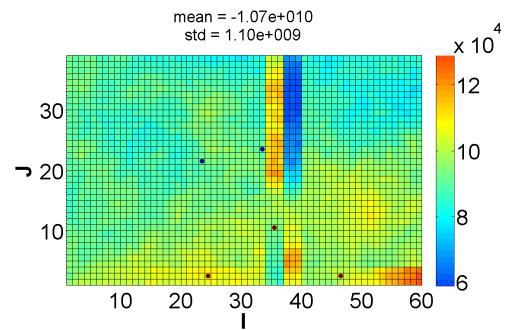
(c) Scenario 9

(d) Scenario 19

Figure 4.25: Comparison of well configurations of reference case and selected scenarios from final Pareto of OIP-NSGA-II

and to plot the liquid production curve as shown from Figure 4.26 to Figure 4.29. Figure 4.26 plots the oil, water gas total production and total water injection (FOPT, FGPT, FWPT and FWIT) while Figure 4.27, Figure 4.28 and Figure 4.29 plot the same for scenarios 4, 9 and 19 respectively.

(a) FOPT

(b) FGPT

(c) FWPT

(d) FWIT
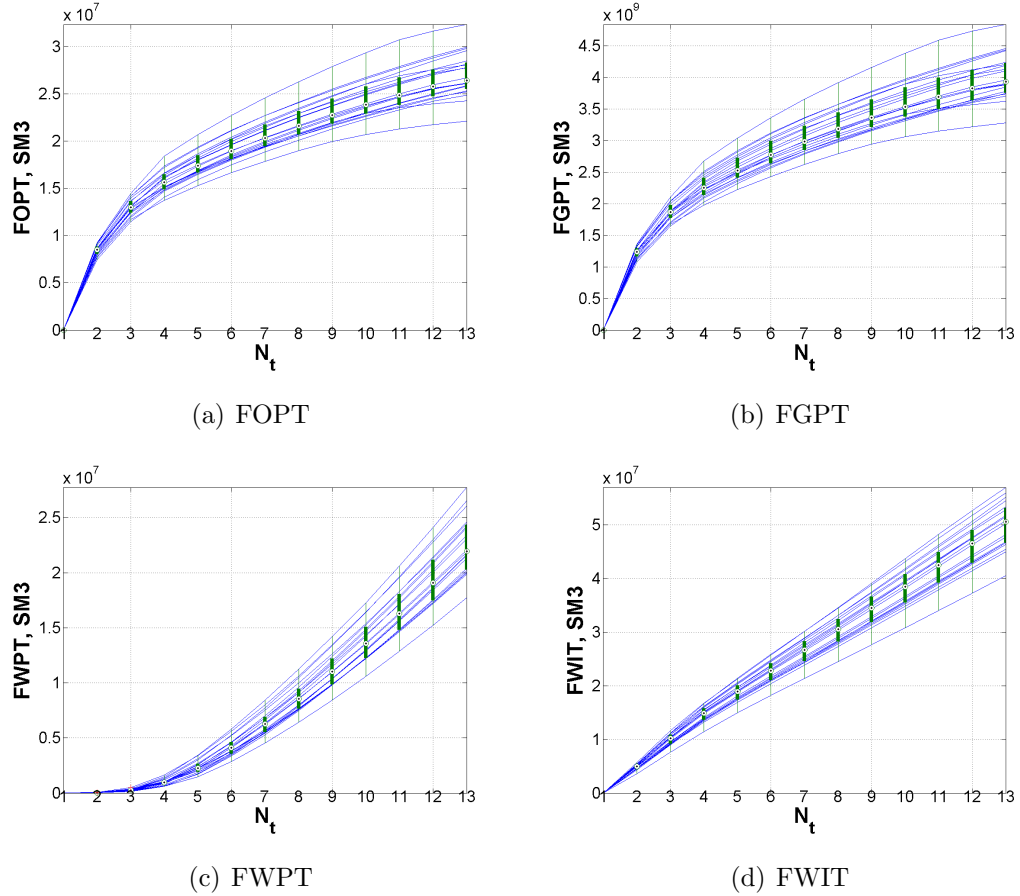
Figure 4.26: Field production profiles of the Sailor reference case for each of the 20 geological realizations

I combine all of the Figures 4.26 to 4.29 into a box plot are shown in Figure 4.30. Blue boxes show the results from reference case, light blue, yellow and red boxes show the results from the Scenario 4, 9 and 19 respectively. Scenario 19 has the highest mean NPV with a fairly high standard deviation. The reference case has a comparable oil and gas production compared to the Scenario 19. However, the reference case is characterized by high water production and high water injection so that it has a lower
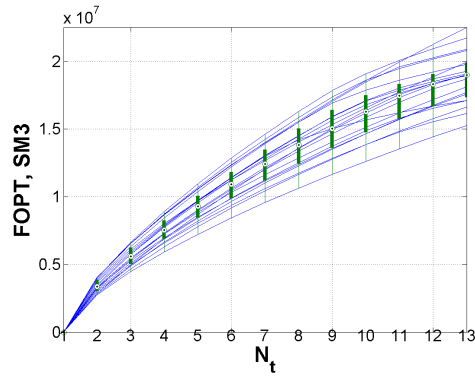
(a) FOPT
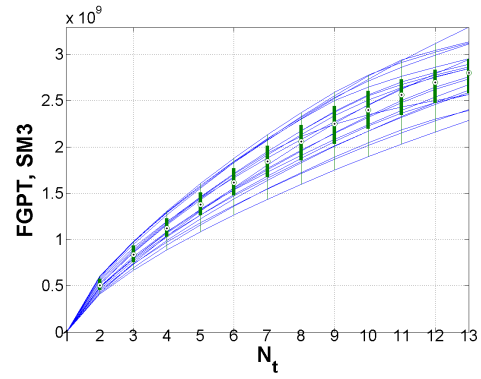
(b) FGPT
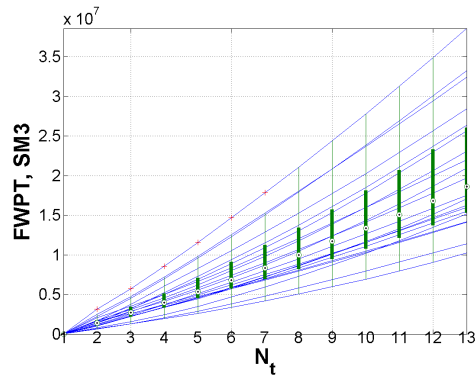
(c) FWPT
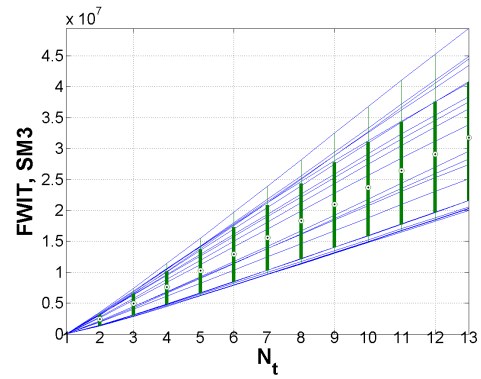
(d) FWIT

Figure 4.27: Field production profiles of well configurations in Scenario 4 from OIP-NSGA-II
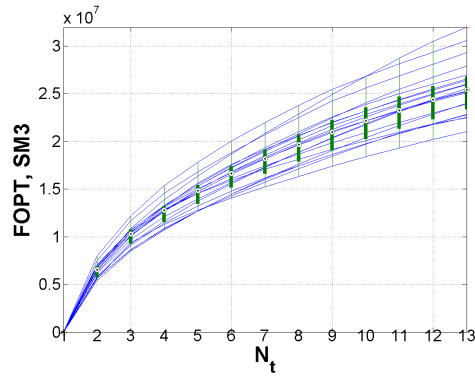
(a) FOPT
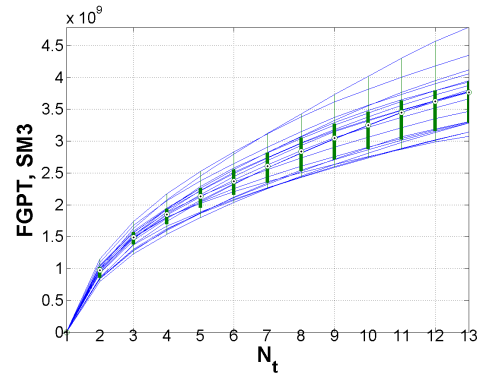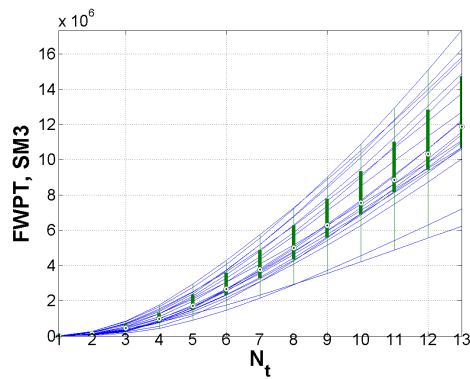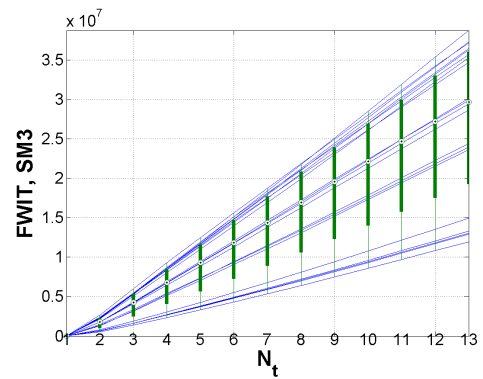
(b) FGPT

(c) FWPT

(d) FWIT

Figure 4.28: Field production profiles of well configurations in Scenario 9 from OIP-NSGA-II
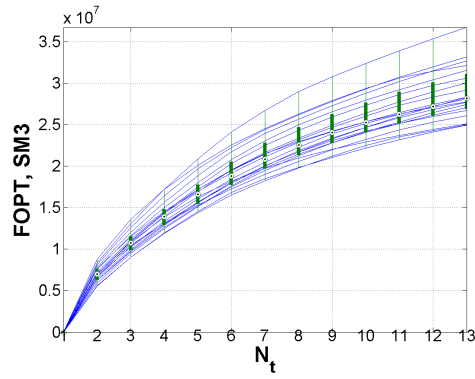
(a) FOPT
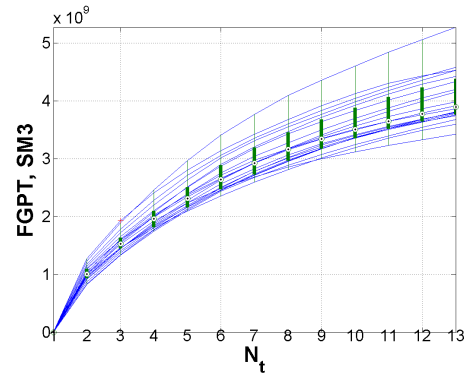
(b) FGPT
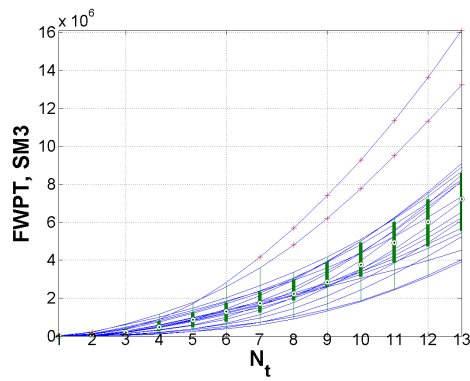
(c) FWPT
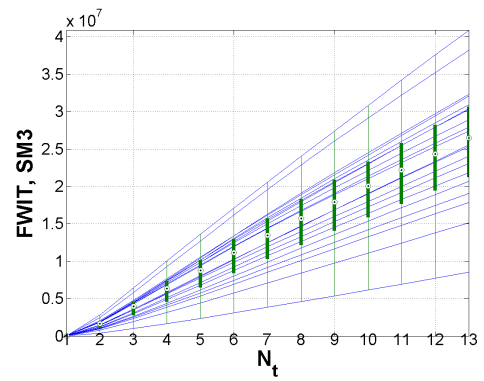
(d) FWIT

Figure 4.29: Field production profiles of well configurations in Scenario 19 from OIP-NSGA-II

NPV. We see the reference case has a smaller quantile range and standard deviation than Scenario 19.

(a) FOPT

(b) FGPT

(c) FWPT

(d) FWIT

(e) Legend
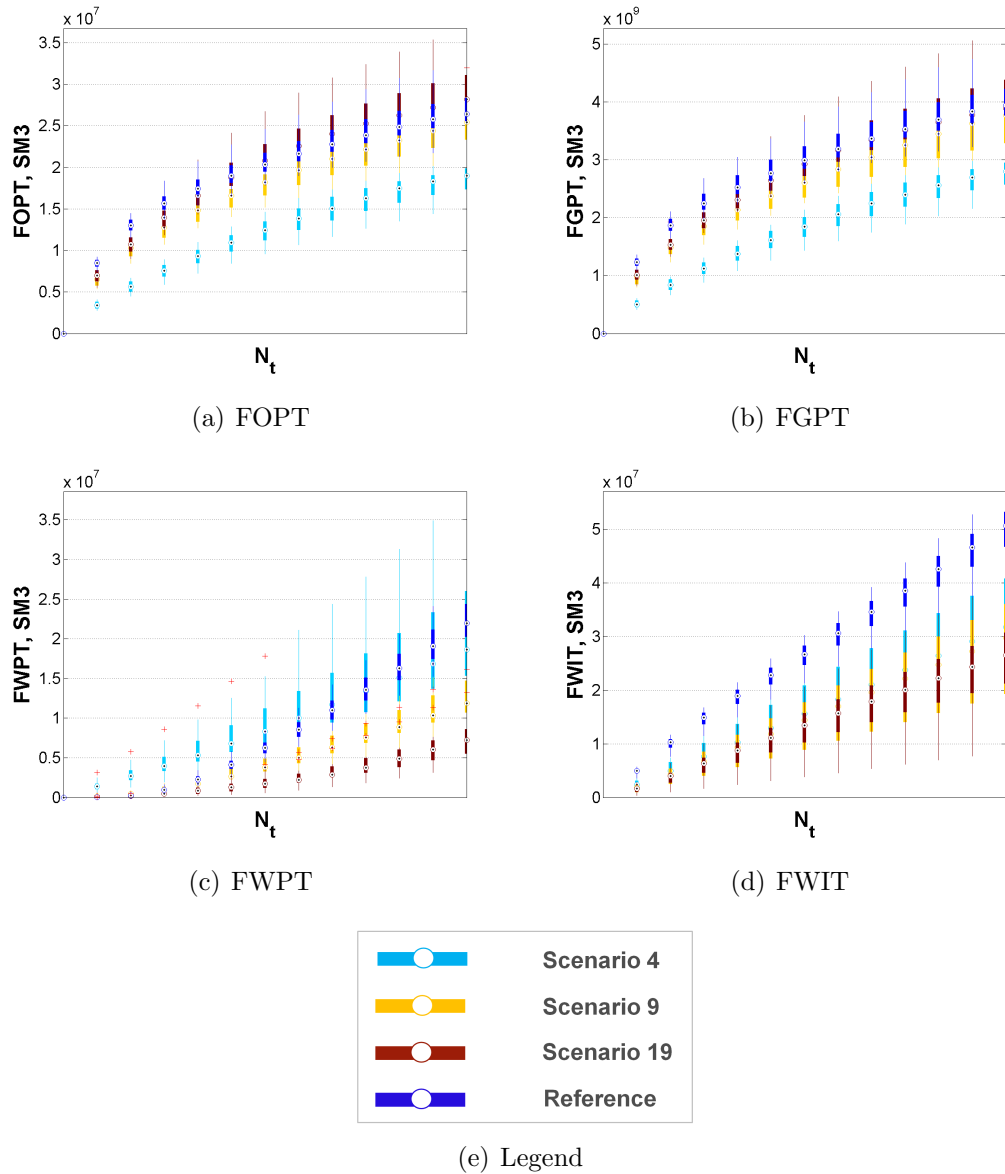
Figure 4.30: Box plot comparisons of field production profiles of well configurations in reference case and selected scenarios from OIP-NSGA-II

With the liquid production data at each time step, the NPV of each scenario can be evaluated on every geological model. The data are shown in Table 4.2 with the box plot of the NPV shown in Figure 4.31. We see that the median of the NPV increases from Scenario 4, Scenario 9 to Scenario 19. The median value and the quantile range

Table 4.2: The NPV of selected scenarios and reference case on all geological models (unit: USD)

$(\times 10^{10})$	Scenario 4	Scenario 9	Scenario 19	Reference
Relz 1	0.6211	0.9163	1.1097	0.9460
Relz 2	0.6493	0.9585	1.2193	0.9667
Relz 3	0.5995	0.9200	1.0096	0.9147
Relz 4	0.6757	0.9128	1.2029	1.0043
Relz 5	0.4906	0.9013	0.8962	0.7774
Relz 6	0.5789	0.7509	1.0023	0.9479
Relz 7	0.5033	0.9638	1.1475	0.9141
Relz 8	0.5120	0.7887	0.9300	0.7104
Relz 9	0.6529	1.0795	1.1786	0.9944
Relz 10	0.5908	0.9366	1.0089	0.8615
Relz 11	0.5319	1.0261	1.1289	0.9425
Relz 12	0.5875	0.8950	1.0166	0.8529
Relz 13	0.5977	0.8663	1.0933	0.8967
Relz 14	0.4890	0.8629	1.0281	0.8860
Relz 15	0.5454	0.8071	0.9050	0.8246
Relz 16	0.6371	0.9269	1.0517	0.8474
Relz 17	0.6460	1.1066	1.3339	1.0912
Relz 18	0.5110	0.9260	1.0507	0.8418
Relz 19	0.6438	0.9043	1.0677	0.8524
Relz 20	0.5356	0.8549	1.0262	0.8392

of Scenario 9 are similar to the reference case due to their relatively close positions on the Pareto as seen in Figure 4.24.
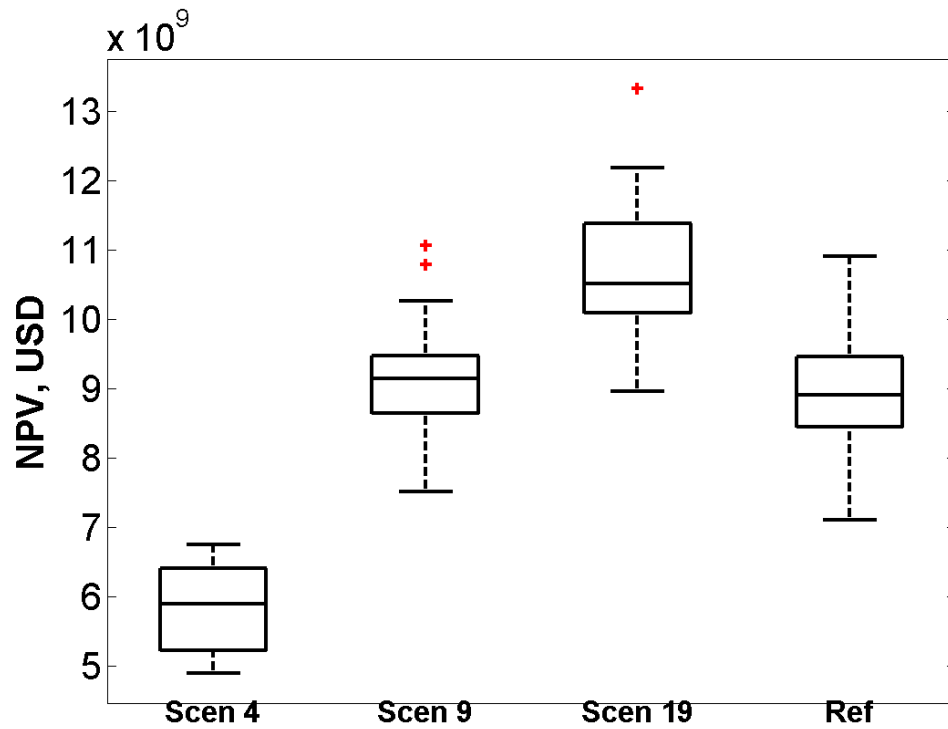
Figure 4.31: Box plot of the NPV over all geological realizations of reference case and selected each scenario from OIP-NSGA-II

The mean of the residual oil in place are plotted in Figure 4.32. Comparing the reference case with Scenarios 4, 9, and 19, we see that the mean of the NPV increases with a clear reduction in the residual oil in place. Moreover, comparing Scenario 9 with the reference case, I observe that it exhibits a similar residual oil in place. In the next section, I describe the application of the proposed multi-objective optimization technique for inclined well placement.
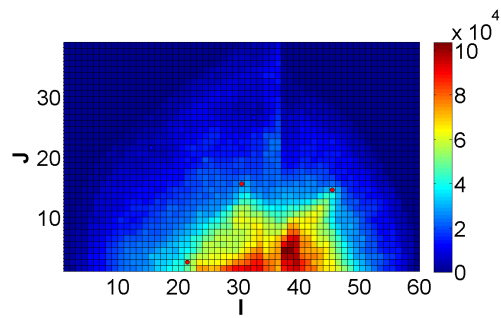
(a) Reference
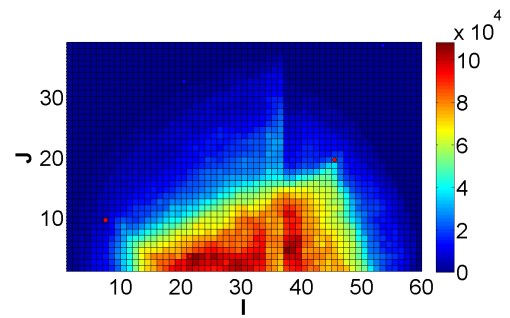
(b) Scenario 4
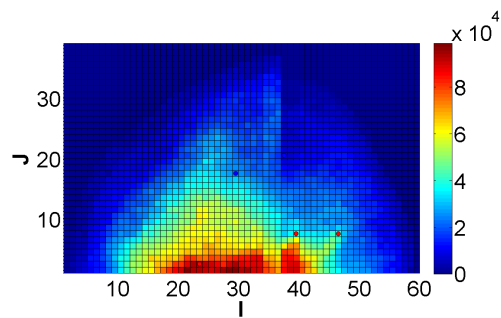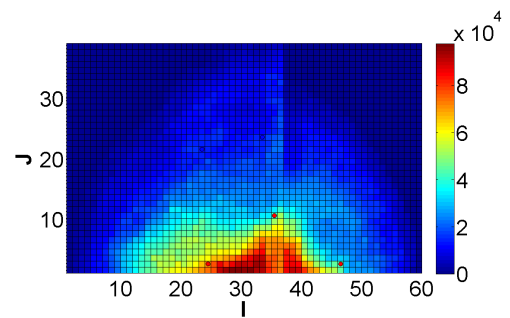
(c) Scenario 9

(d) Scenario 19

Figure 4.32: Comparison of residual OIP mean maps for the reference case and the selected scenarios from the final Pareto of OIP-NSGA-II

4.5 Inclined Well Placement on the Faro Field[2]

In large fields, thin reservoir layers or multiple pay zones may exist in the subsurface, it is more practical to place inclined or horizontal wells in order to maximize reservoir contact while minimizing the cost of drilling. In this section, multi-objective optimization is presented using the Faro field case for placement of inclined wells.

4.5.1 Reservoir Description

The Faro field is a 3-D highly heterogeneous reservoir model with a few faults located in the reservoir shown in Figure 4.33. The 3-D reservoir model was discretized on a $130 \times 100 \times 61$ grid lattice. In the base case, 4 producers and 3 injectors contribute to the drainage strategy for a total production time of 20 years. Because this is a large field, the use of computational resources can be prohibitively high when geological uncertainty is taken into account. Therefore, in this case study, I use the NSGA-II algorithm on upscaled reservoir models with the ratio $2 \times 2 \times 6$ in x-, y- and z-directions to accelerate the flow simulation. For the upscaled Faro reservoir model, it was discretized to $65 \times 50 \times 11$ grid cells with 5000 active cells. The geological uncertainty is represented by using 20 geological realizations.

In order to evaluate the performance of the optimization algorithm, the NPVs from the optimization study are compared with the one from the reference case. The NPV of the reference case is obtained from the reservoir model with well locations manually evaluated for optimality by the operator. In this study, for the optimization case, the same number of wells is used as the reference case but the well locations will be planned based on the solutions obtained from the optimization method. All the planned wells are inclined with a length constraint of 1500 meters. The NPV is calculated from the constants defined in Table. 4.3.

---

[2]**Part of the results in this section has been published in Chang et al. (2015).**
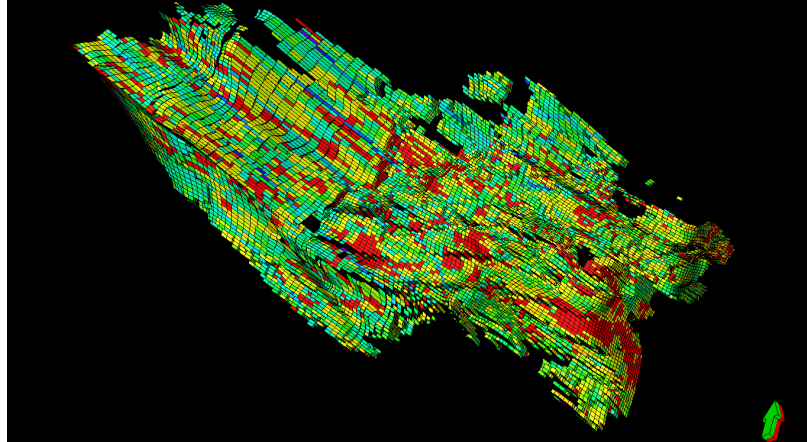
Figure 4.33: The 3-D reservoir model of Faro field

Table 4.3: Constant parameters for NPV calculation

Oil price, \$/SM3	500.0
Gas price, \$/SM3	0.15
Water disposal cost, \$/SM3	-30
Water injection cost, \$/SM3	-50
Drilling cost coefficient A	5000
Wellbore diameter, m	0.2159
Discount rate	0.1

4.5.2 Well Trajectory Design

The parameters for optimization in this specific problem are the locations of the heel and toe of each well. However, in a reservoir simulator, because wells are completed at the grid block centers, well trajectories for inclined wells proceed in stair-step manner as shown in Figure 4.34. The blue line is the real inclined well and the red line is the well trajectory from the reservoir simulator.

(a) Cross-section view   (b) Top view
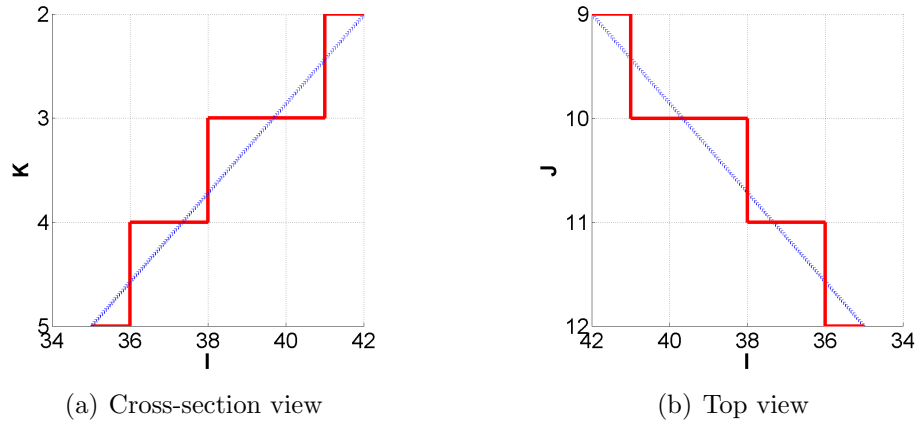
Figure 4.34: Front view and top view of an inclined well trajectory

We see in Figure 4.34 that the length of well trajectory is longer than the real well. Consequently, the productivity index (AI) of the well is adjusted by a coefficient factor to reflect the PI of an actual inclined well following Yeten (2003). This coefficient factor is defined as

$$\zeta = \frac{l_w}{l_g}, \tag{4.12}$$

where l_w is the real length of the well and l_g is the length of the stair-step trajectory.

4.5.3 Performance of NSGA-II and OIP-NSGA-II

We now use the NSGA-II algorithm to determine optimal well configurations for 7 inclined wells, including 4 producers and 3 injectors. Each well is associated with 6

variables — (h_i, h_j, h_k) grid index for the heel and (t_i, t_j, t_k) for the toe. So the total number of variables for optimization is 42 (6 wells $\times$ 4 variables) in this case.

In the Sailor field study case, the population size is set as 20 for the optimization problem with an optimization variable dimension of 20. For this case study, with a larger variable dimension, a larger population size is necessary to ensure an adequate search over the entire variable domain. A larger population size requires however significantly more reservoir simulation runs that are computationally intensive. This study therefore includes two experiments with population sizes of 20 and 40. With the population size of 20, the results in Figure 4.35 show that over 30 iterations, there is no satisfactory improvement of the Pareto front. This indicates that the population size of 20 may not be sufficient for addressing this problem. But for the population size of 40 in Figure 4.36, we see a very good improvement of the Pareto front over 30 iterations. The solutions possess a comparable mean NPV and a much smaller standard deviation in comparison to the reference case. Moreover, the Pareto solutions at the last iteration exhibit relatively good continuity and diversity as seen in the final Pareto front at the last iteration in Figure 4.37.

The mean NPV and standard deviation of the top-ranked individuals for each iteration are shown in Figures 4.38(a) and 4.38(b) respectively. There is clear improvement in the solutions at the 5th and 15th iteration. However, as with all multi-objective studies, the improvement in one objective function is associated with a degradation of another objective function as seen in both Figures 4.38(a) and 4.38(b).

For simulator-based optimization problems, minimizing the computation issue may be achieved by improving the optimization routine by providing prior knowledge before placing wells. Since our main goal is to maximize NPV, I use an oil-in-place map (OIP map) as described earlier to constrain the well placement. In this manner, the search domain for the optimization process can be reduced thereby makes the optimization more efficient.
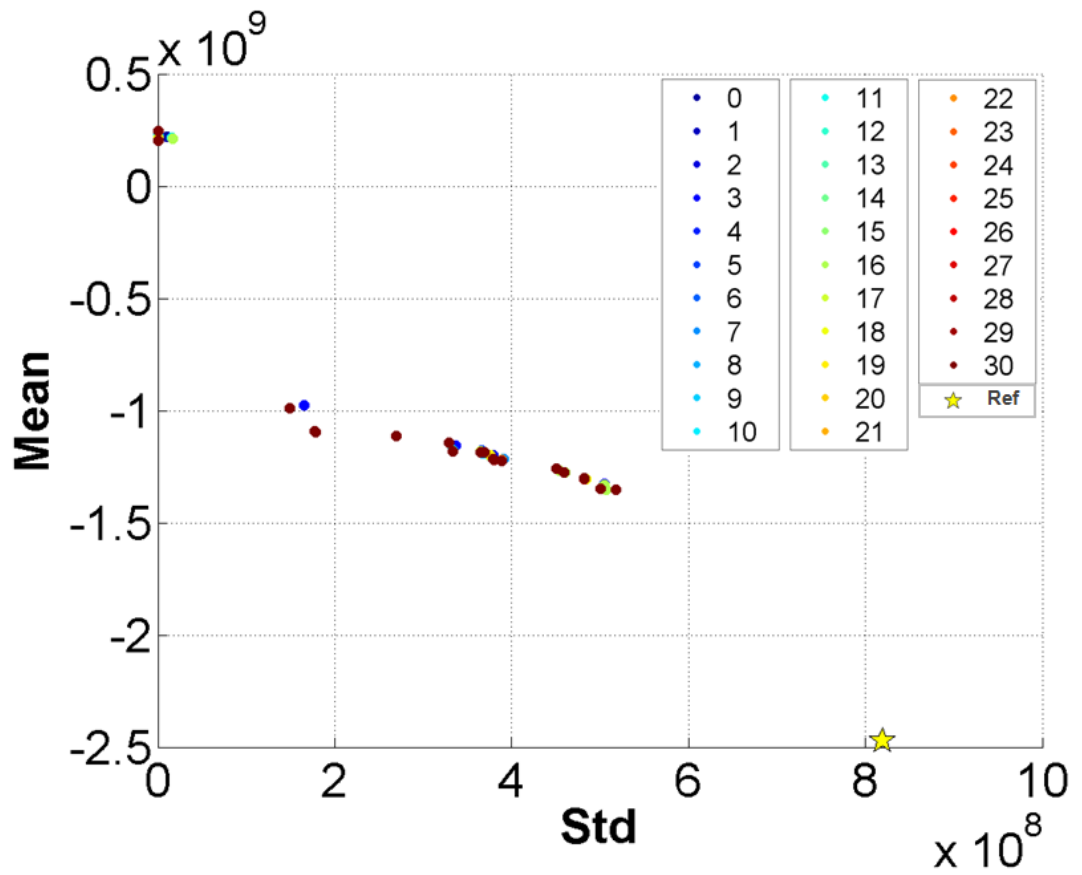
(a) Pareto

Figure 4.35: Pareto evolutions of top-ranked scenarios from NSGA-II with population size 20

146
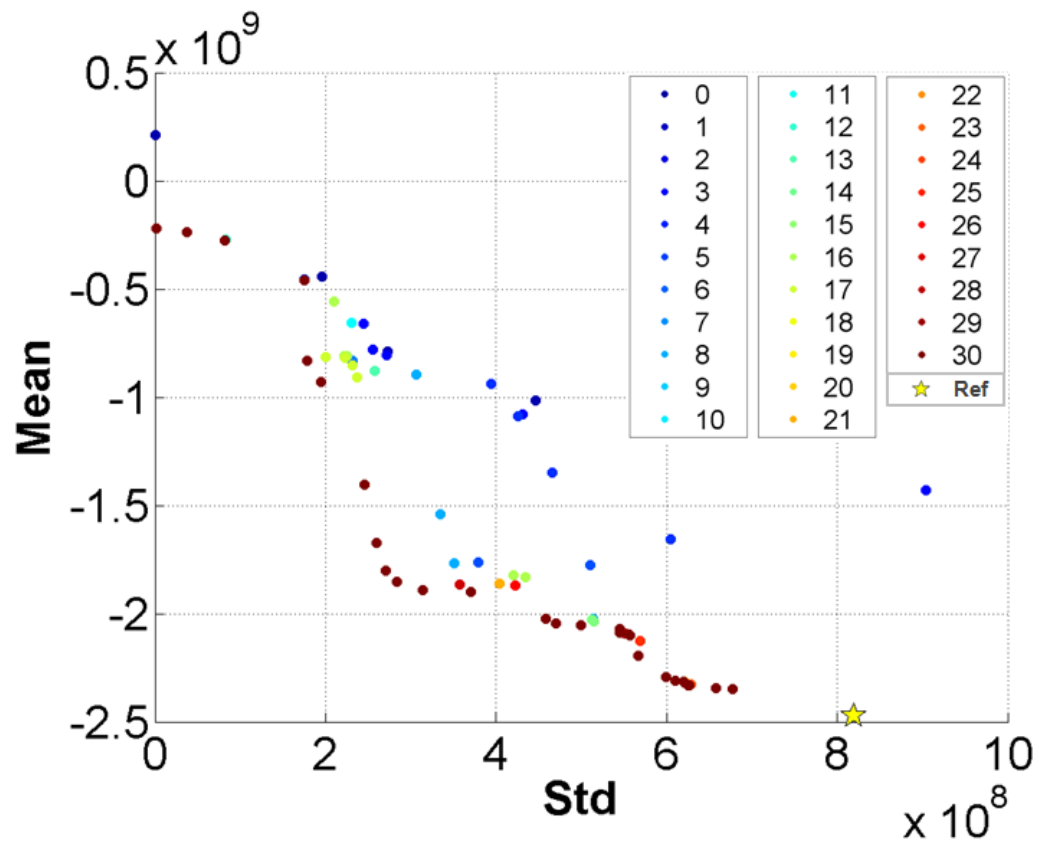
Figure 4.36: Pareto evolutions of top-ranked scenarios from NSGA-II with population size 40
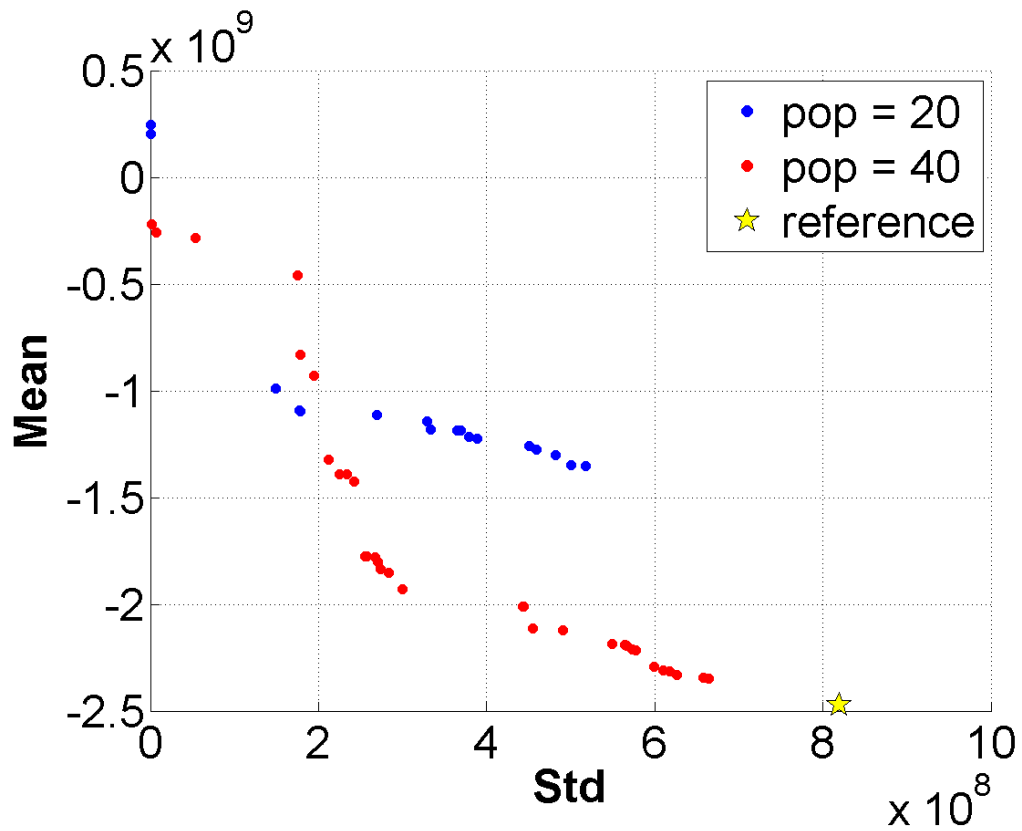
Figure 4.37: Comparison of pareto at last iteration of NSGA-II with different population size

(a) Mean NPV vs. iteration

(b) NPV standard deviation vs. iteration
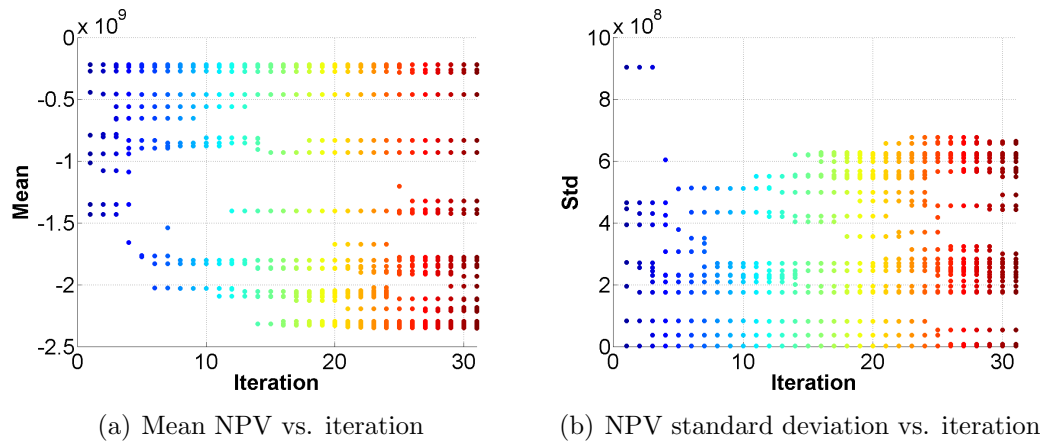
Figure 4.38: Mean NPV and standard deviation evolutions of top-ranked scenarios during iterations of NSGA-II

4.5.3.1 OIP Maps of the Faro Field

As in the Sailor case study, the OIP value of each grid is calculated by the multiplication of pore volume and initial oil saturation in each grid. The 2-D OIP map is the summation of all OIP values from each layer. The same process is repeated to obtain the 2-D OIP map for each geological model to generate the mean OIP map in Figure 4.39(a). The grid cells are ranked based on the OIP percentiles. Figure 4.39(b) shows the reservoir regions with cells colored by the OIP values with 20th, 40th, 60th and 80th percentiles. We use a threshold of 40 percentile to screen out the less productive reservoir regions with low OIP values as shown in Figure 4.39(c). This region is used as a search domain for well placement optimization.

(a) OIP contour map

(b) OIP percentile map
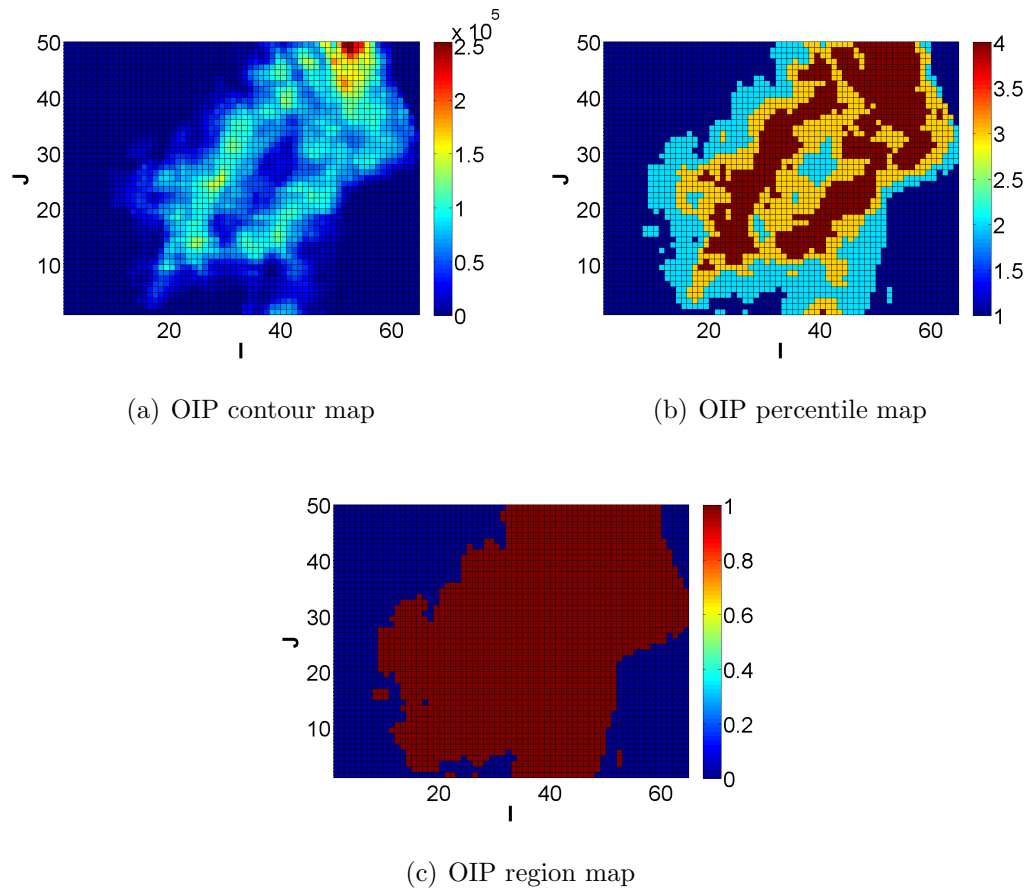
(c) OIP region map

Figure 4.39: OIP contour, percentile and region maps of the Faro case

4.5.3.2 OIP-NSGA-II performance

A quality map based on the OIP is used to assist the NSGA-II (OIP-NSGA-II) for inclined well placement on the Faro field case study where the Pareto evolutions during each iteration are shown in Figure 4.40 while the final Pareto of NSGA-II and OIP-NSGA-II are shown in Figure 4.42. The figures show that the OIP-NSGA-II method results in solutions with higher mean NPV and lower standard deviation compared to the reference case.
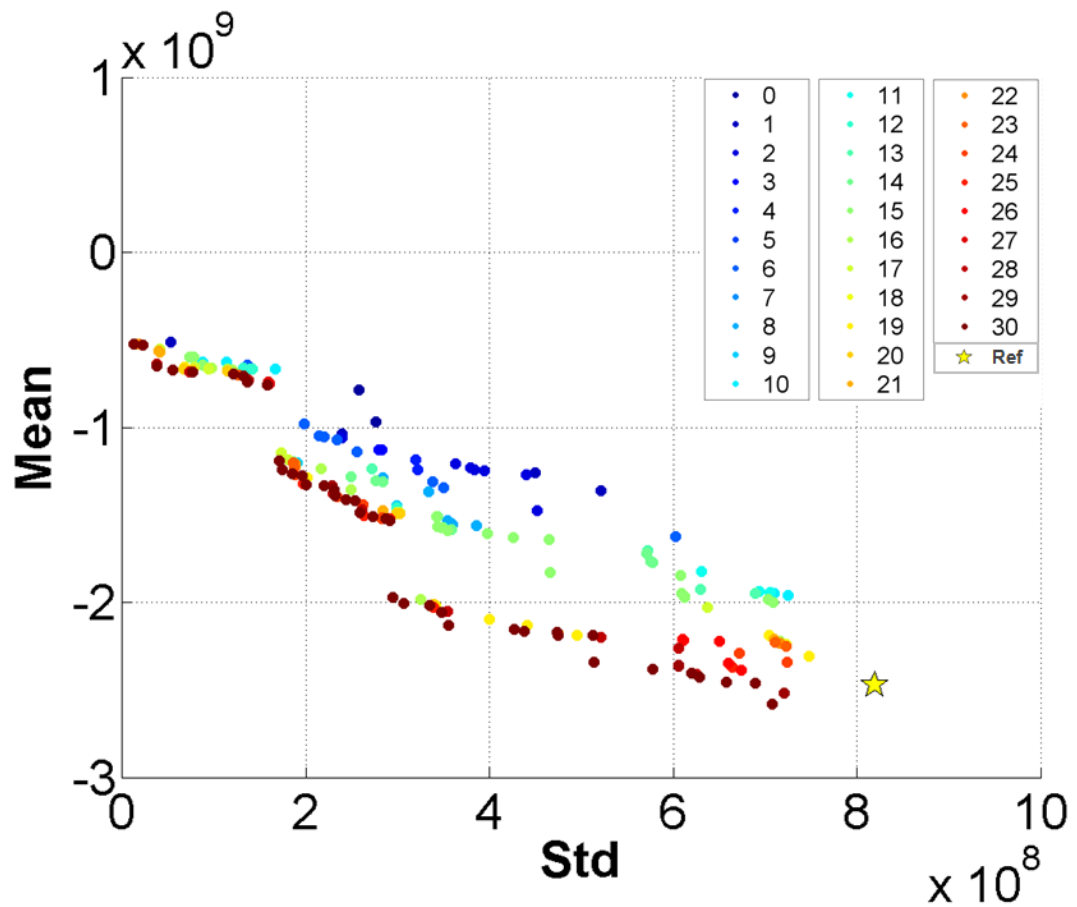
Figure 4.40: Pareto evolutions of top-ranked scenarios from OIP-NSGA-II

The mean and standard deviation of NPV obtained from the top-ranked individuals for each iteration are shown in Figure 4.41. We see the improvement of the mean NPV in the 5th, 15th and 28th iteration, the algorithm was terminated at the

30th iteration because of computational time limits. To have a fair comparison of the algorithm performance, the results at the 30th iteration are used for analysis.

(a) Mean NPV vs. iteration   (b) NPV standard deviation vs. iteration
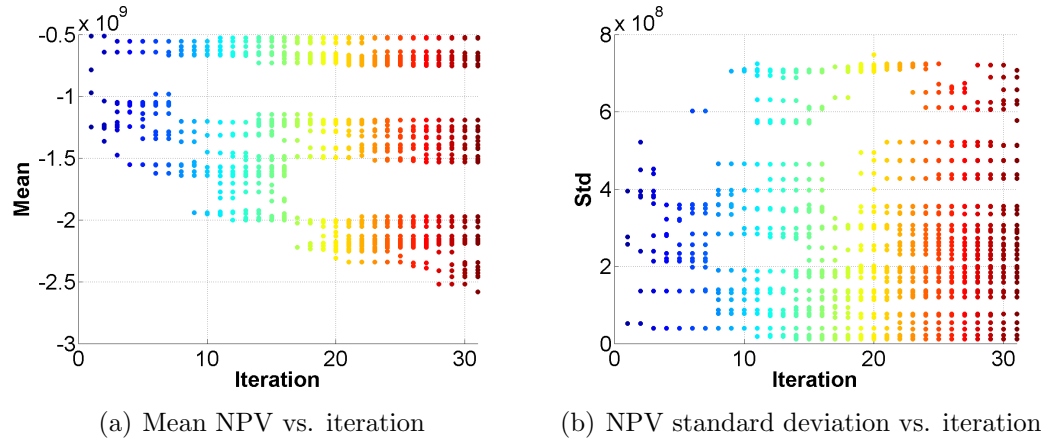
Figure 4.41: Mean NPV and standard deviation evolutions of top-ranked scenarios during iterations of OIP-NSGA-II

4.5.4 Comparisons of NSGA-II and OIP-NSGA-II

The comparison of the final Pareto solutions from NSGA-II and OIP-NSGA-II are shown in Figure 4.42. As mentioned previously, the OIP-NSGA-II is not only able to search for the solutions with higher mean NPV and lower standard deviation, but it also increases the continuity of the Pareto front for each iteration.

The computation time of both the NSGA-II and the OIP-NSGA-II is shown in Figure 4.43 where the OIP-NSGA-II requires only half of the computation time of the NSGA-II; this is achieved by limiting the search domain by utilizing the prior knowledge which also provides a more meaningful and diverse set of solutions.

4.5.5 OIP-NSGA-II Solution Analysis

We select three solutions from the final Pareto of the OIP-NSGA-II. The Scenarios 1, 2 and 9 are selected to compare the production profiles and the residual oil in place with the reference case. From Scenarios 1, 2 and 9, we see in Figure 4.44 that the negative mean NPV value decreases with the standard deviation.
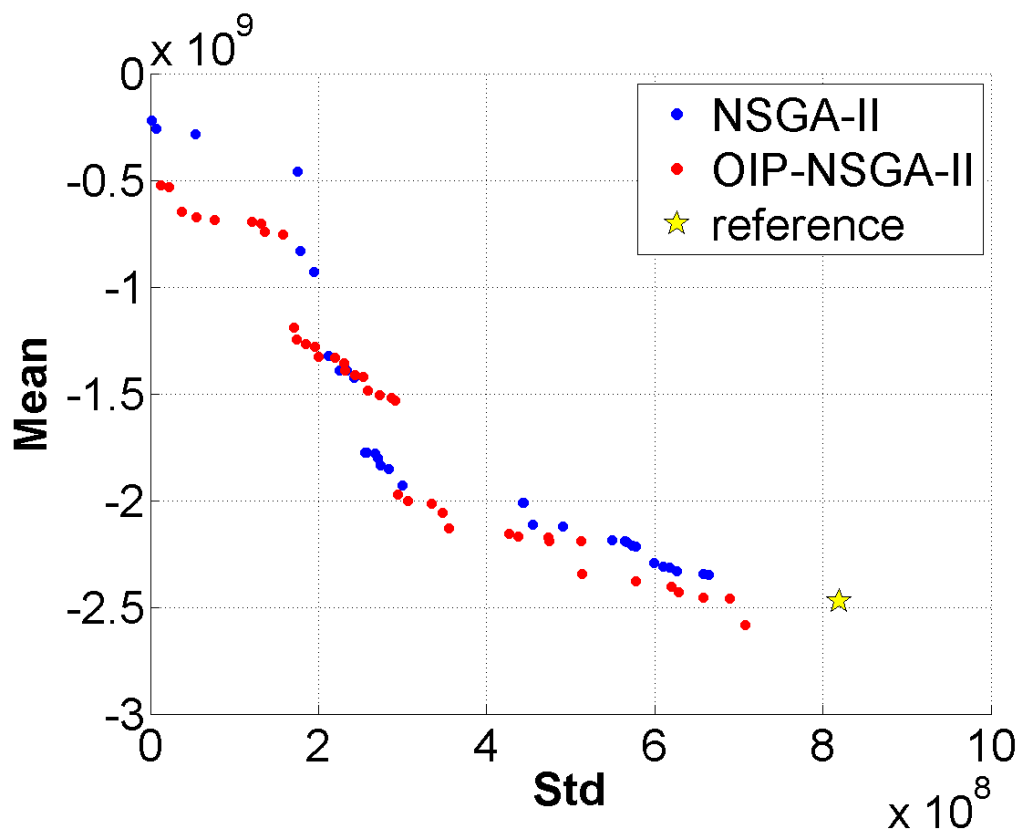
Figure 4.42: Comparison of Pareto at last iteration of NSGA-II & OIP-NSGA-II
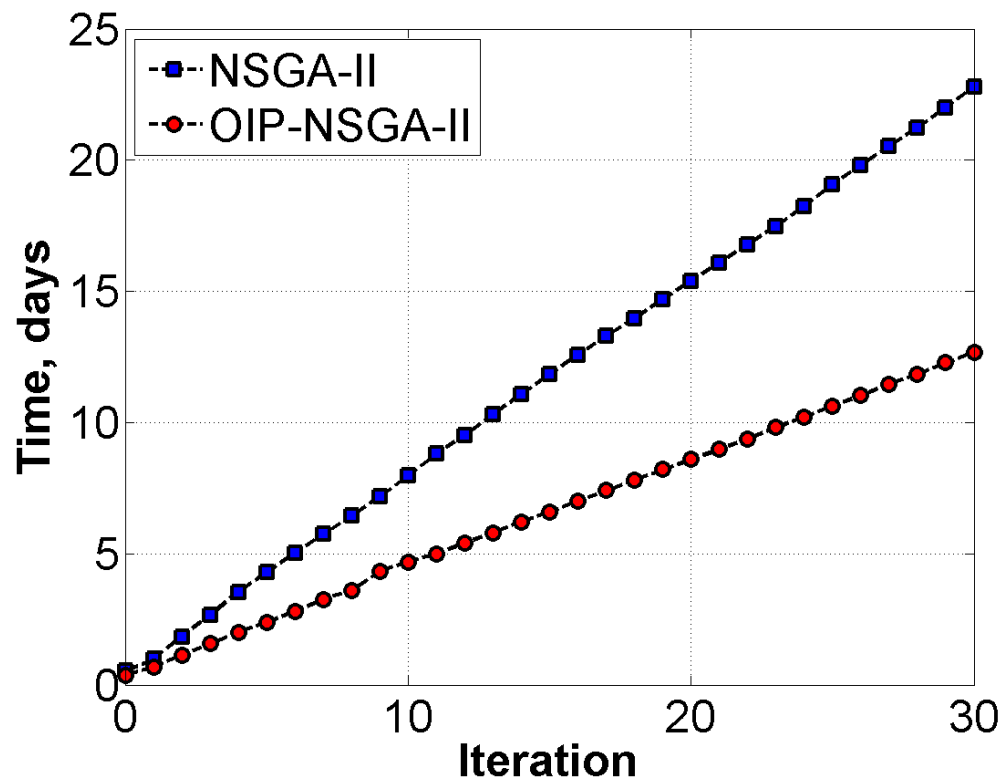
Figure 4.43: Comparison of computation time for NSGA-II & OIP-NSGA-II
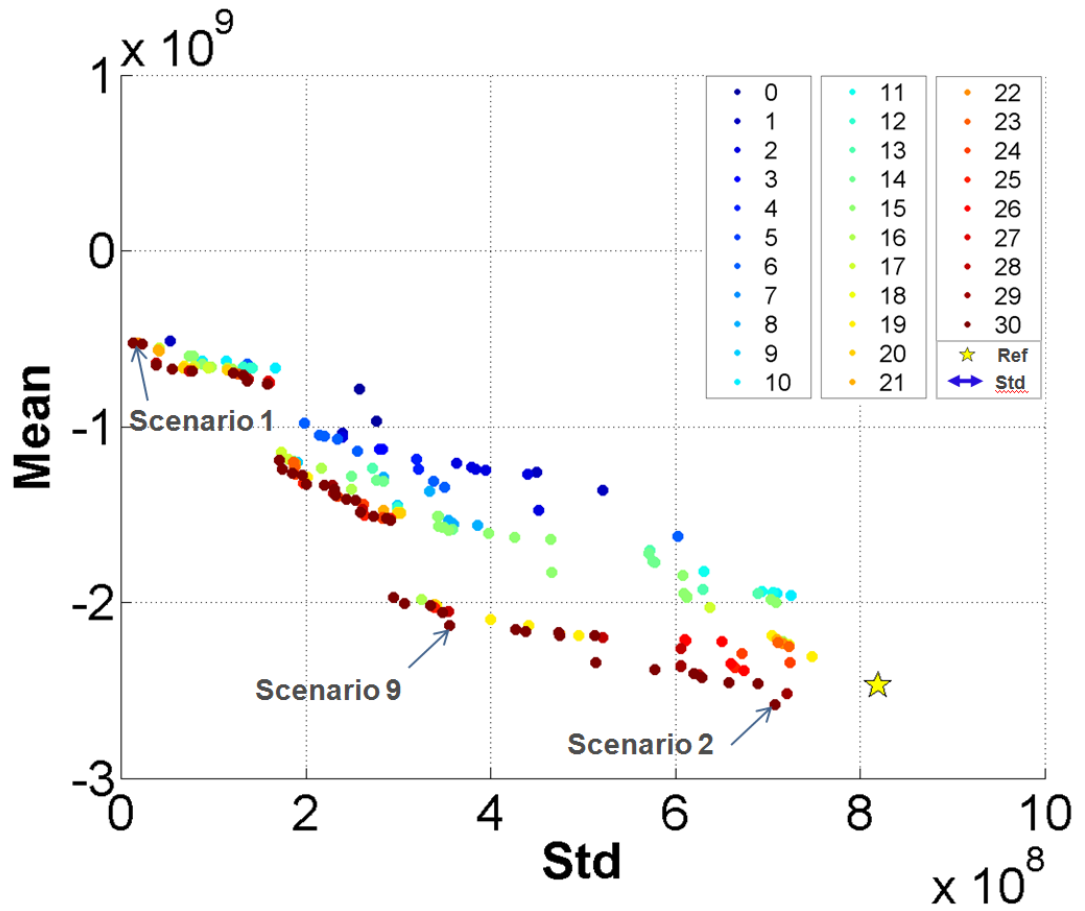
Figure 4.44: Selected scenarios from the final Pareto of the OIP-NSGA-II

The top-view and the 3-D view of well configurations for the three scenarios are shown in Figure 4.45 where the reference case has 2 producers and 2 injectors perforated from the top 6 layers while 2 producers and 1 injector were perforated at the bottom 5 layers. In Scenario 2, the solution with a lower negative mean NPV has 1 producer and 1 injector producing from the top 6 layers while the other 3 producers and 2 injectors are completed in the bottom 5 layers. The better mean NPV achieved by Scenario 2 may be because of better pressure support of the injectors in the bottom layers.

The cumulative liquid production data over all 20 geological realizations at each simulation time step are shown with the box plots in Figure 4.46 where the blue boxes present the results from the reference case. The red boxes correspond to the Scenario 2 that has the highest value for both mean NPV and standard deviation. The reference case has comparable oil and gas production in comparison to Scenario 2 but also has higher water production and injection in this case. Therefore, the negative mean NPV is relatively higher than the one from the Scenario 2. By comparing the data ranges of these scenarios, Scenario 2 has a smaller quantile range than the reference case and this indicates that Scenario 2 is associated with a smaller risk (standard deviation).

With all the liquid production data at each time step, the NPV of each scenario can be evaluated on every geological model. The data are shown in Table 4.4. We plot the box plot of the NPVs in Figure 4.47. We see that the median of the NPV increases from the Scenario 1 towards the Scenario 2. The median value of the Scenario 2 is relatively higher than the one from the reference case, which is also in line with their positions on the Pareto front in Figure 4.44.

The means of the residual oil in place are shown in Figure 4.48 where we see that the amount of residual oil is correlated with the NPV; the scenario with a higher NPV has smaller amount of residual oil. For example, by comparing Scenario 2 with

155
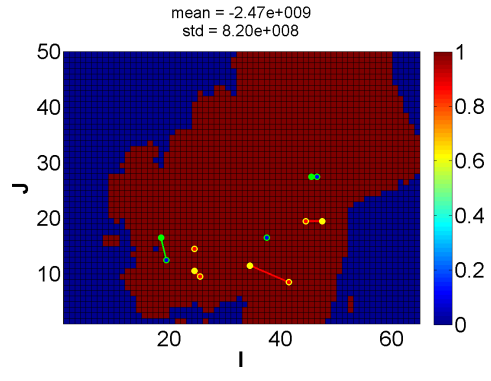
(a) Reference, top view
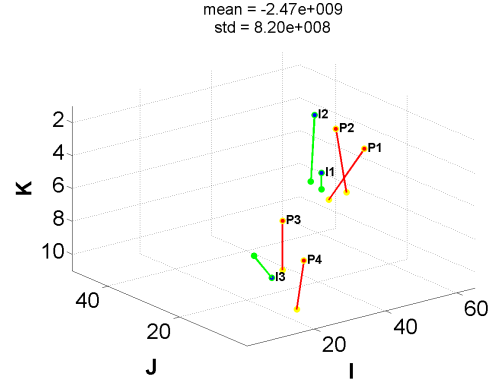
(b) Reference, 3-D
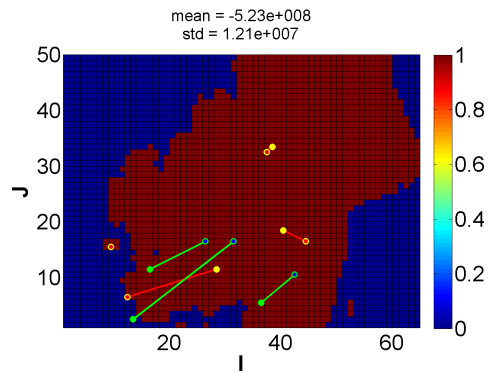
(c) Scenario 1, top view
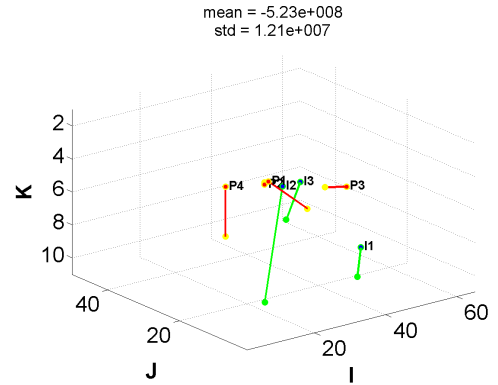
(d) Scenario 1, 3-D
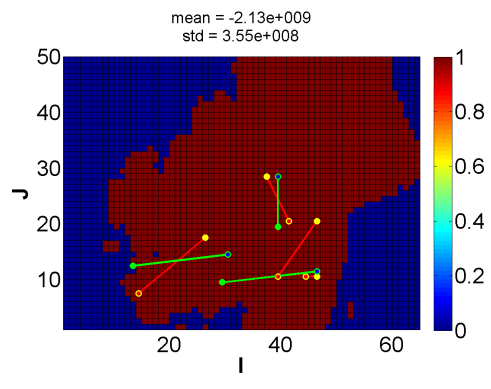
(e) Scenario 9, top view

(f) Scenario 9, 3-D

(g) Scenario 2, top view
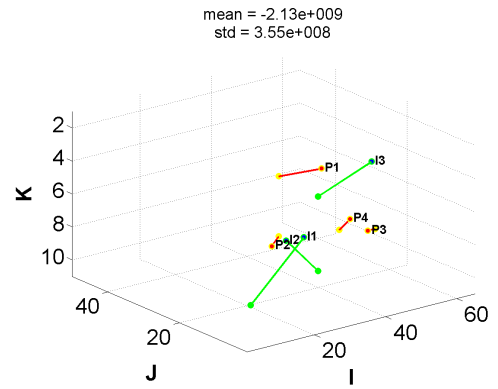
(h) Scenario 2, 3-D
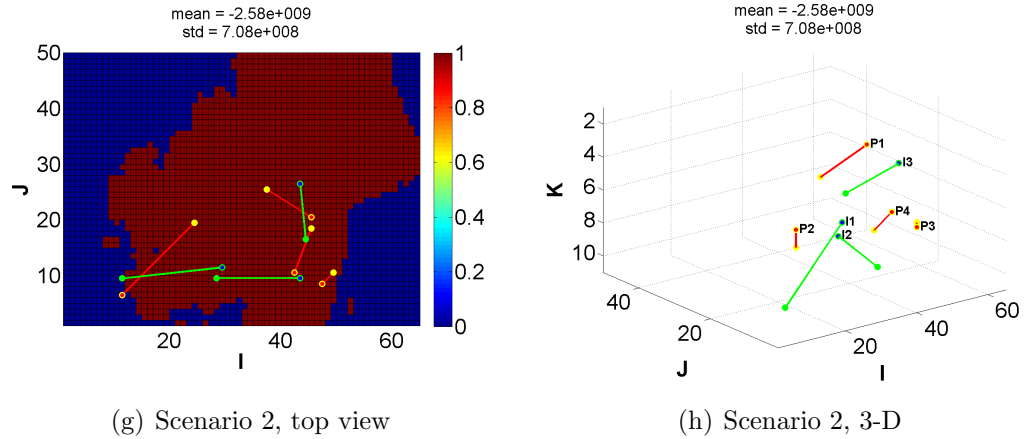
Figure 4.45: Top view and 3-D comparisons of well configurations of base case and selected scenarios from final Pareto of OIP-NSGA-II

Table 4.4: The NPVs of selected scenarios and reference case on all geological models

$(\times 10^9)$	Scenario 4	Scenario 9	Scenario 19	Reference
Relz 1	0.5345	1.7661	1.9724	2.2021
Relz 2	0.5199	1.7104	1.9658	1.5930
Relz 3	0.5262	1.5708	1.5967	1.9508
Relz 4	0.5319	0.5036	1.3253	1.5930
Relz 5	0.5092	2.2545	3.0816	3.0040
Relz 6	0.5200	2.3396	2.6981	2.5236
Relz 7	0.5127	2.4059	2.7072	2.5357
Relz 8	0.5158	2.0557	3.2707	3.0810
Relz 9	0.5296	1.9277	2.3344	2.3869
Relz 10	0.5245	2.0443	2.2372	2.2475
Relz 11	0.5123	2.8753	4.1182	4.0940
Relz 12	0.5329	2.2749	2.6609	2.6233
Relz 13	0.5118	2.2343	2.7282	2.3565
Relz 14	0.5263	2.3648	2.6999	2.6595
Relz 15	0.5161	2.3581	3.6164	3.4291
Relz 16	0.5342	1.8513	2.0383	2.1539
Relz 17	0.5179	2.0764	2.3445	2.4086
Relz 18	0.5606	1.8011	1.8501	1.9884
Relz 19	0.5170	2.5383	2.9237	2.9446
Relz 20	0.5106	2.6048	3.4835	3.2677

157
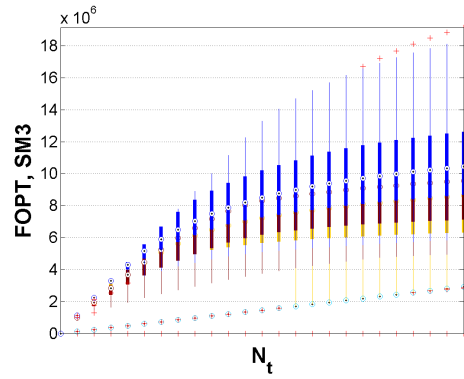
(a) Reference
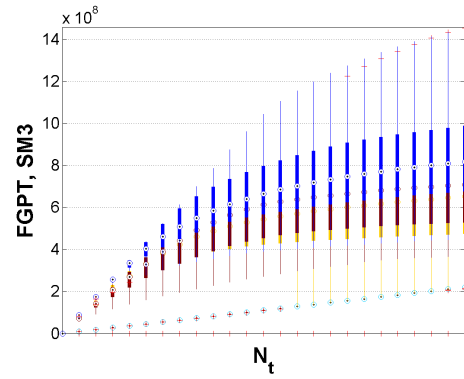
(b) Scenario 1
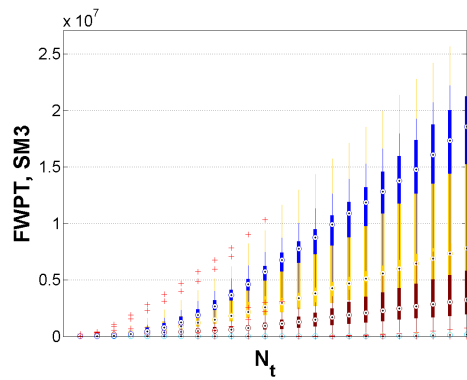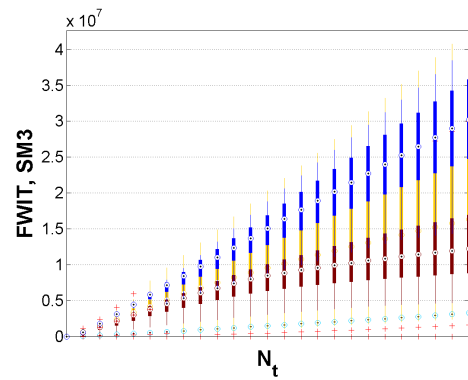
(c) Scenario 9
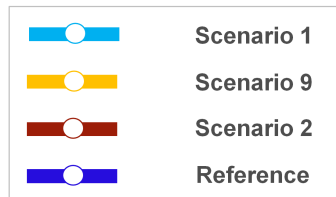
(d) Scenario 2

(e) Legend

Figure 4.46: Box plot of field production profiles of well configurations in base case and selected scenarios from OIP-NSGA-II
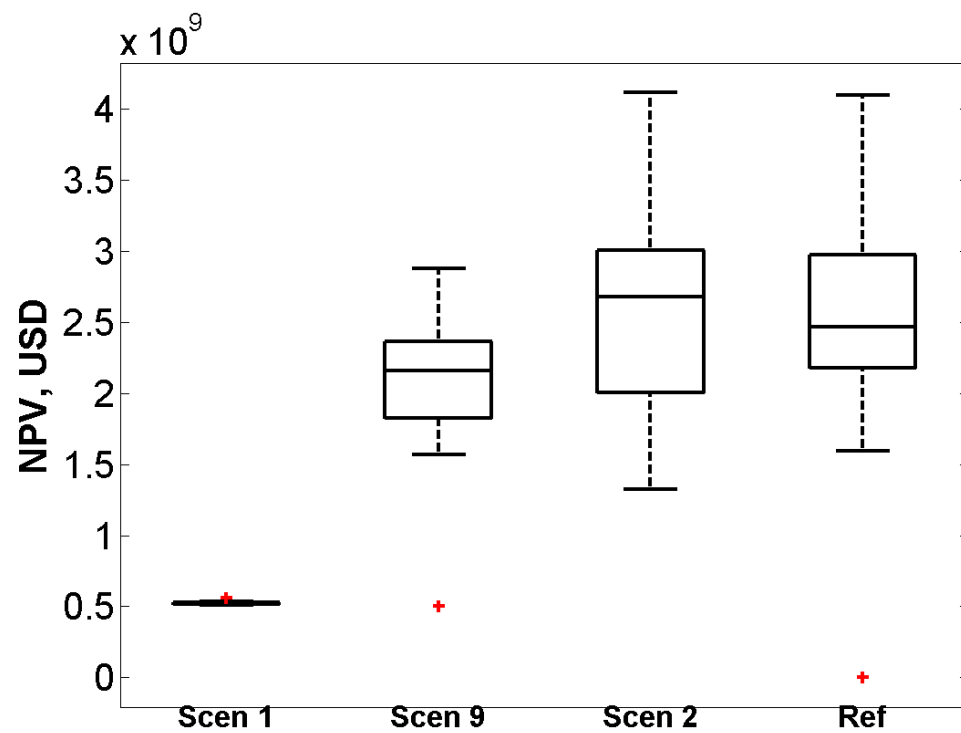
Figure 4.47: Box plot of the NPVs over all geological realizations of reference case and selected each scenario from OIP-NSGA-II

the reference case, we see that the Scenario 2 has slightly less residual oil in place but it has relatively higher NPV.

(a) Reference

(b) Scenario 1

(c) Scenario 9
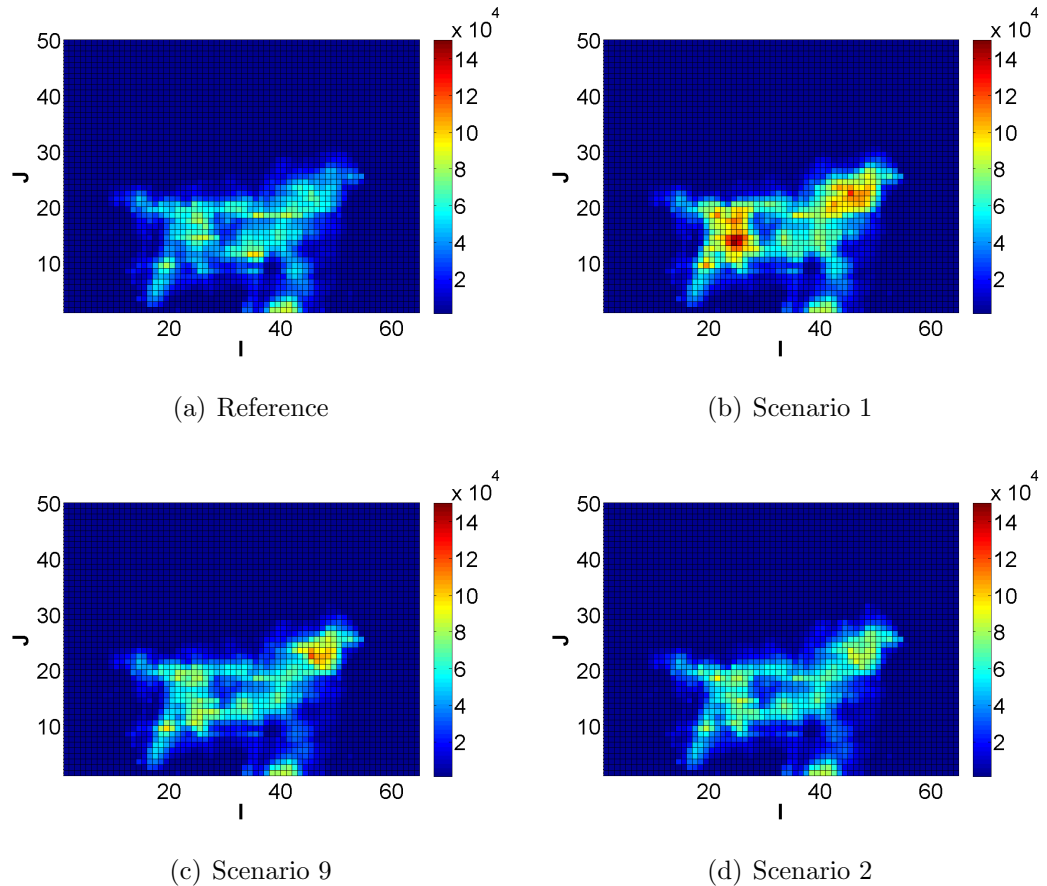
(d) Scenario 2

Figure 4.48: Comparison of residual mean OIP maps for base case and selected scenarios from final Pareto of OIP-NSGA-II

4.6   Summary

In this chapter, I present a promising workflow to place a group of wells while considering geological uncertainty. A mean-variance approach is proposed to handle geological uncertainty and to find robust solutions for well placement. And a multi-objective Pareto-based evolutionary algorithm NSGA-II is applied, with which I am able to obtain a group of optimization solutions which provides decision-makers with the ability to make such weighted decisions. The NSGA-II algorithm applied to the case studies is efficient in searching for multiple solutions in the variable domain,

160

and it is able to find a Pareto front after a few iterations during the optimization process. In order to accelerate the optimization process, I reduce the variable domain by applying an oil in place (OIP) map and constraint the well placement to a smaller region. We see that oil in place (OIP) is an important indicator as prior knowledge for placing wells and the OIP-assisted NSGA-II (OIP-NSGA-II) can largely improve the optimization efficiency.

CHAPTER V

SUMMARY AND CONCLUSIONS

In this dissertation, I present multiple promising approaches and the workflow for decision-making with well placement optimization in oil field development. In general, the studies are carried out in the following order. First, I study and compare two stochastic approximated-gradient-based approaches: the ensemble based optimization method (EnOpt) and the fixed-gain simultaneous perturbation stochastic approximation (FSP) for single well placement. It is shown that FSP is more efficient than the EnOpt method. Second, considering the computational efficiency, I propose the idea of using quality map assisted fixed gain SPSA algorithm (QM-FSP) to identify regions within the reservoir with high connectivity and high oil production potential and to place an optimal number of wells. Third, I consider the multi-objective optimization in real decision-making situations with geological uncertainty. I propose a workflow which incorporates a multi-objective optimization method and is able to place a group of wells efficiently while considering geological uncertainty. The method applied in this work is a multi-objective pareto-based evolutionary algorithm NSGA-II, with which I am able to obtain a group of optimization solutions, and the decision-makers could make decisions based on their risk attitude. In order to accelerate the optimization process, I reduce the variable domain by applying an oil in place (OIP) map and constrained the well placement to smaller regions.

In summary, the following key conclusions can be drawn from this work:

1. I develop an automated process to evaluate productive reservoir regions using quality maps that are then probed using FSP for optimal multiple well placement when the number of wells is not known a priori. The methodology

162

proposed here allows the reservoir engineer to optimally place a number of wells at his/her desktop PC without the need for additional computational hardware as is the case with several other approaches.

2. The advantage of EnOpt and FSP is that they do not require access to simulator code and are designed to work only with simulator output, irrespective of the simulator formulations.

3. Results from the comparison of EnOpt and FSP show that FSP is more efficient in terms of function evaluations, computation time and improvement in objective function values. Comparing EnOpt and FSP, FSP generally requires fewer function evaluations and is recommended as one of the better approaches for well placement.

4. Multiple well placement using QM-FSP has been demonstrated for several case studies and is able to provide a solution with an order of magnitude reduction in computational effort over traditional applications. While other approaches outlined in the literature review chapter are promising, the number of function evaluations required are usually very large. Additionally, they do not extend very well to the placement of multiple wells and may require the use of exhaustive searches in those situations.

5. The difference of the quality map proposed in this work from the one introduced in other literature is the calculation of the quality values. The transmissibility and the relative oil permeability are the parameters incorporated into the formula of quality calculation. The quality map proposed in this work is superior to other previous approaches due to its computational efficiency. We do not need any simulation runs to estimate the quality map.

6. I apply a mean-variance approach to seek for robust solutions for well placement

while handling geological uncertainty. In this manner, not only the average NPV is considered but also the risk of the possible solutions can be quantified in the decision-making.

7. The multi-objective optimization technique NSGA-II applied in this work is efficient in searching for multiple solutions in variable domain, and it is able to find a group of Pareto front solutions during the optimization.

8. Oil in place is an important indicator as prior knowledge for well planning and OIP map assisted NSGA-II (OIP-NSGA-II) can largely improve the optimization efficiency by restrain the search to a smaller feasible domain of optimization variables.

BIBLIOGRAPHY

Aanonsen, S. I., A. L. Eide, and L. Holden, Optimizing reservoir performance under uncertainty with application to well location, 1995.

Artus, V., L. J. Durlofsky, J. Onwunalu, and K. Aziz, Optimization of nonconventional wells under uncertainty using statistical proxies, **10**(4), 389–404, 2006.

Badru, O., *Well Placement Optimization Using The Quality Map Approach*, Master's thesis, Stanford University, Stanford, California, 2003.

Bangerth, W., H. Klie, V. Matossian, M. Parashar, and M. Wheeler, An autonomic reservoir framework for the stochastic optimization of well placement, *Cluster Computing*, **8**, 255–269, 2005.

Bangerth, W., H. Klie, M. F. Wheeler, P. L. Stoffa, and M. K. Sen, On optimization algorithms for the reservoir oil well placement problem, *Computational Geosciences*, **10**(3), 303–319, 2006.

Barnhart, C. M., J. E. Wieselthier, and A. Ephremides, Admission-control policies for multihop wireless networks, *Wireless Networks 1*, pp. 373–387, 1995.

Beckner, B. and X. Song, Field development planning using simulated annealing - optimal economic well schedulling and placement, SPE-30650, in *1995 SPE Annual Technical Conference Exhibition. Dallas, USA*, pp. 209–221, 1995.

Bhatnagar, S. and H. J. Kowshik, A discrete parameter stochastic approximation algorithm for simulation optimization, *Simulation*, **81**(11), 757–772, 2005.

Bittencourt, A. C. and R. N. Horne, Reservoir development and design optimization SPE-38895, in *SPE Annual Technical Conference Exhibition. San Antonio, Texas, USA*, 1997.

Bléhaut, J.-F., The assessment of geological uncertainties in development project planning, 1991.

Bouzarkouna, Z., *Well Placement Optimization*, Ph.D. thesis, University of Paris-Sud, Paris, France, 2012.

Bouzarkouna, Z., A. Auger, and D. Y. Ding, Investigating the local-meta-model CMA-ES for large population sizes, in *Applications of Evolutionary Computation*, (edited by C. Di Chio, S. Cagnoni, C. Cotta, M. Ebner, A. Ekárt, A. Esparcia-Alcazar, C.-K. Goh, J. Merelo, F. Neri, M. Preuß, J. Togelius, and G. Yannakakis), vol. 6024 of *Lecture Notes in Computer Science*, pp. 402–411, Springer Berlin / Heidelberg, 2010.

Bouzarkouna, Z., D. Y. Ding, and A. Auger, Well placement optimization under uncertainty with CMA-ES using the neighborhood, in *13th European Conference on the Mathematics of Oil Recovery (ECMOR XIII)*, EAGE, 2012.

Bouzarkouna, Z., D.-Y. Ding, and A. Auger, Partially separated metamodels with evolution strategies for well-placement optimization, *SPE Journal*, (SPE-143292-PA), 2013.

Brouwer, D. R., G. Nævdal, J. D. Jansen, E. H. Vefring, and C. P. J. W. van Kruijsdijk, Improved reservoir management through optimal control and continuous model updating, in *SPE Annual Technical Conference and Exhibition, 26-29 September, Houston, Texas*, 2004.

Chang, Y., Z. Bouzarkouna, and D. Devegowda, Handling geological uncertainty in oil field development with multi-objective optimization technique, in *14th European Conference on the Mathematics of Oil Recovery ECMOR 2014, Catania, Italy*, EAGE, 2014.

Chang, Y., Z. Bouzarkouna, and D. Devegowda, Multi-objective optimization for rapid and robust optimal oilfield development under geological uncertainty, *Computational Geosciences*, **19**(4), 933–950, 2015.

Chaudhri, M. M., H. A. Phale, N. Liu, and D. S. Oliver, An improved approach for ensemble-based production optimization (SPE 121305), 2009.

Chen, Y., *Ensemble-based closed-loop optimization*, Ph.D. thesis, University of Oklahoma, Norman, Oklahoma, 2008.

Chen, Y. and D. S. Oliver, Ensemble-based closed-loop optimization applied to Brugge Field (SPE 118926), in *Proc. of the 2009 SPE Reservoir Simulation Symposium*, 2009.

Chin, D. C., Comparative study of stochastic algorithms for system optimization based on gradient approximations, *IEEE Transactions on Systems, Man and Cybernetics–Part B: Cybernetics*, **27**(2), 244–249, 1997.

Conn, A., K. Scheinberg, and L. Vicente, *Introduction to Derivative-Free Optimization*, Society for Industrial and Applied Mathematics, 2009.

Cottini-Loureiro, A. and A. Araujo, Optimized well location by combination of multiple realization approach and quality map methods, 2005.

Cruz, P. S., R. N. Horne, and C. V. Deutsch, The quality map: A tool for reservoir uncertainty quantificatio and decision making, 1999.

Cruz, P. S., R. N. Horne, and C. V. Deutsch, The quality map: A tool for reservoir uncertainty quantificatio and decision making, *SPE Reservoir Evaluation & Engineering*, 2004.

Custódio, A. L., H. Rocha, and L. N. Vicente, Incorporating minimum frobenius norm

models in direct search, *Computational Optimization and Applications*, **46**(2), 265–278, 2010.

Custódio, A. L. and L. N. Vicente, Using sampling and simplex derivatives in pattern search methods, *SIAM Journal on Optimization*, **18**(2), 537–555, 2007.

Das, I. and J. Dennis, A closer look at drawbacks of minimizing weighted sums of objectives for pareto set generation in multicriteria optimization problems, *Structural Optimization*, **14**, 63–69, 1997.

Deb, K. and R. B. Agrawal, Simulated binary crossover for continuous search space, *Complex Systems*, **9**, 115–148, 1995.

Deb, K., A. Pratap, S. Agarwal, and T. Meyarivan, A fast and elitist multiobjective genetic algorithm: Nsga-ii, *IEEE Transactions on Evolutionary Computation*, **6**, 182–197, 2002.

Dehdari, V. and D. S. Oliver, Sequential quadratic programming (sqp) for solving constrained production optimization – case study from brugge field, in *2011 SPE Reservoir Simulation Symposium, The Woodlands, Texas, USA*, pp. 1–15, 2011.

Devegowda, D. and H. Gao, Integrated uncertainty assessment for unconventional gas reservoir project development (SPE-111203), in *2007 SPE Eastern Regional Meeting, Lexington, Kentucky, USA*, 2007.

Ding, S., H. Jiang, J. Li, and G. Tang, Optimization of well placement by combination of a modified particle swarm optimization algorithm and quality map method, *Computational Geosciences*, **18**(5), 747–762, 2014.

Do, S., F. Forouzanfar, and A. Reynolds, Estimation of optimal well controls using the augmented lagrangian function with approximate derivatives, *IFAC Workshop*

on *Automatic Control in Offshore Oil and Gas Production, Trondheim, Norway*, 2012.

Do, S. and A. Reynolds, Theoretical connections between optimization algorithms based on an approximate gradient, *Computational Geosciences*, **17**(6), 959–973, 2013.

Do, S. T., *Application of SPSA-type Algorithms to Production Optimization*, Ph.D. thesis, Tulsa, OK, USA, 2012, AAI3507104.

Emerick, A. A., P. S. A., E. Silva, B. Messer, and L. F. Almeida, Well placement optimization using a genetic algorithm with nonlinear constraints, in *2009 SPE Reservoir Simulation Symposium, The Woodlands, Texas, USA*, 2009.

Emmerich, M., N. Beume, and B. Naujoks, An EMO algorithm using the hypervolume measure as selection criterion, in *2005 International Conference*, pp. 62–76, Springer, 2005.

Ferraro, P. and F. Verga, Use of evolutionary algorithms in single and multi-objective optimization techniques for assisted history matching, in *Proc. of the Offshore Mediterranean Conference and Exhibition in Ravenna, Italy, March 25-27, 2009*, 2009.

Ferreira, J., C. Fonseca, and A. Gaspar-Cunha, Methodology to Select Solutions from the Pareto-Optimal Set: A Comparative Study, in *2007 Genetic and Evolutionary Computation Conference (GECCO'2007)*, (edited by D. Thierens), vol. 1, pp. 789–796, ACM Press, London, UK, 2007.

Fonseca, R., O. Leeuwenburgh, and J. Jansen, Ensemble based multi-objective production optimization of smart wells, in *Proceedings of the 13th European Conference on the Mathematics of Oil Recovery (ECMOR XIII)*, Biarritz, France, 10 - 13 September, 2012.

Forouzanfar, F., G. Li, and A. C. Reynolds, A two-stage well placement optimization method based on adjoint gradient, in *SPE Annual Technical Conference and Exhibition, Florence, Italy*, 2010.

Gao, G., G. Li, and A. C. Reynolds, A stochastic optimization algorithm for automatic history matching, *SPE Journal*, **12**(2), 196–208, 2007.

Gerencsér, L. and S. D. Hill, Optimization over discrete sets via spsa, in *Conference on Decision & Control, Phoenix, Arizona, USA*, pp. 1791–1795, 1999.

Gerencsér, L., S. D. Hill, and Z. Vágoó, Discrete optimization via SPSA, in *Proceedings of American Control Conference, Arlington, VA June 25-27, 2001*, 2001.

Gerencsér, L., S. D. Hill, Z. Vágoó, and Z. Vincze, Discrete optimization, SPSA and markov chain monte carlo methods, in *2004 American Control Conference, Boston, Massachusetts*, 2004.

Gokbayrak, K. and C. G. Cassandras, Online surrogate problem methodology for stochastic discrete resource allocation problems, *Journal of optimization Theory and Applications*, **108**(2), 349–375, 2001.

Guyaguler, B. and R. Horne, Optimization of well placement, *Journal of Energy Resources Technology*, **122**, 64–70, 2000.

Guyaguler, B. and R. N. Horne, Uncertainty assessment of well-placement optimization, *SPE Reservoir Evaluation & Engineering*, **7**(1), 24–32, 2004.

Hajizadeh, Y., M. Christie, and V. Demyanov, Towards multiobjective history matching: faster convergence and uncertainty quantification, SPE-141111, *SPE Reservoir Simulation, The Woodlands, Texas, USA, 21-23 February 2011*, 2011.

Handels, M., M. J. Zandvliet, D. R. Brouwer, and J. D. Jansen, Adjoint-based well-placement optimization under production constraints (SPE 105797), in *Proceedings*

of the SPE Reservoir Simulation Symposium, Houston, Texas, USA, 26-28 February 2007, 2007.

Hill, S. D., Discrete stochastic approximation with application to resource allocation, *Johns Hopkins Apl Technical Digest*, **26**(1), 2005.

Horn, J., N. Nafpliotis, and D. E. Goldberg, Multiobjective optimization using the niched pareto genetic algorithm, Tech. rep., 1994.

Imperial College, L., PUNQ-S3 model, 2009.

Ishibuchi, H., N. Tsukamoto, and Y. Nojima, Evolutionary many-objective optimization: A short review., in *IEEE Congress on Evolutionary Computation*, pp. 2419–2426, IEEE, 2008.

Kiefer, J. and J. Wolfowitz, Stochastic estimation of a regression function, *Ann. Math. Statist.*, **23**, 462–466, 1952.

Land, A. H. and A. G. Doig, An automatic method of solving discrete programming problems, *Econometrica: Journal of the Econometric Society*, pp. 497–520, 1960.

Leeuwenburgh, O., P. J. P. Egberts, and O. A. Abbink, Ensemble methods for reservoir life-cycle optimization and well placement (SPE 136916), *Proceedings of SPE/DGS Annual Technical and Symposium and Exhibition, 04-07 April 2010, Al-Khobar, Saudi Arabia*, 2010.

Li, G. and A. Reynolds, Uncertainty quantification of reservoir performance predictions using a stochastic optimization algorithm, *Computational Geosciences*, **15**(3), 451–462, 2011.

Li, L., B. Jafarpour, and M. R. Mohammad-Khaninezhad, A simultaneous perturbation stochastic approximation algorithm for coupled well placement and control

optimization under geologic uncertainty, *Computational Geosciences*, **17**(1), 167–188, 2013.

Little, J. D., K. G. Murty, D. W. Sweeney, and C. Karel, An algorithm for the traveling salesman problem, *Operations research*, **11**(6), 972–989, 1963.

Liu, N., S. Betancourt, and D. S. Oliver, Assessment of uncertainty assessment methods, in *Proceedings of the 2001 SPE Annual Technical Conference and Exhibition*, pp. 1–15, 2001.

Liu, N. and Y. Jalali, Closing the loop between reservoir modeling and well placement and positioning, 2006.

Liu, X., A. C. Reynolds, et al., Multi-objective optimization for maximizing expectation and minimizing uncertainty or risk with application to optimal well control, in *SPE Reservoir Simulation Symposium*, Society of Petroleum Engineers, 2015.

Lorentzen, R. J., A. M. Berg, G. Nævdal, and E. H. Vefring, A new approach for dynamic optimization of waterflooding problems, in *SPE Intelligent Energy Conference and Exhibition*, pp. 1–11, 2006.

Marler, R. and J. Arora, Survey of multi-objective optimization methods for engineering, *Structural and Multidisciplinary Optimization April 2004*, **26**(6), 369–395, 2004.

Maryak, J. L. and D. C. Chin, Global random optimization by simultaneous perturbation stochastic approximation, *IEEE Transactions on Automatic Control*, **53**(3), 780–783, 2008.

Maschio, C. and D. J. Schiozer, A new methodology for assisted history matching using independent objective functions, *Petroleum Science and Technology*, **26**(9), 1047–1062, 2008.

Maschio, C., A. C. Vidal, and D. J. Schiozer, A framework to integrate history matching and geostatistical modeling using genetic algorithm and direct search methods, *Journal of Petroleum Science and Engineering*, **63**(1–4), 34–42, 2008.

Mishra, V., S. Bhatnagar, and N. Hemachandra, Discrete parameter simulation optimization algorithms with applications to admission control with dependent service times, 2007.

Mohamed, L., M. Christie, and V. Demyanov, History matching and uncertainty quantification: Multiobjective particle swarm optimisation approach, (SPE 143067), in *Proceedings of the SPE EUROPEC/EAGE Annual Conference and Exhibition, Vienna, Austria, 23-26 May 2011*, 2011.

Mullins, L., Reserves uncertainty quantification − an executive perspective, 2014.

Nævdal, G., D. R. Brouwer, and J.-D. Jansen, Waterflooding using closed-loop control, *Computational Geosciences*, **10**(1), 37–60, 2006.

Nakajima, L. and D. Schiozer, Horizontal well placement optimization using quality map definition, *SPE Canadian International Petroleum Conference, Alberta, Canada. June 10-12, 2003*, 2003.

Nwaozo, J., *Dynamic optimization of a water flood reservoir*, Masters thesis, University of Oklahoma, 2006.

Onwunalu, J. and L. Durlofsky, Development and application of a new well pattern optimization algorithm for optimizaing large-scale field development, in *2009 SPE Annual Technical Conference and Exhibition, New Orleans, Louisiana, USA*, pp. 1–18, 2009.

Onwunalu, J. E. and L. Durlofsky, Application of a particle swarm optimization algorithm for determining optimum well location and type, *Computational Geosciences*, **14**(1), 183–198, 2010.

Ozdogan, U. and R. N. Horne, Optimization of well placement under time-dependent uncertainty, 2006.

Pan, Y. and R. N. Horne, Improved methods for multivariate optimization of field development scheduling and well placement design (SPE 49055), in *SPE Annual Technical Conference and Exihibition, New Orleans, Louisiana, USA, 27-30 September 1998*, pp. 1–16, 1998.

Papadimitriou, C. H. and K. Steiglitz, *Combinatorial optimization: algorithms and complexity*, Courier Corporation, 1998.

Park, H.-Y., A. Datta-Gupta, and M. J. King, Handling conflicting multiple objectives using pareto-based evolutionary algorithm during history matching of reservoir performance, *Journal of Petroleum Science and Engineering*, **125**(0), 48 – 66, 2015.

Pettingill, H. S., The global deepwater play: A historical and geological perspective 27 years after first discovery, in *AAPG Hedberg Research Conference, Veracruz, Mexico*, 2006.

Petvipusit, R., *Dynamic Well Scheduling and Well Type Optimization Using Ensemble-based Method (EnOpt)*, Master's thesis, University of Oklahoma, 2011.

Pradlwarter, H., Relative importance of uncertain structural parameters. part i: algorithm, *Computational Mechanics*, **40**(4), 627–635, 2007.

Raghuwanshi, M. M. and O. G. Kakde, Survey on multiobjective evolutionary and real coded genetic algorithms, in *Proceedings of the 8th Asia Pacic Symposium on Intelligent and Evolutionasy Systems*, pp. 150–161, 2004.

Reynolds, A. and X. Liu, Gradient-based multiobjective optimization with applications to waterflooding optimization, in *ECMOR XIV-14th European conference on the mathematics of oil recovery*, 2014.

Robbins, H. and S. Monro, A stochastic approximation method, *Ann. Math. Statist.*, **22**, 400–407, 1951.

Sadegh, P. and J. C. Spall, Optimal random perturbations for stochastic approximation using a simultaneous perturbation gradient approximation, *IEEE Transactions on Automatic Control*, **43**(10), 1480–1484, 1998.

Salmachi, A., M. Sayyafzadeh, and M. Haghighi, Infill well placement optimization in coal bed methane reservoirs using genetic algorithm, *Fuel*, **111**(0), 248 – 258, 2013.

Sarma, P. and W. Chen, Efficient well placement optimization with gradient-based algorithms and adjoint models (SPE 112257), in *2008 SPE Intelligent Energy Conference and Exhibition, Amsterdam, The Netherlands, 25-27 February 2008*, pp. 1–18, 2008.

Schulze-Riegert, R., M. Bagheri, M. Krosche, N. Kueck, and D. Ma, Multiple-objective optimization applied to well path design under geological uncertainty (SPE 141712), in *SPE Reservoir Simulation Symposium, 21–23 February, The Woodlands, Texas, USA*, 2011.

Schulze-Riegert, R., M. Dong, K. L. Heskestad, M. Krosche, H. Mustafa, K. Stekolschikov, and M. Bagheri, Well path design optimization under geological uncertainty: Application to complex north sea field, in *2010 SPE Russian Oil & Gas Technical Conference and Exhibition, Moscow, Russia*, 2010.

Schulze-Riegert, R., M. Krosche, A. Fahimuddin, and S. Ghedan, Multi-objective optimization with application to model validation and uncertainty quantification, in

SPE Middle East Oil and Gas Show and Conference, 11–14 March 2007, Kingdom of Bahrain, 2007.

Seshadri, A., A fast elitist multiobjective genetic algorithm: NSGA-II, Class project, Oklahoma State University, 2006.

Spall, J., S. Hill, and D. Stark, Theoretical framework for comparing several stochastic optimization approaches, in *Probabilistic and Randomized Methods for Design under Uncertainty*, (edited by G. Calafiore and F. Dabbene), pp. 99–117, Springer London, 2006.

Spall, J. C., A stochastic approximation technique for generating maximum likelihood parameter estimates, in *American Control Conference*, pp. 1161–1167, 1987.

Spall, J. C., Multivariate stochastic approximation using a simultaneous perturbation gradient approximation, *IEEE Transactions Automat. Control.*, **37**(3), 332–341, 1992.

Spall, J. C., Implementation of the simultaneous perturbation algorithm for stochastic optimization, *IEEE Transactions on Aerospace and Electronic Systems*, **34**(3), 817–823, 1998a.

Spall, J. C., An overview of the simultaneous perturbation method for efficient optimization, *Johns Hopkins APL Technical Digest*, **19**(4), 482–492, 1998b.

Spall, J. C., Adaptive stochastic approximation by the simultaneous perturbation method, *IEEE Transactions on Automat. Control.*, **45**(10), 1839–1853, 2000.

Spall, J. C., Accelerated second-order stochastic optimization using only function measurements, *Proc. of the 2001 Winter Simulation Conf.*, 2001.

Spall, J. C., *Introduction to Stochastic Search and Optimization*, John Wiley & Sons, Inc., Hoboken, New Jersey, 2003.

Srinivas, N. and K. Deb, Muiltiobjective optimization using nondominated sorting in genetic algorithms, *Evolutionary Computation*, **2**(3), 221–248, 1994.

Su, H. and D. S. Oliver, Smart well production optimization using an ensemble-based method (SPE 126072), *SPE Reservoir Evaluation & Engineering*, 2010.

Tarantola, A., *Inverse problem theory and methods for model parameter estimation*, Society for Industrial Mathematics, 2005.

Vlemmix, S., G. Joosten, D. Brouwer, and J. Jansen, Adjoint-based well trajectory optimization in a thin oil rim, in *2009 SPE EUROPC/EAGE Annual Conference and Exhibition, Amsterdam, The Netherlands*, pp. 1–15, 2009.

Wang, C., G. Li, and A. C. Reynolds, Optimal well placement for production optimization, SPE-111154, in *Proceedings of the SPE Eastern Regional Meeting, 17–19 October 2007, Lexington, Kentucky*, 2007.

Wang, C., G. Li, and A. C. Reynolds, Production optimization in closed-loop reservoir management, SPE-109805, *SPE Journal*, **14**(3), 506–523, 2009.

Wang, H., D. E. Ciaurri, L. J. Durlofsky, and A. Cominelli, Optimal well placement under uncertainty using a retrospective optimization framework (SPE 141950), in *SPE Reservoir Simulation Symposium, The Woodlands, Texas, USA*, pp. 1–19, 2011.

Whitney, J. E., L. I. Solomon, and S. D. Hill, Constrained optimization over discrete sets via spsa with application to non-separable resource allocation, *2001 Winter Simulation Conference*, 2001.

Wolsey, L. A., *Integer programming*, vol. 42, Wiley New York, 1998.

Yan, X. and A. C. Reynolds, An optimization algorithm based on combining finite-difference approximations and stochastic gradients (SPE-163613-MS), in *SPE*

Reservoir Simulation Symposium, 18-20 February, 2013, The Woodlands, Texas, USA, 2013.

Yeten, B., *Optimum Deployment of Nonconventional Wells*, Ph.D. thesis, Stanford University, 2003.

Yeten, B., L. Durlofsky, and K. Aziz, Optimization of nonconventional well type, location and trajectory, SPE-86880, *SPE Journal*, **8**(3), 200–210, 2003.

Yoon, K. and C.-L. Hwang, *Multiple Attribute Decision Making, An Introduction*, SAGE Publications, Inc, London, 1995.

Zandvliet, M., M. Handels, G. van Essen, D. Brouwer, and J. Jansen, Adjoint-based well-placement optimization under production constraints, in *SPE Journal*, vol. 13, pp. 392–399, 2008.

Zitzler, E., K. Deb, and L. Thiele, Comparison of Multiobjective Evolutionary Algorithms: Empirical Results, *Evolutionary Computation*, **8**(2), 173–195, 2000.

Zitzler, E., M. Laumanns, and S. Bleuler, A Tutorial on Evolutionary Multiobjective Optimization, in *Metaheuristics for Multiobjective Optimisation*, (edited by X. Gandibleux et al.), vol. 535 of *Lecture Notes in Economics and Mathematical Systems*, Springer, 2004.

Zitzler, E. and L. Thiele, An evolutionary algorithm for multiobjective optimization: The strength pareto approach, Tech. Rep. 43, Computer Engineering and Communication Networks Lab (TIK), Swiss Federal Institute of Technology (ETH), Gloriastrasse 35, CH-8092 Zurich, Switzerland, 1998.

Zitzler, E. and L. Thiele, Multiobjective evolutionary algorithms: a comparative case study and the strength pareto approach, *IEEE Transactions on Evolutionary Computation*, **3**(4), 257–271, 1999.

Zitzler, E., L. Thiele, M. Laumanns, C. M. Fonseca, and V. Grunert da Fonseca, Performance Assessment of Multiobjective Optimizers: An Analysis and Review, *IEEE Transactions on Evolutionary Computation*, **7**(2), 117–132, 2003.